




Rik Westendorp

C-arm conebeam CT guided
 ^{125}I prostate brachytherapy:
Dynamic dose calculation
and implant dynamics

About the cover: X-ray radiograph (april 7, 2014) of a thornback ray (*Raja clavata*) from the fish market. Tube settings: 30 kVp, 15 mA, output at 100 cm: 190 mGy/min; exposure time 2 minutes. Film: Kodak X-Omat V; Ffd 100 cm. Equipment: Machlett OEG-50 water cooled tube with W focus and Be window, no additional filter; Enraf Nonius generator with Graetz circuit; Agfa Curix-60 film processor.

ISBN: 978-90-9030207-2
Cover Design: Arie van 't Riet
Layout: Rik Westendorp
Typesetting: \LaTeX 2 ϵ with Tufte- \LaTeX
Printing: Gildeprint
Author ORCID: 0000-0001-9549-2391

Copyrights:

Chapter 2 © 2007 American Brachytherapy Society
Chapter 3 © 2012 American Brachytherapy Society
Chapter 4 © 2015 The authors. Published by IOP 
Chapter 5 © 2016 The authors. Published by Elsevier 
Chapter 6 © 2017 The authors. Published by Wiley 
Chapter 7 © 2017 American Brachytherapy Society

© 2017, Hendrik Westendorp

This work is licensed under a [Creative Commons 'Attribution-NonCommercial-ShareAlike 4.0 International'](https://creativecommons.org/licenses/by-nc-sa/4.0/) licence.



C-arm conebeam CT guided ^{125}I prostate brachytherapy

Dynamic dose calculation & implant dynamics

C-boog conebeam CT geleide ^{125}I prostaat brachytherapie

Dynamische dosisberekening & dynamica van het implantaat
(met een samenvatting in het Nederlands)

Proefschrift

ter verkrijging van de graad van doctor aan de Universiteit Utrecht op
gezag van de rector magnificus, prof. dr. G.J. van der Zwaan, ingevolge
het besluit van het college voor promoties in het openbaar te verdedigen
op donderdag 18 mei 2017 des middags te 12.45 uur

door

Hendrik Westendorp

geboren op 13 oktober 1977, te Woerden

Promotor: Prof. dr. ir. J.J.W. Lagendijk
Copromotoren: Dr. ir. A.W. Minken
Dr. ir. M.A. Moerland

De druk van dit proefschrift werd (mede) mogelijk gemaakt met financiële steun van Elekta, Radiotherapiegroep en RaySearch Laboratories.

Contents

1	Introduction	7
1.1	Prostate cancer	7
1.2	Prostate radiotherapy	7
1.3	Dosimetry	9
1.4	Outline of this thesis	12
2	Intraoperative adaptive ^{125}I brachytherapy	15
	Intraoperative adaptive brachytherapy of ^{125}I prostate implants guided by C-arm conebeam CT-based dosimetry	
3	Time trends in prostate edema after ^{125}I implantation	27
	Objective automated assessment of time trends in prostate edema after ^{125}I implantation	
4	Automated seed linking method	43
	An automated, fast and accurate registration method to link stranded seeds in permanent prostate implants	
5	Edema and seed displacements	59
	Edema and seed displacements affect intraoperative permanent prostate brachytherapy dosimetry	
6	CBCT based adaptive planning improves dosimetry	75
	Conebeam CT-based adaptive planning improves permanent prostate bra- chytherapy dosimetry: An analysis of 1266 patients	

7	Registration and contouring variability	93
	Dosimetric impact of contouring and image registration variability on dynamic ^{125}I prostate brachytherapy	
8	Summary	109
9	Discussion & future outlook	115
	Bibliography	133
	Samenvatting	141
	Dankwoord	144
	List of Publications	147
	Curriculum Vitae	148
	List of Abbreviations	150

Chapter 1

Introduction

1.1 Prostate cancer

Prostate cancer is a frequently diagnosed malignant disease, with currently an annual incidence of about 10 thousand cases in the Netherlands. The mortality due to prostate cancer in the Netherlands is approximately 2500 annually (figure 1.1). Since 1990 the diagnosed incidence of prostate cancer has increased considerably as a result of the increased use of Prostate Specific Antigen (PSA) testing to diagnose prostate cancer (figure 1.1). With PSA testing, prostate cancer is diagnosed earlier.

For low risk prostate cancer, expectative strategies such as watchful waiting or active surveillance can be good options.¹ Besides that, multiple treatment options are available, with surgery and radiotherapy being the most common.²

1.2 Prostate radiotherapy

Radiotherapy can be administered as external beam radiotherapy (EBRT) or as brachytherapy, where radioactive sources irradiate from within the prostate. Brachytherapy treatments are subdivided in three categories. (1) High-dose-rate (HDR): a high activity source stays inside the target for a limited amount of time, the treatment is performed in one or more fractions, (2) Pulsed-dose-rate (PDR): similar to HDR, but the

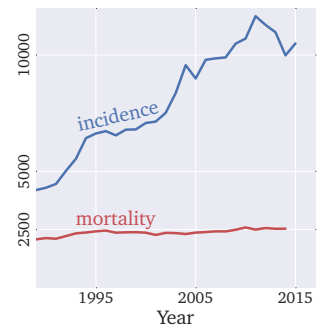


Figure 1.1: The incidence of prostate cancer in the Netherlands increased over the last decades (IKNL, 2016a).

¹ UpToDate®, 2016.

² Grimm *et al.*, 2012; IKNL, 2016b.

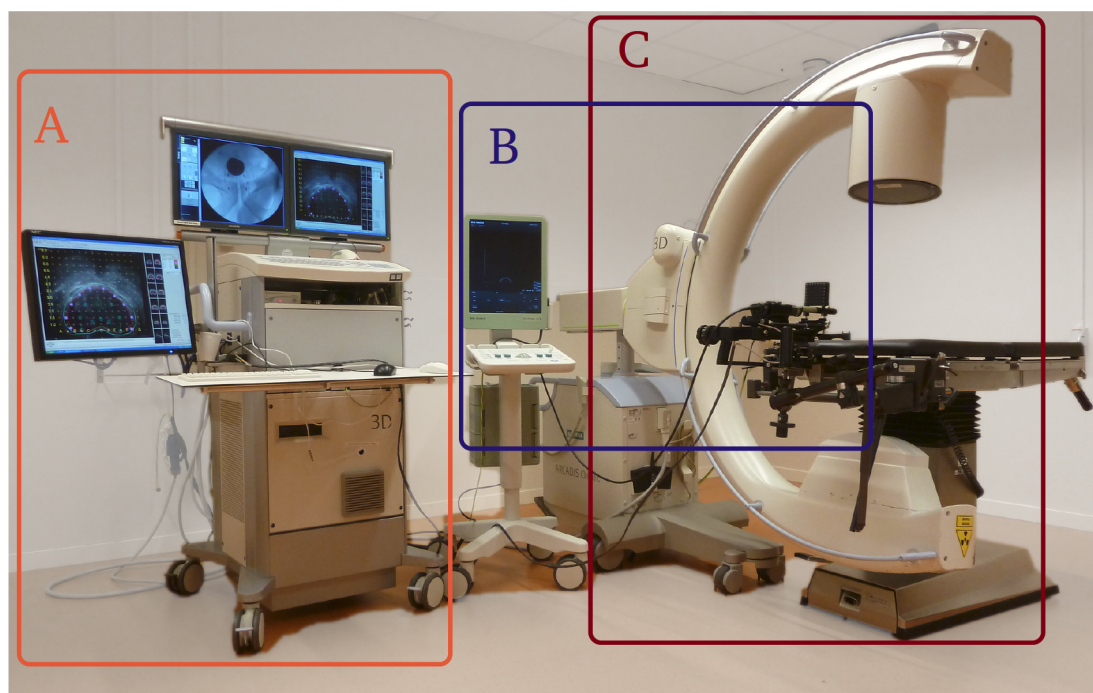


Figure 1.2: The implantation procedure in Deventer is performed with this equipment.

A: (all) computer equipment integrated in a cabinet, B: ultrasound system, C: C-arm CBCT

treatment is performed with a lower activity source in high number of short interval fractions, or (3) with low-dose-rate (LDR): low activity sources are placed in the target for a long time, or permanently. In case of LDR prostate treatment, sources stay in the prostate permanently.

^{125}I prostate brachytherapy

LDR brachytherapy is a well established form of radiotherapy to treat prostate cancer. The first reported brachytherapy treatment for prostate cancer dates back to the early twentieth century.³ Since the 1980's ^{125}I has become a standard isotope for prostate low-dose-rate brachytherapy.⁴ In the 1990's, with an increasing number of low risk patients needing treatment, ^{125}I brachytherapy has become more popular and has proven to be an effective treatment with limited toxicity.⁵

³ Pasteau *et al.*, 1914.

⁴ Holm *et al.*, 1983.

⁵ Potters *et al.*, 2008.

Implantation procedure

The implantation of ^{125}I sources in the prostate is performed in an operating theater (figure 1.2). The simplest implantation procedure is the *preplanning* method.⁶ Prior to the implantation procedure a treatment plan is made in which the locations of the sources are planned, commonly referred to as the ‘preplan’.

The implantation procedure start with (spinal) anaesthetising the patient. After positioning the patient according to the preplan, Trans Rectal Ultrasound (TRUS) images of the prostate and surrounding tissues are acquired. These images form the base for the treatment. The radiation oncologist contours the prostate, urethra, bladder and rectum. The preplan provides the locations at which seeds need to be placed. The radiation oncologist places the seeds in the prostate with needles that are inserted through a template (figure 1.3). When all seeds are placed, the treatment is finished.

1.3 Dosimetry

Approximately one month after implantation, a computed tomography (CT) scan of the implant is made and contoured.⁷ Seed positions found on the CT dataset are used to reconstruct a dose distribution. A Magnetic Resonance Imaging (MRI) scan can be acquired to obtain the actual prostate shape and can be used for contouring to improve target definition compared with CT. Alternatively the pre implant TRUS contours can be registered to the CT dataset.⁸ This proces, *postimplant dosimetry*, provides a good estimate of the dose that is delivered⁹ and gives an indication of the quality of the implant. Furthermore, it provides feedback to the brachytherapy team.

Multiple studies have shown the correlation between postimplant dosimetry and treatment outcome.¹⁰ Prostate cancer usually shows relatively slow progression. Most men diagnosed with prostate cancer die of other causes than prostate cancer. Outcome is therefore generally measured as biochemical disease free survival (BDFS).

Prostate irradiation may lead to complications in healthy tissues. These complications are mainly urinary, bowel and sexual dysfunction. To limit complications, dose to organs at risk should be limited.¹¹ This leads to a relatively narrow therapeutic window in which the prostate

⁶ Nag et al., 1999.

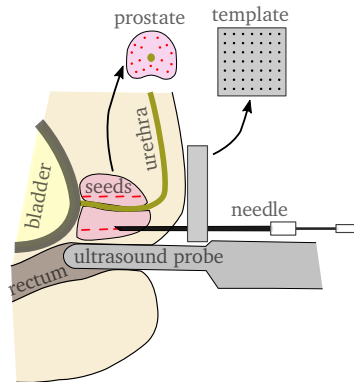


Figure 1.3: Seeds are implanted in the prostate transperineally. A template helps to position the seeds. Transrectal ultrasound visualizes the needle, prostate and organs at risk.

⁷ Ash et al., 2000; Davis et al., 2012; Nath et al., 2009; Salembier et al., 2007.

⁸ Bowes et al., 2013.

⁹ Moerland, 1998; Yue et al., 1999.

¹⁰ Henry et al., 2015; Hinnen et al., 2010a; Al-Qaisieh et al., 2009; Stone et al., 2010.

¹¹ Potters et al., 2001; Salembier et al., 2007.

receives an adequate dose while the complication rates are still low. While postimplant dosimetry gives a good indication of the quality of the implant, it does not allow for simple corrections in case an underdosage is observed. Ideally underdosages are resolved during the implantation procedure, with the patient still anaesthetized.

Intraoperative planning

The preplanning technique, originally used, is a simple approach. Some weeks prior to the implantation procedure a volume study is made, on which the prostate is contoured and the positions of the seeds are planned. During the implantation procedure the situation of the study needs to be reproduced exactly. In practice this leads to several limitations.¹²

¹² Polo *et al.*, 2010.

The TRUS probe setup and template need to be positioned exactly to reproduce the volume study images. Furthermore the size and shape of the prostate might have changed in the period between the volume study and the implantation procedure. As a result, the contours of the preplan can deviate from the actual situation and may lead to poor dose distributions.

To overcome these limitations, intraoperative treatment planning techniques have been developed. In contrast to the preplanning approach, the planning, imaging and seed placement during an intraoperative approach all take place in the operating theater. Intraoperative techniques have become the standard in the field. There are multiple approaches to perform intraoperative planning.

Intraoperative preplanning With intraoperative preplanning the planning is not performed several days to weeks before implantation, but in the operating theater, just before the implantation begins.¹³ The actual situation, including the imaging setup, is accurately reflected. This obviates the repositioning step that is involved in a preplanning approach.

¹³ Nag *et al.*, 1999.

Both dosimetry and outcome can be improved with intraoperative preplanning.¹⁴ Still, this procedure is limited since it does not adapt to a continuously changing shape of the prostate and deviations from the planned positions of the needles and seeds.

¹⁴ Gewanter *et al.*, 2000; Shah *et al.*, 2006; Wilkinson *et al.*, 2000.

Interactive planning With interactive planning, the radiation oncologist uses TRUS images to record the actual positions of the needles in the prostate.¹⁵ Deviations between the planned and actual positions of needles affect the dose distribution. According to the actual position of the needles, the plan is updated. The updated plan compensates for the difference between the actual and planned dose distribution. The positions of the remaining seeds are adjusted to reflect the deviations in dosimetry.

While the interactive planning technique shows improved dosimetry and outcome,¹⁶ no final check of all seed positions is available during the implantation procedure. Displacements of seeds and retraction of strands stay unnoticed and will not be discovered before postimplant dosimetry (day 30). Multiple studies show that postimplant dosimetry shows poorer results than intraoperative dosimetry¹⁷ using interactive planning.

Dynamic dose calculation The goal of dynamic dose calculation technique is to further enhance the accuracy of the implantation procedure.¹⁸ A step beyond interactive planning, in which needle positions are used, goes dynamic dose calculation where the position of each deposited seed is registered and used to calculate the actual dose distribution. Dynamic dose calculation takes all anatomy and implant dynamics into account.

While providing good visualization of the anatomy, TRUS does not allow for accurate final localisation of all seeds and can therefore not be used in a full dynamic dose calculation approach.¹⁹ In addition to TRUS, to show anatomy, a C-arm can be used to visualize the position of seeds. Most C-arm units only have (2D) fluoroscopy capabilities. Several groups investigated the use of multiple fluoroscopy images to reconstruct an implant.²⁰ Currently however, this type of reconstruction is not supported in treatment planning software, nor are there reports of large scale implementation of fluoroscopy based dynamic dosimetry.

Since 2006 C-arm equipment capable of acquiring 3D volumes has become available. These 3D volumes can be reconstructed as CT slices. This CT reconstruction facilitates integration in the intraoperative procedure greatly. It enables a workflow similar to postimplant dosimetry.

Seeds can be identified using the CT based seed finder algorithm that is available in the TPS. Following, anatomy (contours) and implant (seed positions) acquired by TRUS and CT, respectively are registered using

¹⁵ Nag *et al.*, 1999; Polo *et al.*, 2010.

¹⁶ Beaulieu *et al.*, 2007; Matzkin *et al.*, 2013; Raben *et al.*, 2004; Shanahan *et al.*, 2002.

¹⁷ Acher *et al.*, 2010; Igidbashian *et al.*, 2008; Moerland *et al.*, 2009; Al-Qaisieh *et al.*, 2009.

¹⁸ Nag *et al.*, 1999; Polo *et al.*, 2010.

¹⁹ Han *et al.*, 2003a; Polo *et al.*, 2010; Xue *et al.*, 2005.

²⁰ Kuo *et al.*, 2014; Todor *et al.*, 2003.

²¹ Westendorp *et al.*, 2007.²² Ishiyama *et al.*, 2016; Zelefsky *et al.*, 2010.

the standard module in the TPS. We have implemented a CBCT based dynamic dosimetry technique.²¹ Other groups have also reported about the use of intraoperative CBCT²² (figure 1.2).

1.4 Outline of this thesis

Since 2006 we use a C-arm CBCT based dynamic planning technique in clinical routine. The *purpose* of the present thesis is to give an overview of the clinical implementation of this dynamic dose calculation technique for ¹²⁵I prostate brachytherapy. The current chapter provides the background, context and rationale for such a technique. The aim is to efficiently generate implants, consistent in high quality, both with respect to target coverage and normal tissue sparing and to confirm this with postimplant dosimetry. Furthermore we sought to gain insight in the mechanisms that cause deviations between intraoperative and postimplant dosimetry.

In chapter 2 the C-arm CBCT based dynamic dosimetry technique is presented. An efficient workflow is introduced, making use of fiducial gold markers to register TRUS and CBCT image datasets. The first intraoperative dosimetry results from a pilot study of 20 patients are reported.

In chapter 3 we introduce two models that help to describe edema induced prostate volume changes. We studied the time course of edema on seven moments in the first month after implantation. The models use the positions of the seeds as surrogate for the prostate size. A simple spherical model is compared to a more complex cylindrical model, that was expected to more closely reflect the implant geometry.

In chapter 4 we present a novel technique that allows for tracking of individual seeds and automated processing of large datasets. The model takes into account that seeds are implanted as strands. It allows to study seed displacements in detail.

Chapter 5 shows an application of the seed tracking algorithm. Seed displacements and edema, taking place during the implantation procedure, were assessed. We studied the correlation of intraoperative and postimplant dosimetry. Analysis was performed for 699 implants and displacements were assessed for 70 subvolumes in the prostate. The effect of edema on dosimetry was analyzed separately.

Chapter 6 describes the dosimetry results of the dynamic CBCT technique for a large group of 1266 patients. The effect of CBCT based

dynamic dosimetry was studied both for the intraoperative and postimplant situation. Besides that, the region in the prostate most prone to underdosage was identified by locating the positions at which remedial seeds were placed.

Chapter 7 reports about the dosimetric uncertainties caused by inter and intra-observer variabilities in image registration and contouring. Dosimetrical consequences of contouring and registration variability are compared to the improvement in dosimetry by adding remedial seeds according to the CBCT based dynamic brachytherapy procedure.

Chapter 8 gives a summary of the preceding chapters. Finally, the position of the CBCT based dynamic technique in the field of permanent prostate brachytherapy is discussed in **chapter 9**.

Chapter 2

Intraoperative adaptive brachytherapy of ^{125}I prostate implants guided by C-arm conebeam CT-based dosimetry

Adapted from: H Westendorp, CJ Hoekstra, A van 't Riet, AW Minken and JJ Immerzeel (2007). 'Intraoperative adaptive brachytherapy of iodine-125 prostate implants guided by C-arm cone-beam computed tomography-based dosimetry.' *Brachytherapy*, 6(4):231–7

Abstract

Purpose: (1) To demonstrate the feasibility of C-arm cone-beam computed tomography (CBCT)-based postplanning and subsequent adaptation of underdosed critical areas by adding remedial seeds during the transrectal ultrasound (TRUS)-guided implantation of ^{125}I seeds and (2) to assess the duration of this procedure.

Methods and materials: After finishing the implant, three fiducial markers were implanted and a TRUS study was performed to delineate the prostate. A C-arm CBCT unit with isocentric design was used to generate a CT data set to localise the seeds. The TRUS and CBCT data sets were coregistered by the radiation oncologist to assess the dosimetry of the implant. If underdosages existed at critical areas, dosimetry was adapted by adding remedial seeds while the patient was still under anesthesia.

Results: Of 20 patients studied, 9 demonstrated underdosage in critical areas. On average four additional seeds were implanted, resulting in a mean D_{90} of 100.7% (increase 4.9%) and 117.5% (increase 17.8%) of the prescribed dose of 145 Gy and 110 Gy respectively. The average additional time involved in performing the adaptation procedure was less than 30 min.

Conclusion: C-arm CBCT guided intraoperative postplanning during TRUS guided brachytherapy for prostate cancer is both feasible and time efficient. The adaptation resulted in improved dosimetry of the prostate implants.

Introduction

The implantation of radioactive seeds in the prostate is a procedure currently undergoing rapid evolution. Shortcomings in a realised source distribution may lead to areas of underdosage within the prostate or insufficient treatment margins¹ with, as a possible result, lower treatment outcome.² For this reason a subsequent postplan on a computed tomography (CT) or magnetic resonance imaging (MRI) scan is recommended, varying from hours to several weeks after the implantation procedure, in order to ensure adequate dosimetry.³ If a postplan is acquired after the implantation procedure and areas of underdosage need to be corrected, a second implantation procedure has to be scheduled to correct the implant.⁴ Ideally, underdosages in the implant should be corrected as part of the implantation procedure while the patient is still anesthetized.⁵ A number of authors have described real-time dosimetric methods for prostate brachytherapy, using transrectal ultrasound (TRUS), fluoroscopy or CT. TRUS has good prostate imaging characteristics, but has a limited ability in accurately identifying all of the implanted sources,⁶ thus restricting its usability in real-time dosimetry. Source localization with multi-image fluoroscopy registered to TRUS combines the seed identification accuracy of fluoroscopy with the prostate imaging characteristics of TRUS.⁷ However, processing of fluoroscopic X-ray images is not yet incorporated in commercially available treatment planning software. Furthermore, the identification of overlapping seeds can be difficult.⁸ Real-time conventional CT based dosimetric feedback and modification are time consuming and the patient has to leave the operating room for CT.⁹ Availability of the department's CT scanner is a limiting factor¹⁰ when seed implantation is performed on a modified CT table.

Since 2003, more than 600 prostate seed implantations have been performed at this Institute in a conventional operating room setting. Preoperative adjustment of treatment plans was applied using TRUS guidance. A followup CT scan was obtained at Day 0 and at 4 – 6 weeks after the procedure for dosimetric evaluation of the implant. TRUS based dynamic dosimetry programs rely on a manual attempt to identify the sources as they are deposited within the prostate gland. However, subsequent movement of the deposited seed on removal of the needle cannot be excluded.¹¹ For this reason we decided to introduce into clinical routine an implant procedure with C-arm cone-beam CT (CBCT)-based

¹ Mueller *et al.*, 2002.

² Ash *et al.*, 2006; Stock *et al.*, 1998.

³ Nag *et al.*, 2000; Stock *et al.*, 1998.

⁴ Keyes *et al.*, 2004.

⁵ Zelefsky *et al.*, 2006.

⁶ Han *et al.*, 2003b; Steggerda *et al.*, 2005.

⁷ Gong *et al.*, 2002; Todor *et al.*, 2003.

⁸ Su *et al.*, 2004.

⁹ Fuller *et al.*, 2005.

¹⁰ Kaplan *et al.*, 2006.

¹¹ Reed *et al.*, 2005.

dosimetric feedback. In this way the dosimetric evaluation of the implant is brought into the operating theatre, using equipment already available in that location. The intraoperative dosimetric evaluation presented is based on the registration of fiducial markers on TRUS images, for prostate contouring, and CT images from a C-arm CBCT unit, for seed localization. In this feasibility study, consideration was given to whether adaptations were achievable within a reasonable amount of time and to the degree of prostate dosimetry improvement.

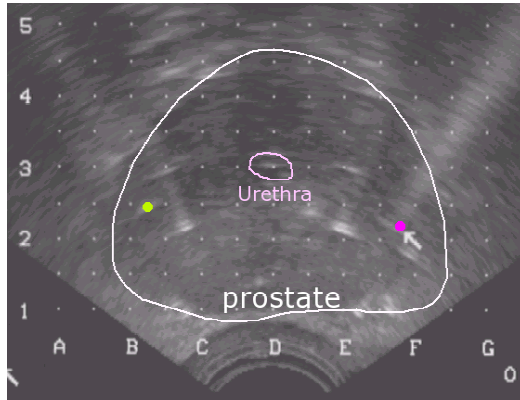
Methods and materials

Twenty-two consecutive patients treated in the period of October 2006 through November 2006 have been analyzed with real-time, intraoperative C-arm CBCT postplanning. Of this group, two patients were excluded from the study because of insufficient registration of the TRUS and CBCT data set during the limited time available in the operating theatre. A dose of 145 Gy was prescribed for ¹²⁵I monotherapy or, in case of a boost, a dose of 110 Gy was prescribed after a 50 Gy external beam treatment. The implantation and delineation of all prostates was performed by a team of experienced radiation oncologists.

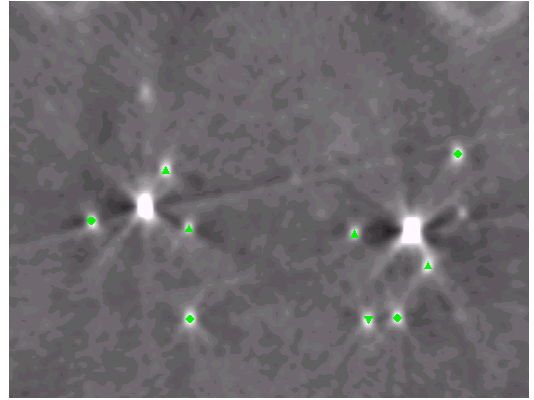
A TRUS volume study was performed on average 2 weeks before implantation. This study was used for preplanning the optimal source geometry and to determine the activity and number of sources.

In this preplan a homogeneous dose distribution was planned with 90% of the target volume receiving a dose (D_{90}) between 110% and 120% of the prescribed dose. The percentage of the target volume receiving at least 100% of the dose (V_{100}) was prescribed to be >98%. A transperineal implantation technique was applied¹² making use of stranded sources. Before implantation, the prostate was imaged with TRUS and delineated anew. Where necessary, the preplan was adjusted in accordance with alterations in prostate geometry. During the implantation procedure, sources were placed as closely as possible in agreement with the latest preplan. Should deviations from this latest preplan occur during implantation, modifications were made dynamically to take these deviations into account. For patients receiving 145 Gy monotherapy, three gold cylinders with a length of 5 mm and a diameter of 1 mm were implanted in the prostate to serve as fiducial markers as soon as the TRUS guided implantation procedure was completed. One marker was placed near the apex,

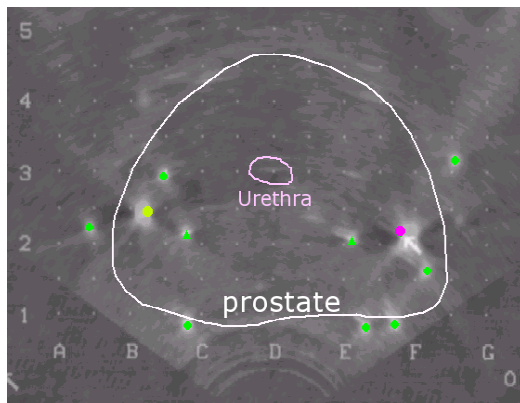
¹² Holm *et al.*, 1983.



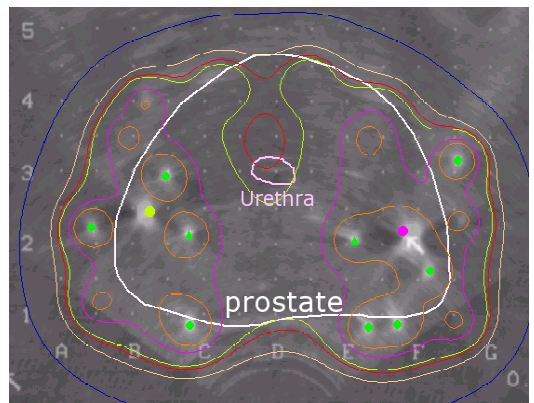
(a) TRUS with contours and labeled fiducial markers



(b) CBCT with fiducial markers and labelled source positions



(c) Registration of TRUS and CBCT on fiducial markers



(d) Isodose lines and contours on registration of TRUS and CBCT

a second near the base, and a third lateral in the prostate to ensure the most reliable registration possible. In the case of the 110 Gy boost, four markers with the same specifications were already present, having been placed for position verification during the external beam treatment. The fiducial markers for the 110 Gy treatment were located one in the apex, one at the base of the prostate and two laterally in the prostate.

The legs of the patient were lowered as far as possible to obviate excessive prostate rotation with respect to the CBCT study that was performed subsequently thus facilitating registration of both studies. A TRUS volume study with 2.5 mm steps was then made. The pressure of the TRUS probe to the prostate was minimized by reducing the amount

Figure 2.1: Registration(c) of TRUS(a) and CBCT(b) on fiducial markers, resulting in isodose-contours on TRUS(d).

of water in the balloon on the TRUS probe. During the acquisition of the TRUS images, fiducial markers were labelled immediately because the visibility of such fiducial markers on static images may be poorer than that during acquisition.

A CT study was made using the C-arm CBCT unit following removal of the TRUS probe from the rectum. The patient was laid flat to provide enough space for the rotation of the C-arm, needed to acquire a CT data set. A C-arm CBCT unit¹³ with an isocentric design and 190° orbital movement was used to generate the CBCT data set. The 3D data set was split into slices at 2.5 mm increment and sent to the planning station¹⁴. The seed finder of the planning station was used to locate the seed positions, which were verified manually.

With the patient still on the treatment couch, the delineated TRUS study was registered on the CT with labelled fiducials using the registration functionality of the treatment planning system as shown in [figure 2.1](#). The registration was performed using a least squares algorithm allowing the marked positions to translate and rotate as a rigid body. The implanted fiducial markers were used as reference positions to align the TRUS and CT data sets. The quality of the resulting registration was judged by comparing positions of seeds on CT with strand trajectories visible on TRUS. Additionally, the positions of the urethra and bladder balloon, visible on both studies, were examined.

After the registration and the identification of all source positions from the CT image set, a slice-by-slice dosimetric analysis was available from the treatment planning system. The dosimetry was evaluated by the radiation oncologist. If the dosimetry was deemed satisfactory, the patient was discharged. Alternatively, the identification of sites with coverage deficiency led to the adoption of a corrective plan and the placement of remedial seeds as shown in [figure 2.2](#). The position of the simulated remedial sources was specified according to the ultrasound targeting grid coordinates, just as in the original standard procedure planned preoperatively. The patient was prepared anew with the legs elevated. The remedial seeds were implanted following the correction plan and the reimplant procedure was completed. A final C-arm CBCT was obtained. The TRUS scan made after the first implantation procedure was registered on the CT images obtained, using the same procedure as used after the first implantation, resulting in final Day-0 dosimetry for the corrected implants. The entire procedure was scheduled to involve a

¹³ Siemens Arcadis Orbic 3D, Siemens Medical Systems, Erlangen, Germany

¹⁴ Variseed 7.1, Varian Medical Systems, Palo Alto, USA

time not exceeding 90 min, with the patient being discharged the same day.

Results

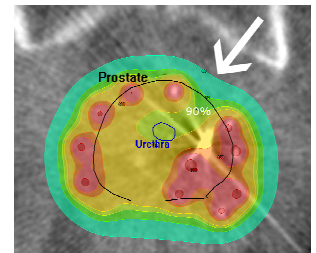
In this study, 16 of 20 patients received ^{125}I monotherapy and the remaining four a ^{125}I boost after 50 Gy external beam radiotherapy. In 9 patients the implant was adapted based on the criterium that underdosed areas were considered to be clinically important.

On average 4 seeds (2 – 8) were added to correct the appearing underdosage. The mean preimplant volume of the prostates in the operating theatre was 40.2 cm^3 (range, $20.7 - 57.8\text{ cm}^3$). Following implantation, a mean increase of volume of 2.5 cm^3 (range, $-1.9 - 9.2\text{ cm}^3$) was observed, both volumes being measured with TRUS. The registration of the postimplant TRUS was performed on the CBCTs before and after reimplantation. After registration, the root mean square (RMS) of the distance between the corresponding fiducials in the TRUS and CT data set was 0.8 mm on average (SD 0.3 mm).

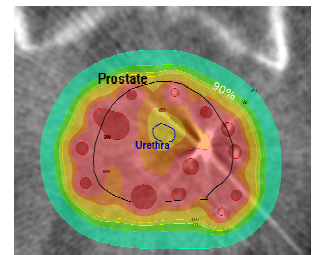
After performing a CBCT for Day-0 postplanning, the additional time involved in performing the correction procedure was 25 minutes (range, 16 – 30 minutes).

Patients with a prescription dose of 145 Gy

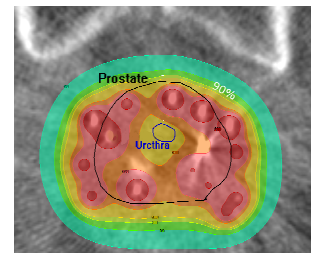
Sixteen cases were treated with a prescribed dose of 145 Gy, five of which (31%) were corrected. Two to four additional seeds were implanted to correct the initial realisation. In [table 2.1](#), D_{90} and V_{100} of the corrected group¹⁵ and uncorrected group¹⁶ are presented. The preplanned D_{90} and V_{100} did not differ between the corrected group and the group not receiving additional seeds. After the initial realisation the average D_{90} of the corrected group was 4.4% lower than that of the uncorrected group. The correction procedure raised D_{90} 4.9% on average (range, 2.4 – 10%). After correction the average D_{90} of the corrected group was not significantly different than in the uncorrected group. Before correction a 4% lower V_{100} is shown in the corrected group with respect to the uncorrected group. A rise in V_{100} of 6.9% on average (range, 2.9 – 17%) is observed after correction. The ultimate V_{100} in the corrected group is 3% higher than that in the uncorrected group. For all 145 Gy implants, a



(a) White arrow marks dose deficiency



(b) Correction plan



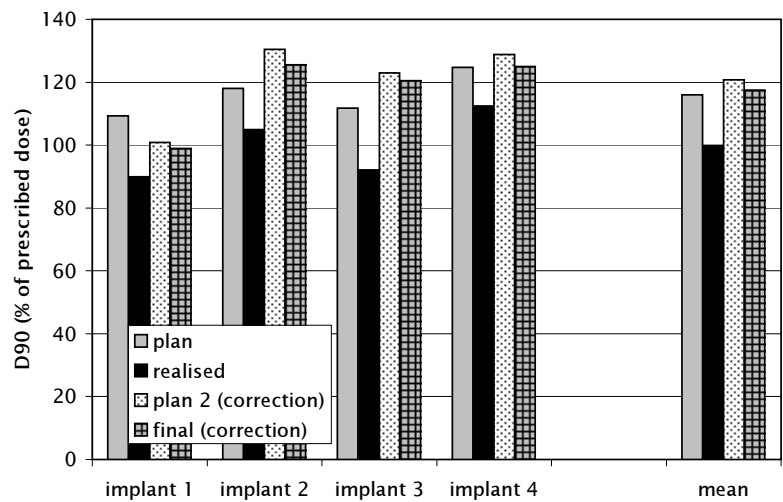
(c) Finally realised dose distribution

Figure 2.2: Example of the adaptation procedure, showing the adaptation of an underdosage in an implant. The 90% isodose contour is displayed in light green.

¹⁵ cases receiving additional seeds

¹⁶ cases not receiving additional seeds

Figure 2.3: D₉₀ of corrected implants with a prescribed dose of 110 Gy



final D₉₀ of 100.3% on average was achieved resulting in a 14.1% lower D₉₀ than originally planned, whereas the average final V₁₀₀ of 88.4% turned out to be 10.5% lower than originally scheduled.

Patients with a prescription dose of 110 Gy

All four implants with a prescription dose of 110 Gy were corrected. To correct these implants, four to eight seeds were added. The results of the correction are presented in table 2.1. D₉₀ increased with 17.8% on average (range, 9.0 – 28.4%). The final D₉₀ was 1.6% higher than the initial plan and 3.3% lower than the correction plan. A mean increase of 11.1% (range, 1.2 – 21.9%) in V₁₀₀ was observed resulting in a value of 97.2%, which corresponds with the correction plan and is 1.8% lower than the initial plan. In figures 2.3 and 2.4, a graphical representation of D₉₀ and V₁₀₀, respectively is shown per case at each step of the procedure; the mean of D₉₀ and V₁₀₀ for these four implants is also indicated.

Discussion

With increasing evidence that dosimetric parameters correlate with biochemical outcome, it is desirable to evaluate the quality of the implant.¹⁷ The timing of postimplant dosimetry is controversial,¹⁸ some authors

¹⁷ Ash et al., 2006; Nag et al., 2000.
¹⁸ Nag et al., 1999.

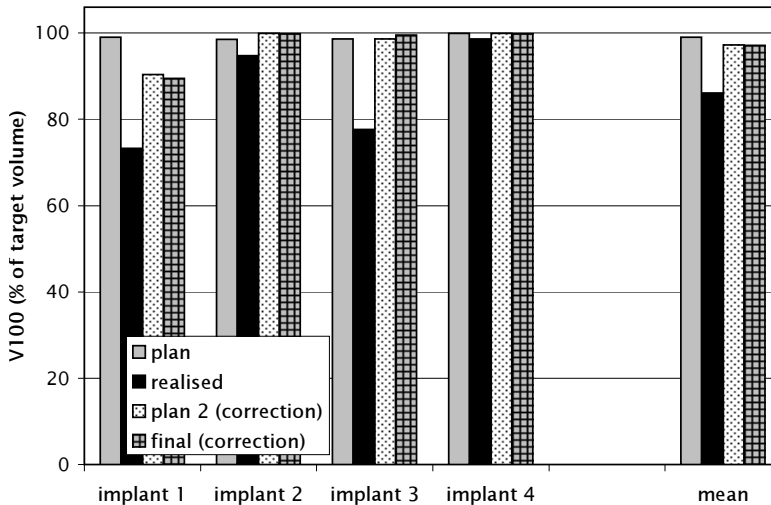


Figure 2.4: V_{100} of corrected implants with a prescribed dose of 110 Gy

suggesting that 24 hour dosimetry is acceptable.¹⁹ The occurrence of possible underestimation of D_{90} due to edema is a reason why other authors prefer to delay postimplant dosimetry by several weeks.²⁰ In this latter case, however, correction of the implant involves a second implantation procedure.²¹ We are of the opinion that it is preferable to perform dosimetric evaluation as an integrated part of the implantation procedure itself, using equipment already available in the operating room.

As a rule, two intraoperative imaging modalities are available, TRUS and fluoroscopy, neither of which is capable of providing accurately consecutive identification of the prostate gland and localisation of the implanted seeds. Xue *et al.* (2005) state that it is possible to identify stranded seeds in an implant with a high-resolution TRUS. This is not only difficult, but also hardly possible without prior knowledge of the implanted seed geometry. Data reported by Chauveinc *et al.* (2004) shows considerable deviations between TRUS and CT derived D_{90} and V_{100} .

In contrast to TRUS, fluoroscopy can indicate seed positions. The modality can also be applied in the operating theatre. At the present time, however, this seed localisation method is not yet integrated in commercial treatment planning software. Furthermore, overlapping seeds can cause incorrect localization of seeds, making a thorough manual check of source positions imperative. The registration of the reconstructed seed

¹⁹ Taussky *et al.*, 2005.

²⁰ Prestidge *et al.*, 1998; Waterman *et al.*, 1998.

²¹ Keyes *et al.*, 2004.

		D ₉₀ (% of prescribed)				V ₁₀₀ (% of prescribed)			
		Initial		Correction		Initial		Correction	
		Plan	Realised	Plan 2	Final	Plan	Realised	Plan 2	Final
145 Gy (not corrected)	mean	114.3	100.2			98.9	87.5		
	min.	108.0	87.7			98.0	75.4		
	max.	121.8	116.2			99.5	99.3		
145 Gy (corrected)	mean	114.6	95.8	100.9	100.7	99.0	83.6	91.0	90.5
	min.	111.5	93.4	97.7	95.9	97.6	77.5	86.3	83.7
	max.	120.3	99.7	104.2	103.5	99.8	89.5	94.8	94.6
110 Gy (all corrected)	mean	115.9	99.8	120.8	117.5	99.0	86.1	97.3	97.2
	min.	109.3	89.9	100.8	98.9	98.5	73.3	90.4	89.5
	max.	124.7	112.5	130.5	125.5	100.0	98.6	100.0	99.8

Table 2.1: Dosimetry of im-
plants represented by D₉₀ and
V₁₀₀, extrema correspond to
the maximum and minimum
of all patients in the corres-
ponding group per stage of the
procedure.

positions to the delineated ultrasound images is difficult. Gong *et al.* (2002) propose the use of needle tips as fiducials but, to the best of our knowledge, this method has not yet been reported clinically. Another disadvantage of this method is possible prostate deformation during TRUS imaging and fluoroscopy. CBCT imaging with a C-arm can overcome most disadvantages of fluoroscopy, making seed identification possible on the reference modality CT.²²

For evaluation, an accurate and reproducible definition of the prostate is needed. Contouring of the prostate on high quality, diagnostic CT images demonstrates a variation in delineation according to the observer's subjective judgment of the prostate outline on CT.²³ Assessing prostate volume from the C-arm CBCT is considerably less reliable since the C-arm CBCT does not possess the imaging qualities of (multislice) CT. The best modality to contour the prostate on is MRI,²⁴ a technique not available in the average operating room. TRUS exhibits reproducibility²⁵ similar to that of MRI. TRUS, available in the operating room, is the reference modality on which to delineate the prostate. Adequate registration of the TRUS delineated contours and the seed positions found on the CT images is essential. Fuller *et al.* (2005) describe a registration based on contours delineated on TRUS and CT, but registering TRUS to CT based on delineation of both modalities which has the shortcoming of limited prostate visibility on CT. We prefer the use of fiducial markers

²² Nag *et al.*, 1999.

²³ Al-Qaisieh *et al.*, 2002; Smith *et al.*, 2007.

²⁴ Salembier *et al.*, 2007.

²⁵ Smith *et al.*, 2007.

as references, these being visible both on TRUS by the cast shadow and on CT by the artifacts. A least-squares fit is performed to minimize the distance between the markers on TRUS and CT, leading to a rigid-body transformation of the TRUS data.

Although the fiducial markers usually demonstrate more cast shadow than seeds, on postimplant TRUS it may occasionally be difficult to distinguish the markers from seeds, calcareous spots or artifacts. This limitation may be overcome by using transverse and sagittal TRUS images to identify fiducial markers from ^{125}I seeds. As noted earlier, improper registration during the limited time available in the operating theatre led to rejection of two patients in the initial phase of this study.

To obtain TRUS images, a probe was inserted in the rectum. The CT data set, however, was obtained without a probe or stabilising device in the rectum. As a result, deviations between CT and TRUS modalities can appear. The most obvious distortions (2 – 5 mm) are reported on the posterior midline of the prostate when using surface coregistration. By contrast, anterior prostate and lateral prostate coregistration are less sensitive to such distortions, agreement generally occurring within the range of 0 – 2 mm.²⁶ The ultrasound probe was positioned inside a balloon, filled with water.

²⁶ Fuller *et al.*, 2005.

To minimise deviations between CT and US coregistration, postimplant TRUS in our series was obtained with the balloon emptied and with the probe positioned dorsal to the rectum; in our experience this results in negligible distortion of the prostate. The fiducial markers were positioned in areas less susceptible to distortion, which is supported by the root mean square of the distance between the corresponding fiducial markers in both imaging studies.

D_{90} is a generally accepted dosimetric parameter that should be reported²⁷ when assessing the quality of implants. For high risk patients, a homogeneous dose distribution is of major importance in the treatment of the prostate. The results obtained in this study show that all patients in the high risk group, receiving a ^{125}I boost of 110 Gy, had to be corrected, leading to significantly higher values of the relative D_{90} than in the low risk group with brachy monotherapy of 145 Gy. With high risk brachytherapy-boosts the aim is a homogeneous dose in the entire prostatic gland, while in the low risk group, depending on the geometry of the dose-distribution, a less homogenous dose is accepted when tumor coverage is adequate. For the low-risk group, the determining factor on

²⁷ Nag *et al.*, 2000.

deciding whether remedial seeds were needed was underdosage in areas considered by the radiation oncologist to be clinically significant.

It should be noted that the intraoperative adaptive dosimetric method here presented is strictly a Day 0 manipulation. Although prostate volume fluctuation beyond Day 0 is a dynamic process which is not constant from patient to patient; in our experience²⁸ the dosimetric impact of prostate swelling is generally clinically insignificant, making the dosimetry representative for the entire treatment time-frame. The results obtained in this study show no clinically significant change of prostate volume immediately after the implantation procedure for most patients.

²⁸ Westendorp *et al.*, 2004.

Conclusion

The feasibility of intraoperative implant corrections using a C-arm CBCT is demonstrated. TRUS was used to contour the prostate. Fiducial markers served as reference points in registering TRUS and CT, rendering adequate dosimetry possible intraoperatively. The correction procedure proved to be feasible within half an hour of additional time.

Chapter 3

Objective automated assessment of time trends in prostate edema after ^{125}I implantation

Adapted from: H Westendorp, R Kattevilder, A van 't Riet, AW Minken, TT Nuver, JJ Immerzeel and CJ Hoekstra (2012). 'Objective automated assessment of time trends in prostate edema after ^{125}I implantation'. *Brachytherapy*, 11(5) (5):327–

Abstract

Purpose: To present an objective automated method to determine time trends in prostatic edema resulting from ^{125}I brachytherapy.

Methods and materials: We followed 20 patients, implanted with stranded seeds, with 7 consecutive CT scans to establish a time trend in prostate edema. Seed positions were obtained automatically from the CT series. The change in seed positions was used as surrogate for edema. Two approaches were applied to model changes in volume. (1) A cylindrical model: seeds from the compared distribution were linked to the reference distribution of Day 28. After alignment the compared distribution was scaled in cylindrical coordinates, leading to the changes in radial and craniocaudal directions. The volume changes were calculated using these scaling factors. (2) A spherical model: distances of seeds to the center of gravity of all seeds were used as a measure to model volume changes.

Results: With Day 28 as reference, the observed volume changes were smaller than $18\% \pm 6\%$ (1 SD) for the cylindrical and $12\% \pm 7\%$ for the spherical model. One day after implantation the implanted prostate was less than 10% larger than in the reference scan for both models. Apart from Day 0, both models showed similar volume changes.

Conclusions: We present an objective automated method to determine changes in the implanted prostate volume, eliminating the influence of an observer in the assessment of the prostate size. The implanted volume change was less than $18\% \pm 7\%$ for the studied group of 20 patients. Edema was $9\% \pm 5\%$ from 1 day after implantation onward.

Introduction

Brachytherapy with ¹²⁵I seed implants is a well-established treatment for low-grade prostate cancer. The implantation of seeds in the prostate causes swelling of the prostate.¹ This swelling or edema can affect the dose distribution in the prostate. Depending on the time trend and amount of edema, this can result in inadequate dose coverage of the target volume. Edema is, therefore, an important clinical parameter to quantify.

Edema can be assessed by contouring the prostate on an imaging study. Both MRI and TRUS are good modalities to visualize the prostate. CT gives poorer prostate visualization.² Positions of seeds though can be determined accurately on CT,³ whereas TRUS and MRI are less suited to localize seeds automatically. Compared with CT and TRUS, access to MRI equipment is limited, and imaging studies with MRI require larger time slots than with CT.

The amount of edema is reported by various groups in a range of 18% to 100%, mostly taking the TRUS-based preimplant volume of the prostate as a reference.⁴ In most studies the prostate volume is assessed by manual contouring, sometimes even comparing different modalities such as TRUS and CT. This introduces inaccuracies as TRUS and CT delineations lead to significant differences in the observed volume.⁵ If a postimplant CT study is compared to a preimplant TRUS study, the observed volume difference could be caused by difficulties in delineating the prostate on the CT study.⁶

All manual determinations of prostate volumes are dependent on the accuracy of the observer. Intra- and inter-observer variability is known to affect the results.⁷ Moreover, if multiple scans per patient are obtained, the workload to accurately contour all studies is enormous. Therefore, most studies analyse edema for a small number of patients and for a limited number of measurements per patient.

Clearly, a fast and objective method to determine the prostate size will be valuable for accurate determination of time trends in edema. Objectivity can be obtained by using an automated procedure to determine the prostate volume. Implanted ¹²⁵I seeds can be detected automatically and they serve as surrogate reference points for the implanted prostate volume. The positions of the seeds can be used to determine the relative volume of the implanted prostate volume over time and they provide

¹ Waterman *et al.*, 1998.

² Smith *et al.*, 2007.

³ Siebert *et al.*, 2007.

⁴ Dogan *et al.*, 2002; Leclerc *et al.*, 2006; Merrick *et al.*, 1998; Moerland *et al.*, 1997; Narayana *et al.*, 1997; Prestidge *et al.*, 1998; Sloboda *et al.*, 2010; Tanaka *et al.*, 2007; Taussky *et al.*, 2005; Waterman *et al.*, 1998.

⁵ Smith *et al.*, 2007.

⁶ Solhjem *et al.*, 2004.

⁷ Al-Qaisieh *et al.*, 2002; Smith *et al.*, 2007.

⁸ Leclerc *et al.*, 2006; Merrick *et al.*, 1998; Steggerda *et al.*, 2007; Waterman *et al.*, 1997; Westendorp *et al.*, 2004.

⁹ Leclerc *et al.*, 2006; Steggerda *et al.*, 2007; Waterman *et al.*, 1997; Westendorp *et al.*, 2004.

time trends in the investigated period.

The use of seeds as reference markers has been reported before.⁸ A 2 dimensional or spherical 3 dimensional approach was used in these cases. The 2 dimensional approach has serious limitations in an accurate comparison of seed distributions due to difficulties in aligning two distributions. Earlier studies⁹ using a 3 dimensional approach treated edema as an isotropic phenomenon by using a spherical model. An isotropic model could be limited: after implantation seeds could move through the implantation channels. Also, if seeds are in strands, the movement of seeds with respect to each other might be limited. Perpendicular to the implantation direction, seeds are expected to be more limited in their movements with respect to the prostatic tissue. The spherical model cannot distinguish between seed displacement in craniocaudal and radial directions.

We developed a new model to quantify the amount of prostate edema. In this model seed movements in the radial and craniocaudal directions are separated. The method is automated and objective.

Seed distributions in 140 CT scans, which were obtained during the first four weeks after implantation, were registered by linking seeds to the reference distribution (Day 28), and relative volumes were determined.

Methods and materials

For each patient, 7 CT scans were made: on Day 0 (just after implantation), 1 or 2, 4 or 6, 9 or 11, 13 or 15, 20 and Day 28 or 29. The first week after implantation multiple CT scans were obtained to track relatively rapid changes in the implanted volume. After that, weekly scans were performed revealing more gradual changes.

Immediately after implantation of the ¹²⁵I seeds the implants were checked for underdosed areas, using in-room C-arm cone-beam CT¹⁰ available in the operating theater. The implants were corrected in the same procedure when necessary.¹¹ In five cases of the analyzed group this correction was deemed necessary, and remedial seeds were implanted.

The first CT scan (Day 0) was acquired with the C-arm Cone Beam CT-unit just after finishing the total implant procedure. Slices of 2.5 mm thickness were reconstructed. The patient was laid flat to provide enough space for the rotation of the C-arm, needed to acquire a CT data set. The pelvic rotation was close to that used for making the conventional

¹⁰ Arcadis Orbic 3D, Siemens, Germany

¹¹ Westendorp *et al.*, 2007.

CT scans. Subsequent CT scans were performed on a conventional CT scanner¹² with a slice thickness of 2 mm. As these studies were used only to track the positions of the seeds, low-dose scans could be used. The accuracy of finding seeds on C-arm cone-beam CT and low-dose scans was verified by a phantom with markers at known positions. The markers were tracked with the same accuracy as with a diagnostic CT protocol on a conventional CT. The final scan (Day 28) had diagnostic quality, but radiation exposure was minimized. Scan protocols were optimized to minimize effective dose from imaging equipment, resulting in a total effective dose of all CT scans equal to the traditionally used CT scan after 1 month. The extra performed CT scans added a total extra effective dose <6 mSv. All patients provided informed consent.

¹² Brilliance Big Bore 16 Slice, Philips, The Netherlands

The seed finder of the treatment planning system¹³ was used to localize the seeds in the datasets. The automatic localization of seeds was manually examined for inconsistencies.

¹³ Variseed 7.2, Varian, Palo Alto, USA

Analysis

In the spherical model, volume changes of seed distributions were modelled as a uniform spherical expansion. The mean of the distances of the seeds to the center of mass of the distribution was taken as a measure for the radius of this sphere (r_s). There is no absolute relevance to r_s , but it can be compared to the radius of a reference distribution $r_{s,\text{ref}}$. The scan of Day 28 was taken as the reference distribution, as this is the common time point for reporting dosimetry.¹⁴

¹⁴ Ash *et al.*, 2000; Nag *et al.*, 1999.

The relative volume ($V_{\text{rel,spher}}$) of the seed distribution was calculated using [equation \(3.1\)](#).

$$V_{\text{rel,spher}} = \left(\frac{r_s}{r_{s,\text{ref}}} \right)^3 \quad (3.1)$$

A spherical approach, however, has limitations. Strands are inserted through channels, possibly allowing migration in the direction of the channel more easily than orthogonally to it.

In our implantation procedure, most seeds are interconnected in strands, and as long as the strand is not weakened or dissolved, the seeds could be restrained to migrate in the z -direction with respect to interconnected seeds. Perpendicular to the strands, seeds are likely to move with the prostatic tissue. Obviously, the spherical model cannot

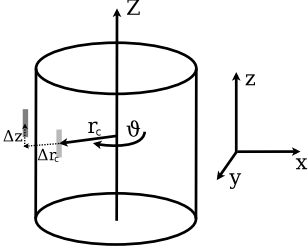


Figure 3.1: A cylindrical geometry is used to analyse the volume changes. r_c , z and θ are the principal directions of the cylindrical geometry. The reference position of a seed is shown in light gray; the registered seed is shown in dark gray. The movement of the seed is reflected in the vectors Δr_c and Δz . A Cartesian coordinate system is shown on the right.

describe these effects. Therefore, the seed distribution was also modelled by a cylindrical shape (figure 3.1). Using the cylinder geometry, expansion in craniocaudal (z) direction is separated from expansion in radial (r_c) direction. We expect that this geometry is a better representation of the physical behaviour of interconnected seeds in implantation channels. Equation (3.2) describes how the relative volume ($V_{\text{rel,cyl}}$) of the cylinder geometry scales with respect to the reference.

$$V_{\text{rel,cyl}} = \frac{r_c^2 z}{r_{c,\text{ref}}^2 z_{\text{ref}}} \quad (3.2)$$

Our cylindrical analysis is shown in figure 3.2 in a schematic way. First, the centers of mass of the seed distributions were merged. After that, seeds close together in the compared distributions were linked, minimizing the root mean square distance between linked seeds.

The compared distribution can differ with respect to location and orientation from the reference distribution because of a different filling of the rectum and bladder and a different positioning of the patient. Because of these changes in location, orientation and scale (edema) the compared distribution was translated, rotated and scaled to obtain optimal agreement between the two distributions. After translating and rotating the compared distribution, scaling was performed in cylindrical coordinates. This scaling provided the mutual independent changes in the z and r_c directions. Subsequently, the seeds between the reference and (optimized) compared distribution were linked again (second iteration). After the first iteration, the seed distributions were more similar in position, orientation and scale, more or other seeds could be linked, enabling further optimization. Taking the mean of the square of the distances between the linked seeds and the number of linked seeds as measures, the optimized distribution was compared to the previous iteration. If additional seeds were linked or a decrease in mean distance was observed, another optimization step was performed. If not, the optimization procedure was stopped. From the final r_c and z the relative volume changes relative to Day 28 were computed. The technical details of the procedure are more elaborately described in [appendix A](#).

To test the robustness of the cylindrical approach, other distributions than Day 28 were taken as a reference. The distribution of Day 0 was taken as a reference comparing later distributions. Also, an incremental procedure was followed, comparing Day 1–0, 2–1 . . . 28–20, thus calculat-

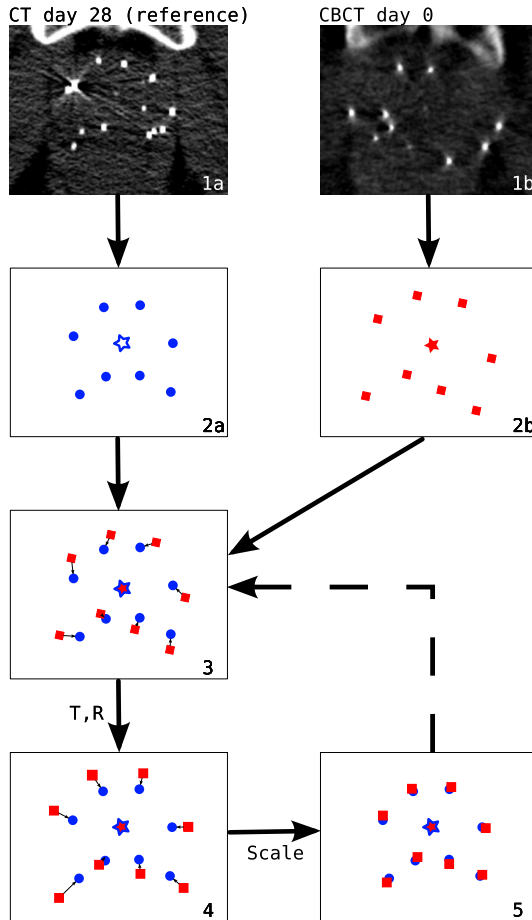


Figure 3.2: Procedure schematically presented. The CT study of Day 28 (1a) is the reference study. In this example the CBCT study of Day 0 (1b) is the compared distribution. Source positions of both distributions are obtained, schematically depicted in 2a,b. The center of mass is determined (star) and merged (3). Seeds of the compared distribution are linked to the closest seeds in the reference distribution, after which a translation (T) and rotation (R) is performed. The compared distribution is transformed to cylindrical coordinates and scaled (4,5). If the result is not optimal another iteration is performed (dashed line). CBCT = cone-beam CT.

ing the total change of r_c and z . These two checks should yield similar same results as taking Day 28 as the reference. The accuracy of the cylindrical model was checked by investigating the residual distances and number of seeds linked.

Time trends in movements of the seeds were investigated in the radial and craniocaudal directions. From these data, the changes in implanted volume were deduced.

The optimization procedure was also performed with scaling in Cartesian coordinates to check if any difference existed in left-right (LR) and anterior-posterior (AP) edema.

Clinical

A group of 20 patients was included in a period of approximately 7 months. Seven patients were also treated with hormonal therapy three months before the brachytherapy procedure. Eighteen patients were treated with ^{125}I monotherapy (prescribed dose 145 Gy). Two patients had an external beam treatment prior to the brachytherapy boost (prescribed dose 110 Gy). Fourteen patients were staged with Stage T1a–T1c and 6 patients with Stage T2a–T2b prostate cancer. The preimplant prostate volume based on TRUS imaging varied from 26 to 62 cm³ (mean 42 cm³). The prostatic gland as well as the capsule were implanted. On average 74 seeds (range, 62–84) were implanted using 18 needles (range, 15–21). Stranded seeds were employed with an activity from 0.38 to 0.58 mCi per seed (mean, 0.48). Implantation was performed by inserting one needle at a time and immediately releasing the strand while removing the needle. Eighteen patients were implanted with 125I¹⁵ seeds, in two cases 125I¹⁶ seeds were used. All implantations were performed at our institute by an experienced team of two radiation oncologists using the same technique.

¹⁵ IBt, Belgium

¹⁶ IBt-BEBIG, Germany

Results

Figure 3.3 shows the time trends of seed distributions for the cylindrical approach in radial (r_c) and craniocaudal (z) directions for each of the 20 patients. The distribution of Day 28 was used as reference. Not all cases showed a similar time trend although a gradual decrease in lateral and craniocaudal directions could be observed. In two cases (○ at Day 15, △ at Day 0) a poor registration result was observed.

In the investigated period, no effects on implanted volume time trends were observed with respect to earlier administered hormone treatment, the migration of a strand, the disappearance of a seed, placement of remedial seeds, boost or monotherapy treatment, number of needles, number of seeds used and type of stranded seed applied.

During the seed finding process, the following observations were made. For 2 patients, migration of a strand (>5 mm) was observed 1 day after implantation. For another patient, one of 68 seeds disappeared from the prostate between Day 0 and 1 and in one further case, one of 73 seeds disappeared between Day 20 and 28.

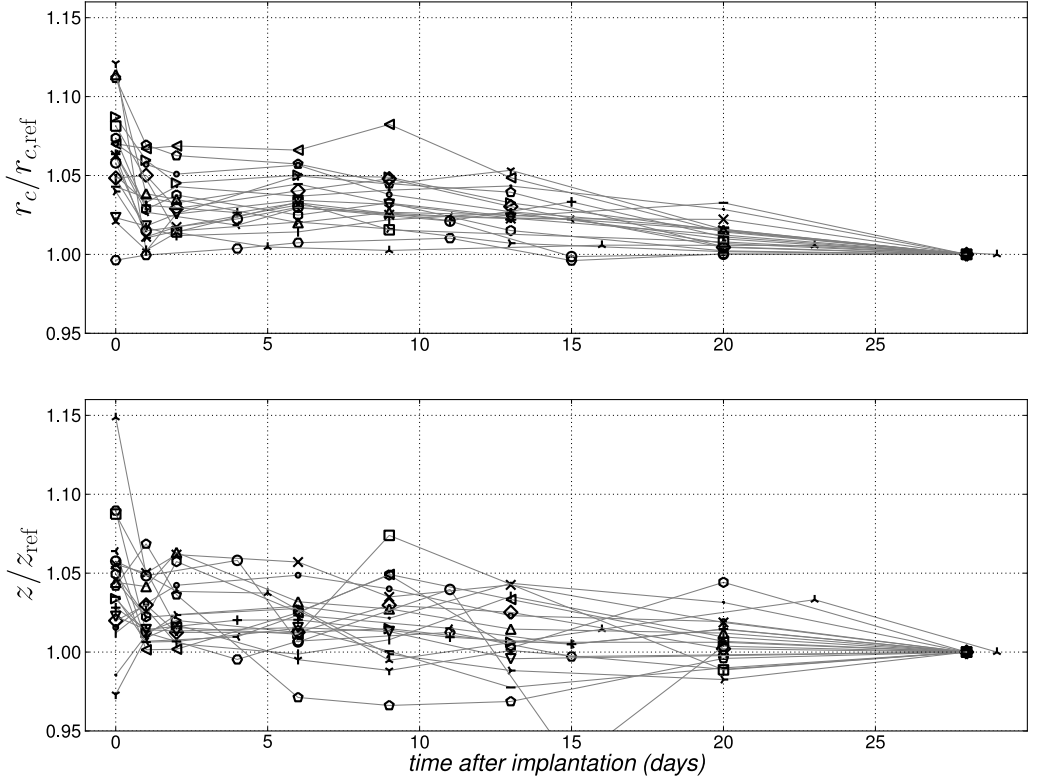


Figure 3.3: Radial (r_c) and craniocaudal (z) time trends of seeds distributions of 20 patients with Day 28 as reference. The results of \circ at Day 15 and Δ at Day 0 are because of poor registration.

Disregarding the two outlier points described previously, on average, a decrease of $6\% \pm 3\%$ (1 standard deviation) in radial and $4\% \pm 4\%$ in craniocaudal directions was observed over the period of 28 days. The time trend of the relative volume for the group of patients is presented in [figure 3.4](#). If the prostate is considered as a cylinder, this corresponds to a mean decrease in prostate volume of $18\% \pm 6\%$ from just after implantation to Day 28.

The seed distribution was also modelled spherically. In [figure 3.4](#) volume changes calculated from the spherical approach, with radius r_s , are shown by the dashed line. In this case a volume decrease of $12\% \pm 7\%$ was observed.

A small difference in LR vs. AP edema was found. Averaged over all measurements the edema in the LR direction was $98\% \pm 4\%$ of the AP edema.

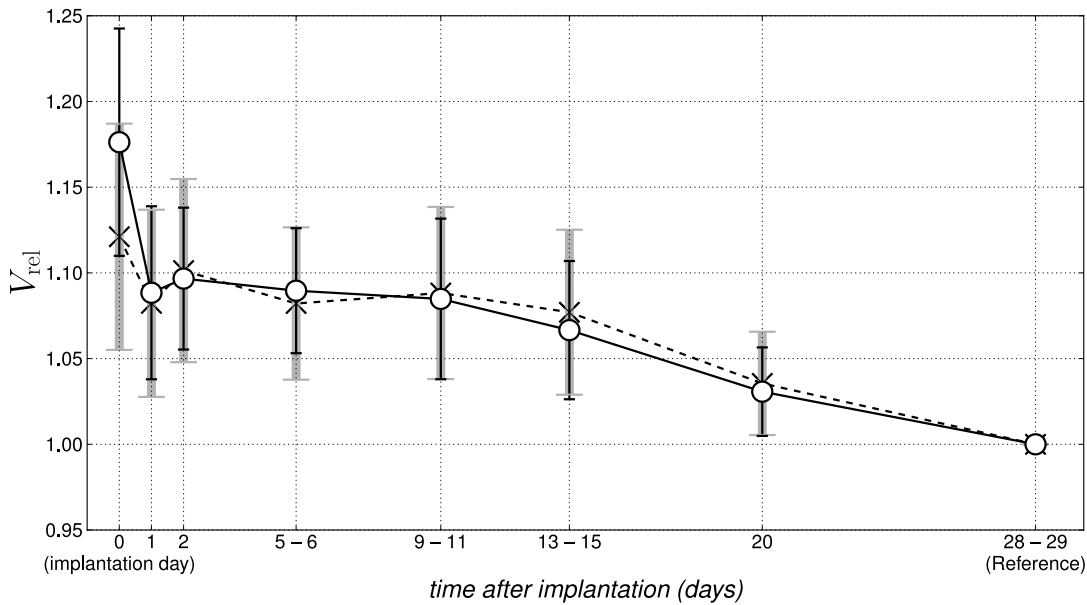


Figure 3.4: Changes in im-
planted volume with Day 28
as a reference, the solid line
with o-marks and black error
bars indicates the cylindrical ap-
proach, the spherical approach
is represented by the dashed
line with x-marks and gray
error bars.

Registration from Day 28–Day 0 resulted in the same changes in volume as registering Day 28–Day 20, Day 20–Day 15 . . . Day 1–Day 0. Taking Day 0 as a reference and comparing following distributions showed a similar result, demonstrating the robustness of the matching procedure.

For the registration of Day 0–Day 28 on average 3.8 (range 1–10) iterations were performed. For Day 1–Day 20 the average number of iterations decreased from 2.3 to 2.0. Residual distances after connecting and registration are reported in [table 3.1](#). Translations in x , y and z directions did not show a relevant deviation from 0. Rotations up to 12° were present around the LR axis. On average more than 97% of the seeds were matched; in [table 3.1](#) the number of matched seeds is presented on a day-by-day basis.

match Day 28 to	residual distance (mm)		% of seeds matched	
	mean	SD	mean	SD
0	2.5	0.3	92	5
1	1.7	0.3	97	3
2	1.6	0.3	97	3
5–6	1.4	0.3	98	1.9
9–11	1.3	0.3	99	1.5
13–15	1.1	0.3	99	1.3
20	0.9	0.3	99.5	1.1

Table 3.1: Residual distances and percentage of seeds matched in registrations after performing the optimization procedure for the cylindrical expansion.

Discussion

Analysis

We developed a method to automatically determine the changes in implanted volume using a cylindrical model and compared it with a spherical model. The prostate implant served as surrogate for the prostate volume.

The registration procedure of the cylindrical approach proved to be reliable: we were able to match over 97% of the seeds in the implant on average. Residual distances between the seeds after the optimization routine can originate from the slice thickness of the CT scans, not all seeds being linked to the reference distribution and limited accuracy of the seed finding algorithm.¹⁷ In general the rotations needed to align distributions were considerable, indicating these were necessary to improve accuracy.

In figure 3.4 good agreement is shown for the spherical and cylindrical model, starting from Day 1. The earlier reported¹⁸ spherical approach seems to be the method of choice, as this procedure is simpler to implement.

Day 0 shows a difference between the two approaches that might relate to the migration of seeds. A possible reason might be that the cylindrical geometry handles migration of seeds better than the spherical geometry. Although the spherical approach takes all seeds into account, the cylindrical approach ensures that seeds that have migrated are not linked to seeds in the reference distribution and that they do not influence the scaling of the distribution and consequently the calculated volume.

The registration on Day 0 is slightly poorer than later registrations (table 3.1). Implantation channels are expected to be still relatively open

¹⁷ Siebert *et al.*, 2007.

¹⁸ Leclerc *et al.*, 2006; Waterman *et al.*, 1998; Westendorp *et al.*, 2004.

¹⁹ Fuller *et al.*, 2004.

on Day 0, enabling migration¹⁹ and therefore possibly influencing the residual distance and the fraction of seeds that could be linked. Although the patient is laid flat while performing the C-arm Cone Beam CT, the pose of the patient on Day 0 could be somewhat different than at other moments, using the CT.

Using the cylindrical approach, almost similar time trends are observed in z as well as r_c direction, which may suggest that the used strands are losing their rigidity in the z direction the first day after implantation. In a simple experiment we put a strand with four seeds in water with body temperature. Within 5 hours the strand was flexible and could be compressed easily a couple of millimeters. A similar process could occur in the implanted prostates.

Other groups also determined implanted volume changes from seed positions. Merrick *et al.* (1998) use fluoroscopic images to determine the positions of the seeds to deduce the volume of the prostate. This method does not generate the seed positions in three dimensions. An accurate correction for the rotations of the prostate cannot be applied, which will hamper the accuracy of the determined prostate size.

²⁰ Leclerc *et al.*, 2006; Steggerda *et al.*, 2007; Waterman *et al.*, 1998.

Others²⁰ used a spherical model. We introduced a cylindrical model and were able to distinguish between lateral and craniocaudal changes. The linking of seeds allows to track individual seed positions over time. This can be useful in determining migration of seeds, which is currently under investigation.

Clinical

An objective assessment of implanted volume changes is presented for a group of 20 patients. Similar results were obtained for the cylindrical and spherical approach. The average amount of volume change was limited, being 18% on average for the cylindrical approach and 12% for the spherical approach.

The most important advantage of our study with respect to other studies is the objective computational approach we used. Compared to previously published data more measurements are presented: 7 measurements per patient within 28 days. Our observations during the first 4 weeks after implantation do not give evidence for an exponential

decrease in prostate volume as has been suggested elsewhere.²¹

Time trends in volume change are highly variable for each individual patient (figure 3.3). The average time trend of the group (figure 3.4) shows a considerable change in prostate volume within the first day after implantation, suggesting that most of the postimplant volume changes take place shortly after implantation.

The amount of volume change after ¹²⁵I seed implantation is in agreement with the data based on MRI contouring published by Sloboda *et al.* (2010). This group reports a volume increase of $18 \pm 14\%$ from the day before implantation to just after implantation. Our study provides additional data in the four weeks directly after implantation.

In literature higher values for the volume changes are reported.²² The difference in observed volume change between this study compared to other studies might be attributed to the design of the study. In other studies, often fewer measurements were taken, volume change was manually assessed by delineating imaging series, sometimes from different imaging modalities.

Other causes for a difference in the observed volume changes may be the implantation technique used. Some groups report the placement of all needles before loading the sources, others immediately load the needle with sources and retract it before placing another needle. Also the type and number of needles used to implant the seeds could influence the amount of edema.

Steggerda *et al.* (2007) reported more edema of the implanted volume than the contoured volume. Previous research of our group did not show more edema based on seed positions than based on delineation of TRUS images²³

In this study, Day 28 was used as a reference. This is an arbitrary moment although it is often used as the reference date for postimplant dosimetry.²⁴ After one month, there may still be an increased prostate volume. Sloboda *et al.* (2010) reported that the volume of the prostate on Day 28 is 1% higher than the preimplant volume on average. Others reported higher values of edema at Day 28 but used different modalities to compare the prostatic edema on.²⁵ The amount of edema present after day 28 remains subject to further investigation.

²¹ Waterman *et al.*, 1998.

²² Dogan *et al.*, 2002; Leclerc *et al.*, 2006; Merrick *et al.*, 1998; Moerland *et al.*, 1997; Narayana *et al.*, 1997; Prestidge *et al.*, 1998; Tanaka *et al.*, 2007; Taussky *et al.*, 2005; Waterman *et al.*, 1998.

²³ Westendorp *et al.*, 2004.

²⁴ Ash *et al.*, 2000; Nag *et al.*, 1999.

²⁵ Taussky *et al.*, 2005.

Conclusion

We present an automated objective method to determine changes in implanted prostate volume. The proposed method is fully automated and thereby eliminates the influence of an observer in the assessment of the prostate size. The implanted prostate volume showed an implanted volume change of $18\% \pm 7\%$ for the studied group of patients. Edema was $9\% \pm 5\%$ one day after implantation. Apart from Day 0, the cylindrical approach provides the same estimate of the swelling of the implanted prostate volume as the spherical approach.

Appendix A: Detailed description of the cylindrical procedure

A program was developed in Python to register the seed distributions, using the following strategy:

1. Take a reference distribution X (with n_X seeds) and a registration distribution Y (with n_Y seeds). Translate both distributions such that their center of mass is $(0, 0, 0)$.
2. Calculate the distance $d_{i,j}$ from every seed in one distribution to every seed in the other distribution.
3. Sort all distances.
4. $n = \min(n_X, n_Y)$. Select the n shortest distances (O_n). Take the maximum distance found after sorting: $d_{\max} = \max(d_{i,j}) \forall i, j \in O_n$ and define the upper limit for distances that are considered: $d_{\text{threshold}} = d_{\max} + 0.5 \text{ mm}$.
5. Iterate over all possible combinations $d_{i,j}$. If $d_{i,j} < d_{\text{threshold}}$ (as determined in previous step) take combination as valid, d_c . After all combinations have been checked, choose the best match of the reference seeds with multiple connections to seeds in the compared distribution. Allow only one connection per seed in each distribution.
6. Using a Powell optimization technique, optimize the distribution with respect to translation, rotation and scale, such that e is minimized.

$$e = \sum_{c \in \text{connections}} d_c^2$$

and

$$Y_{\text{transl, rot}}(x, y, z) = T_{xyz} R_z R_y R_x Y(x, y, z)$$

where T is the translation from the center of mass. And R_x , R_y and R_z are the rotations around the x , y and z axis respectively.

7. For the scaling, the seed optimal translated and rotated distribution $Y_{\text{transl, rot}}$ is transformed to cylindrical coordinates as shown in [figure 3.1](#). A scaling in radial, r_c and craniocaudal z direction is

performed also using a Powell optimization. After that, the distribution is transformed back to Cartesian coordinates to enable another iteration.

$$Y_{\text{scale,transl,rot}}(\vartheta, r, z) = S_{r,z} Y_{\text{transl,rot}}(\vartheta, r, z)$$

8. Iterate through Steps 2–6 until the number of connected seeds does not increase and the error e does not decrease anymore. The optimal registration has been found. Store the error as well as the mean distance for d_c .

Chapter 4

*An automated, fast and accurate
registration method to link
stranded seeds in permanent
prostate implants*

Adapted from: H Westendorp, TT Nuver, MA Moerland and AW Minken (2015).
'An automated, fast and accurate registration method to link stranded seeds in
permanent prostate implants'. *Phys Med Biol*, 60(20):N391–N403

Abstract

The geometry of a permanent prostate implant varies over time. Seeds can migrate and edema of the prostate affects the position of seeds. Seed movements directly influence dosimetry, which relates to treatment quality.

We present a method that tracks all individual seeds over time, allowing quantification of seed movements. This linking procedure was tested on transrectal ultrasound (TRUS) and cone-beam CT (CBCT) datasets of 699 patients. These datasets were acquired intraoperatively during a dynamic implantation procedure that combines both imaging modalities.

The procedure was subdivided in four automatic linking Steps. (I) The Hungarian Algorithm was applied to initially link seeds in CBCT and the corresponding TRUS datasets. (II) Strands were identified and optimized based on curvature and linefits: non optimal links were removed. (III) The positions of unlinked seeds were reviewed and were linked to incomplete strands if within curvature and distance thresholds. (IV) Finally, seeds close to strands were linked, also if the curvature threshold was violated. After linking the seeds, an affine transformation was applied. The procedure was repeated until the results were stable or the 6th iteration ended.

All results were visually reviewed for mismatches and uncertainties. Eleven implants showed a mismatch and in 12 cases an uncertainty was identified. On average the linking procedure took 42 ms per case.

This accurate and fast method has the potential to be used for other time spans, like Day 30, and other imaging modalities. It can potentially be used during a dynamic implantation procedure to faster and better evaluate the quality of the permanent prostate implant.

Introduction

The dosimetry of permanent prostate implants depends critically on the localization of ^{125}I seeds.¹ Difficult visualization of seeds on transrectal ultrasound (TRUS) hampers the localization of seeds and consequently accurate dosimetry.² C-arm cone-beam computed tomography (CBCT) allows, like CT,³ for accurate localization of seeds, but visualizes the prostate boundary poorly.⁴ Combining TRUS and CBCT improves the accuracy of the dosimetry of implants.⁵ We developed a dynamic dosimetry procedure in which we assess the dosimetry during implantation by combining TRUS and CBCT.⁶ This live method allows for immediate adaptation of the implant: if an implant shows a cold spot remedial seeds are placed in the same intraoperative procedure.

The geometry of an implant is not stable over time.⁷ Edema of the prostate pushes seeds away from the center⁸ and seeds migrate after implantation. Better understanding of implant geometry changes may help to improve the implantation practice and could assist in a modified strand and seed design.

Migration of seeds can only be quantified if each seed can be tracked over time. In each image dataset all seed positions have to be identified and related to positions in a reference dataset. It is impossible to perform this task manually. An automated model is needed to connect the seed positions for each image dataset, after which the result can be visually inspected.

We developed a linking procedure to track movements of individual seeds and validated it on 699 intraoperative TRUS and CBCT datasets. With adjustments, the linking procedure may also be used to study implant geometry changes for longer time spans, like the time from implantation to Day 14 or Day 30.

Methods and Materials

TRUS and CBCT datasets

Intraoperatively obtained TRUS and CBCT datasets of 740 consecutive patients, treated in the period from October 2007 to May 2012, were reviewed. Forty one cases lacked an image dataset due to technical reasons, leaving 699 cases eligible for analysis. All patients were treated accord-

¹ Kuo *et al.*, 2014.

² Polo *et al.*, 2010.

³ Brabandere *et al.*, 2012.

⁴ Smith *et al.*, 2007.

⁵ Polo *et al.*, 2010.

⁶ Westendorp *et al.*, 2007.

⁷ McLaughlin *et al.*, 2006; Moerland *et al.*, 2009; Steggerda *et al.*, 2015.

⁸ Westendorp *et al.*, 2012.

⁹ Falcon 2101 EX and Flex Focus 400, BK Medical; Herlev, Denmark and Siemens Arcadis Orbic 3D; Siemens Medical Systems, Erlangen, Germany

¹⁰ Westendorp *et al.*, 2007.

¹¹ IBt 1251L; Seneffe, Belgium, IBt-Bebig I25.S06; Berlin, Germany, Bard STM1251; Murray Hill, NJ USA

¹² Variseed 7.2 – 8.02; Varian Medical Systems, Inc., Palo Alto, CA USA

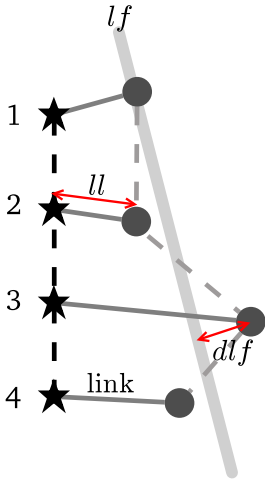


Figure 4.1: Links between reference distribution (★, TRUS) and compared distribution (●, CBCT). *lf*: linefit, *ll*: link-length, *dlf*: distance to linefit.

ing to our protocol that makes use of combined TRUS-CBCT imaging^{9, 10}. Stranded seeds of $\varnothing 1 \times 5$ mm were used¹¹. Spacing was equidistant in most strands, but also strands with varying spacing were used. Seed positions were initially localized on the TRUS datasets directly after releasing the strands from the needles. The seed finder of the treatment planning system¹² was used to identify seeds on CBCT, after which the seed positions were visually inspected. These CBCT seed positions were used for clinical dosimetry.

Linking procedure

DICOM RT objects were exported from the treatment planning system. The DICOM RT Plan objects provided the seed positions as identified on the treatment planning system for both TRUS and CBCT.

TRUS seed positions were acquired first and served as the reference distribution (X). The CBCT distribution was the compared distribution (Y , figure 4.1). The center of mass (COM) of both seed distributions was set to (0, 0, 0). After that, four linking steps (I, II, III and IV) were performed. The linking procedure is visualized in figure 4.2 and depicted as a flowchart in figure 4.3.

Step I The initial distance between both distributions was defined as the minimum total squared distance, similar to the approach described by Chng *et al.* (2011) and Jain *et al.* (2005).

First, a cost matrix was generated with all squared distances from the reference, TRUS, distribution X (with seeds $\mathbf{x}_1, \mathbf{x}_2, \dots, \mathbf{x}_n$) to the compared, CBCT, distribution Y (with seeds $\mathbf{y}_1, \mathbf{y}_2, \dots, \mathbf{y}_m$):

$$c_{ij} = \begin{bmatrix} |\mathbf{x}_1 - \mathbf{y}_1|^2 & \dots & |\mathbf{x}_1 - \mathbf{y}_m|^2 \\ \vdots & \ddots & \vdots \\ |\mathbf{x}_n - \mathbf{y}_1|^2 & \dots & |\mathbf{x}_n - \mathbf{y}_m|^2 \end{bmatrix}, \quad (4.1)$$

$$i = 1, 2, \dots, n,$$

$$j = 1, 2, \dots, m.$$

Occasionally, due to human error, the number of seeds in both distributions was not equal. In some cases a seed was not identified on one of the image datasets. In other cases a misidentification led to too

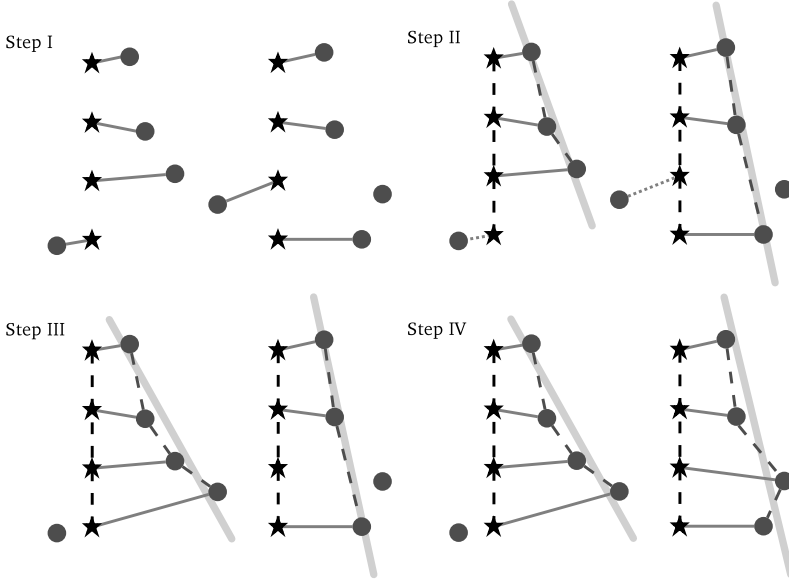


Figure 4.2: Linking procedure for two strands. In this example the compared distribution (\bullet, Y) contains one seed more than the reference (\star, X) distribution. Dashed lines: connections of seeds in strand. Thin solid lines: links between reference and compared seeds. Step I: seeds are initially linked. Step II: A linefit of the (compared) strand is added (lf , thick gray lines) and links causing violation of strand constraints (dotted lines) are removed. Step III: New links, not violating strand constraints, are generated. Step IV: Residual seeds are linked if close to the linefit, even if the curvature constraint is violated.

many seeds in a distribution. In case $n \neq m$, the distribution with the lowest number of seeds determined the number of links.

After the cost matrix (c_{ij}) was defined, the total cost σ was determined:

$$\sigma = \sum_{i=1}^n \sum_{j=1}^m c_{ij} p_{ij},$$

where

$$p_{ij} = \begin{cases} 1 & \text{if } i^{\text{th}} \text{ seed from } X \text{ is assigned to } j^{\text{th}} \text{ seed from } Y \\ 0 & \text{if not,} \end{cases}$$

under the restriction that each seed is used once.

(4.2)

The Hungarian algorithm¹³ was used to solve the linear assignment problem, resulting in the minimum value for σ . The resulting links represented the lowest cost but could be physically incorrect, a mismatch (figure 4.2, Step I). In the next steps strand properties were used to correct the mismatches originating from step I.

¹³ Kuhn, 1955.

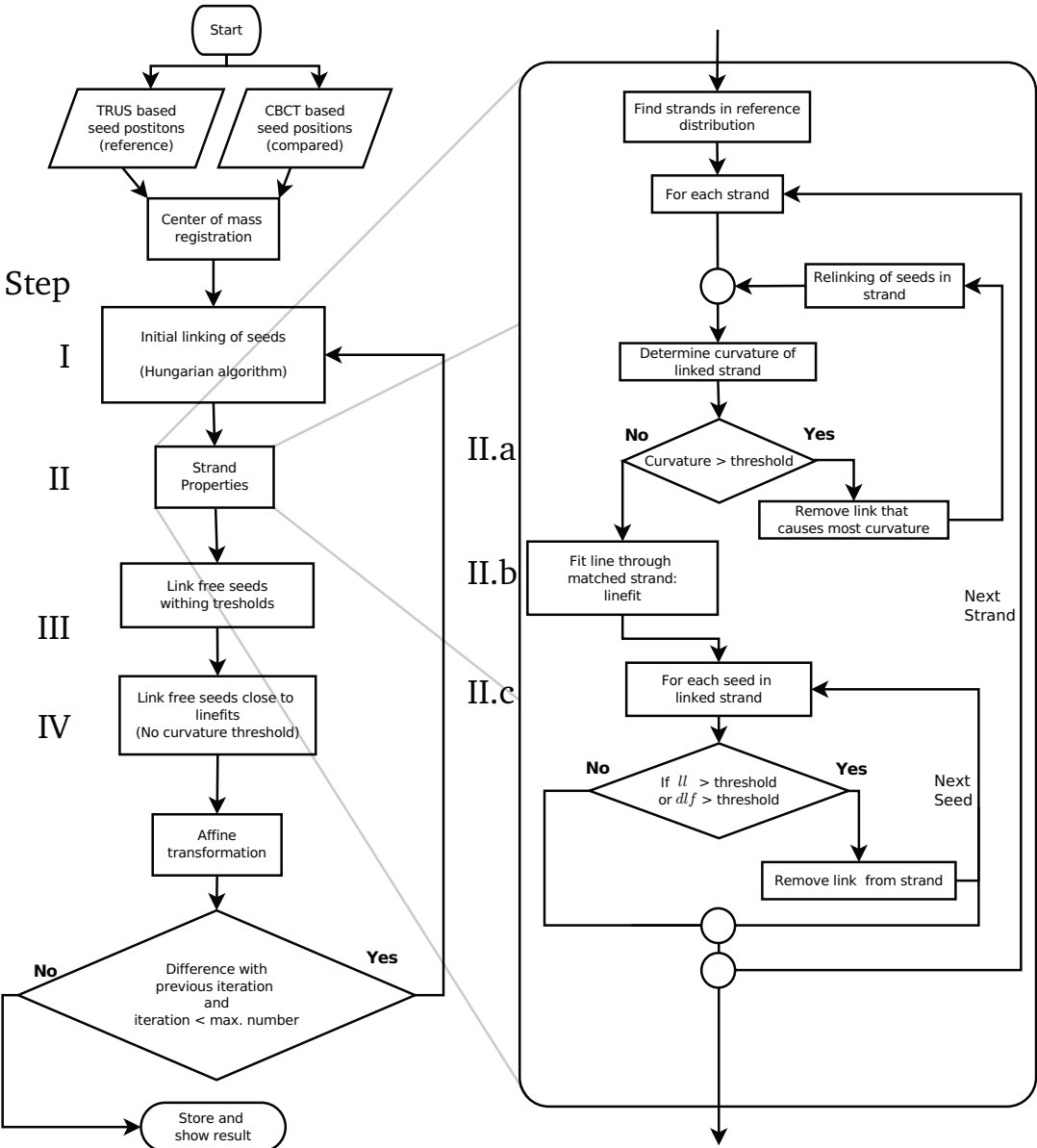


Figure 4.3: Flow chart showing the linking procedure. The right part shows details of Step II. *ll*: link-length, *dlf*: distance to linefit.

Step II In this step strand properties of Y were determined and, if links were physically unlikely, i.e. thresholds are exceeded, links were removed. This is visualized in detail in the right part of [figure 4.3](#) and in [figure 4.2](#), Step II.

Based on the TRUS DICOM RT Plan object (seed coordinates) all strands were identified in X . The reference strands contained the seeds (\mathbf{x}_i) and provided links to \mathbf{y}_j . The links to \mathbf{y}_j provided an initial estimate of strands in Y . Following, the curvature (κ)¹⁴ of each strand in Y was determined.

¹⁴ Stewart, 2015, p. 877–882.

$$\kappa = \frac{1}{r}, \quad (4.3)$$

where r is the radius of curvature. The coordinates of a strand can be parametrised as $\boldsymbol{\gamma}$. Under the assumption that $\boldsymbol{\gamma}$ is a function of z ($\boldsymbol{\gamma} = f(z)$), where z is the needle insertion direction, the curvature is defined as:

$$\kappa = \frac{\frac{d^2\boldsymbol{\gamma}}{dz^2}}{\left(1 + \left(\frac{d\boldsymbol{\gamma}}{dz}\right)^2\right)^{3/2}}. \quad (4.4)$$

In case the angle of the strand with respect to the z -axis is small, ($d\boldsymbol{\gamma}/dz \ll 1$) the denominator is approximately equal to unity and κ can be approximated by

$$\kappa \approx \frac{d^2\boldsymbol{\gamma}}{dz^2}. \quad (4.5)$$

Note that the second derivative is a measure of the position variation of seeds around a straight line. The total curvature (K) of a strand (with N seeds) in the discrete situation (with $\mathbf{y}_p = (x_p, y_p, z_p)$) is:

$$K = \sum_{p=2}^{N-1} \kappa_p,$$

where

$$\kappa_p = \frac{\sqrt{|x_{p+1} - 2x_p + x_{p-1}|^2 + |y_{p+1} - 2y_p + y_{p-1}|^2}}{\Delta z_p^2}, \quad (4.6)$$

$$\Delta z_p = \max(10, |z_{p+1} - z_{p-1}|).$$

Only strands with ≥ 3 seeds could be taken into account, as the discrete second derivative can only be computed if $N \geq 3$. Seeds close together in the z -direction can increase the curvature excessively. Therefore, a lower limit of 10 mm was applied for Δz . This limit equals the minimum physical distance between the upper and lower neighbours of a seed in a strand.

II.a If the curvature of a strand in Y exceeded a curvature threshold (see § [Parameters](#)), the link that accounted for most curvature was removed from the links of that strand.

After removal of a link, the remaining links of the strand were re-evaluated using [equations \(4.1\) and \(4.2\)](#) and solving this system with the Hungarian algorithm, for the involved \mathbf{x}_i and \mathbf{y}_j ([figure 4.3](#)).

II.b A line was fitted through all \mathbf{y}_j of a strand by least square regression, using singular value decomposition. The linefit (lf) is visualized in [figure 4.1](#). The linefit extended 10 mm beyond the first and last seed in the strand.

II.c Also shown in [figure 4.1](#) is the distance of a seed in Y to the linefit (dlf , for calculation see [appendix A](#)). Furthermore the link-length (ll) was calculated ([figure 4.1](#)). All links with ll and dlf exceeding the maximum distance threshold (see § [Parameters](#)) were excluded from the strand.

Next, all loose seeds were unlinked. Consequently, at the end of Step II less links between X and Y were present than at the end of Step I.

Step III Seeds that were unlinked in step II were, if possible, linked anew, taking into account the restrictions of the thresholds. First, a cost matrix ([equation \(4.1\)](#)) was generated with dlf^2 of non linked seeds to strands missing a link. Seeds without dlf 's within the distance threshold were discarded. The Hungarian Algorithm was used to solve the cost matrix. If the curvature as well as ll or dlf were within the curvature and distance thresholds, \mathbf{y}_j was linked to the corresponding \mathbf{x}_i . Finally, free \mathbf{y}_j closest to loose \mathbf{x}_i were linked based on proximity if ll was within the distance threshold. At the end of Step III, only a small fraction of seeds was not linked.

Step IV The linefits that originated from step II were taken as starting point again. The dlf 's of the remaining non-linked \mathbf{y}_j to linefits of incomplete strands were determined. Seeds of which the dlf was below the distance threshold were linked. There was no threshold for the curvature in this step.

After finishing the linking steps, Y was transformed with an affine transformation. The transformation was determined using a linear least squares regression of $\sum l_{ij}^2$ with singular value decomposition. The transformed compared distribution (Y_{k+1}) forms the starting point for the next iteration. The transformation took place in the following order:

$$\begin{aligned} Y_{k+1} &= T_k Y_k \\ T &= T_{\text{scale}} T_{\text{shear}} T_{\text{rotate}} T_{\text{translate}}, \end{aligned} \quad (4.7)$$

of which more details are shown in [appendix B](#).

From the second iteration on, the links were compared to the preceding iteration. If no differences were observed in the links the linking procedure was ended. A maximum of 6 iterations was allowed.

Parameters

In the linking procedure two parameters had considerable effect on the resulting links. First of all, the distance threshold for the dlf and ll determined if links were allowed. Secondly the curvature threshold strongly affected the outcome. Increasing the thresholds led to more links but also allowed more mismatches.

Initial parameters were set by visual inspection of all 699 linked distributions. Inspection was performed using a rotatable 3D graph similar to the graphs displayed in [figure 4.4](#). Cases in which a mismatch was present were identified. A subset of 24 cases with mismatches was created. The parameters were adjusted to minimize the number of mismatches in the subset. Subsequently the new settings were validated on the remaining cases by visual assessment. This process was repeated until the results were not further improved. The tuning of the parameters lead to values of 8 mm for the distance threshold and 0.0125 mm^{-1} for the curvature threshold. The visual inspection was performed in approximately 10 s per implant.

Analysis

The results of the linking procedure were compared to that of the initial linking only (iteration 1, step I).

All implants were visually inspected by one observer (HW). If the observer could improve the automatically generated links, the match was classified as *mismatch*; if the observer considered the result as possible mismatch, but he could not improve it, the match was classified as *uncertain*. For each implant, the mismatched and uncertain links, and involved strands were registered.

Computation

The linking procedure was implemented in Python code.¹⁵ All DICOM RT Plan objects were parsed to a SQLite database. Most scientific calculations were carried out with Numpy and Scipy.¹⁶ For specific parts of the code, computation speed was greatly improved by using Numba¹⁷, a just-in-time compiler. Visualizations were realized with the Matplotlib plotting library.¹⁸ Analysis was performed using IPython¹⁹ and the Pandas framework.²⁰ Code was run on a 3.0 GHz AMD Phenom™ II X4 945 CPU (2009).

¹⁵ Rossum *et al.*, 1989.

¹⁶ Oliphant, 2007.

¹⁷ Continuum Analytics, Austin, TX, USA

¹⁸ Hunter, 2007.

¹⁹ Perez *et al.*, 2007.

²⁰ McKinney, 2010.

Results

An example of the linking procedure is depicted in figure 4.4. Step I shows the initial linking of seeds, resulting in multiple mismatches in this case. In Step II, strand constraints are introduced and links causing curvature or distance thresholds violations are excluded. The next step, III, shows the relinking of seeds that were unlinked in Step II, restricted by curvature and distance thresholds. In Step IV, seeds close to linefits are linked, regardless of the curvature of the resulting strand. Then, the ll of all seeds was minimized by transforming Y with an affine transformation: $[T_1]$. Next the linking procedure (Step I – IV) was restarted on the transformed distribution. Notice that the transformation improved the initial results of Step I. In this example Step IV of Iteration 2 shows that one seed was not linked: the distance (d_{lf}), between the residual seed and the strand missing a seed, exceeded the distance threshold.

Comparing the final result of the linking procedure with the results after the initial linking in Step I, iteration 1, 233 out of 699 (33.3%) cases showed differences. This illustrates the added value of introducing the

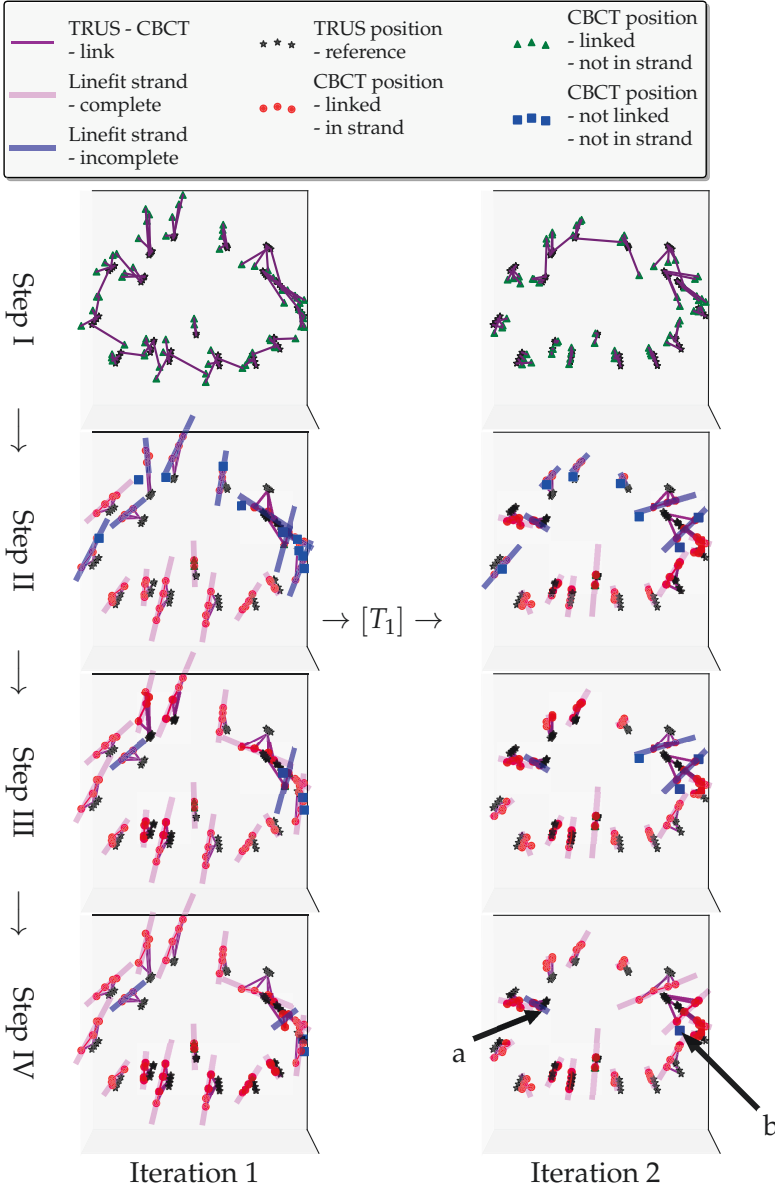
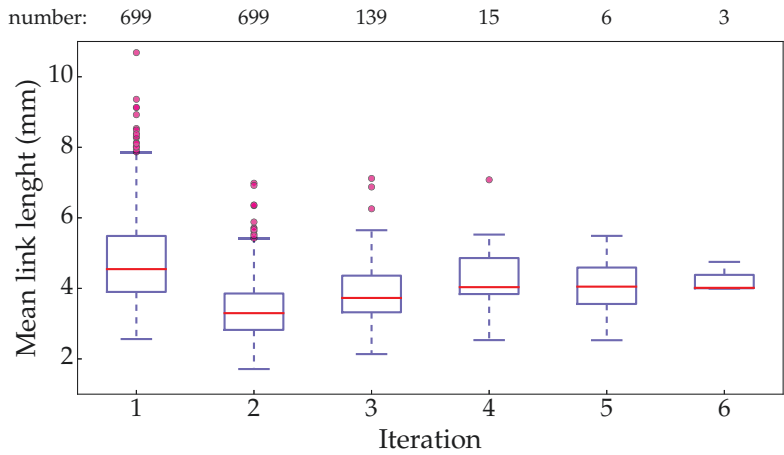


Figure 4.4: The steps of the linking procedure (figure 4.3) in an example. After Step IV in iteration 1, the compared distribution is transformed with $[T_1]$. The final result in Step IV, Iteration 2 does not link the incomplete strand (a) with the seed available (b), d_{lf} exceeds distance threshold.

Figure 4.5: Mean (per implant) link-length (ll) at the end of each iteration. On top the number of implants.



strand properties. The number of links after Step I is by definition equal to the maximum number possible (100%). In Step II the linked percentage decreases ($\sim 97\%$), whereas in Step III ($\sim 99\%$) and IV ($>99.8\%$) most seeds are linked again leaving a small fraction of links not feasible due to the thresholds.

Of all implants the observer classified 11 (1.6%) to contain a mismatch, 12 (1.7%) as uncertain. On the strand level 13 of 12860 (0.10%) strands were mismatched, 25 (0.19%) uncertain. Of 49897 seeds 17 (0.026%) were mismatched and 28 (0.050%) had an uncertain link. The results of the linking procedure, subdivided according to their final iteration, are shown in [table 4.1](#). In this table the number of implants (second column) that reached their final linking are shown per iteration (row). The last three columns show the percentage of linked seeds, the mean ll and the mean dlf of the registered implants, respectively. The mean ll after finishing the linking procedure was 3.4 ± 0.8 mm (1 SD). The average dlf equalled 1.6 ± 0.7 mm (1 SD). Of all seeds more than 99.8% was linked after the final iteration.

In [figure 4.5](#) the mean link-length per implant is visualized after each iteration. In iterations 1 and 2 all implants were incorporated, this number was much smaller in the last four iterations, shown in the top of [figure 4.5](#). Notice, the reduction in mean link-length values from iteration 1 to 2, resulting from the transformation ([equation \(4.7\)](#)). On average, the linking procedure was performed in 42 ms per case.

Iteration	Number ending in iteration ^a			Mismatch ^b	% Linked ^c mean \pm SD	<i>ll</i> (mm) mean \pm SD	<i>dlf</i> (mm) mean \pm SD
	Implants	Strands	Seeds				
2	560	10259	39866	4	99.94 \pm 0.37	3.3 \pm 0.7	1.6 \pm 0.7
3	124	2310	8899	4	99.74 \pm 0.64	3.8 \pm 0.8	1.8 \pm 0.7
4	9	177	678	1	99.38 \pm 0.75	4.6 \pm 1.1	2.0 \pm 0.9
5	3	55	229	1	98.69 \pm 1.35	3.8 \pm 1.5	2.1 \pm 1.5
6	3	59	225	1	98.56 \pm 1.47	4.3 \pm 0.4	1.6 \pm 0.4

ll: link-length, *dlf*: distance to linefit.

^a Number of implants that ended linking procedure in that iteration.

^b Number of implants with a mismatch.

^c Percentage of all possible links that is realized.

Table 4.1: Characteristics of results of linking procedure subdivided by implants ending in iteration. In total 699 implants, 12860 strands and 49897 seeds were analyzed.

Discussion

We present an automated method that allows tracking of seeds between intraoperatively acquired TRUS and CBCT. Our linking procedure improved in 33% of the cases the initial linking (Iteration 1, Step I) that is based on minimization of the cost matrix using the Hungarian Algorithm. Figure 4.4 exemplifies that the linking procedure made changes to the initial linking of Step I. Especially the transformation applied after the first iteration improved the results as illustrated in figure 4.5. The linking procedure ended after the second (560 cases, 80%) or third iteration (124 cases, 18%) for most implants (table 4.1), which shows that the linking procedure was rapidly converging.

One observer visually inspected all results. Currently a metric that takes into account all considerations of a human observer, for example the classification of links as *uncertain* or *mismatch*, is not available. The linking procedure could be extended with a method that only presents cases with a risk of mismatches. Note that it is impossible to link seeds manually if only seed coordinates are presented. The visual inspection revealed only a small percentage of implants with uncertainties (1.7%) or mismatches (1.6%).

The linking method we present partly resembles work of Chng *et al.* (2011). Both methods use the properties of strands and make use of the Hungarian Algorithm to make an initial estimate of the links. There are however important differences between both methods. The work of Chng *et al.* (2011), *S*-reconstruction, was developed to compare seed positions of pretreatment plans to realized seed positions, localized on Day 0 CT. We primarily developed the linking procedure to compare

intraoperatively acquired TRUS and CBCT based seed positions. The number of parameters that needs to be set was two in the current study instead of 12 in case of the *S*-reconstruction. Contrary to our method *S*-reconstruction relies on a fixed interseed distance. Our study showed 1.6% mismatches and 1.7% uncertainty while *S*-reconstruction showed mismatches in 26% of the cases. This might be caused by the fact that other types of data were analysed. Finally, the linking procedure was performed in 42 ms per case, whereas the *S*-reconstruction took 5 – 10 s to complete. The number of implants (699) used to design and validate the procedure in the present work is approximately ten times larger than that for the design of *S*-reconstruction.

In future work we will use the linking procedure to analyse differences between intraoperatively obtained TRUS and CBCT seed positions. In that work we will be able to quantify the early migration of seeds based on two intraoperatively acquired image datasets. Currently the cause of migration is explained in several ways. McLaughlin *et al.* (2006) suggested that anchoring of strands in the levator ani may explain migration. Steggerda *et al.* (2015) hypothesized that strands are pushed out during voiding. The currently presented linking procedure may help to characterize the migration patterns and corresponding time trends and provide a better understanding.

Potentially, the linking procedure can be extended to allow for incorporation in an intraoperative dynamic procedure²¹ allowing high accuracy registration and dosimetry prediction. As the presented procedure does not restrict seed spacing, the concept of strands might be extended to implantation channels, making it possible to study migration of loose seeds as well. Seed positions extracted from other data than TRUS or (CB)CT, like MRI, can be processed with the presented linking procedure. Other time spans could possibly be studied with adjustments of the threshold parameters. For example migration from Day 0 to Day 30 could be investigated using the presented linking procedure.

²¹ Polo *et al.*, 2010.

Conclusion

A high accuracy, high speed seed linking procedure for intraoperatively acquired TRUS and CBCT datasets is presented and validated. This method has the potential to be generalized to other time spans and imaging modalities.

Appendix A: Distance to linefit

dlf , the distance of the seeds \mathbf{y}_j to the linefits lf 's was calculated as follows:

$$\begin{aligned}
 \mathbf{y}_j &= \begin{bmatrix} x_j \\ y_j \\ z_j \end{bmatrix}, \\
 lf &= [lf_1, lf_2], \\
 P &= \mathbf{y}_j - lf_2, \\
 V &= lf - lf_2, \\
 w &= (V^T V)^{-1} V^T P, \\
 dlf &= \begin{cases} |wV - P| & \text{if } w \in [0, 1] \\ \min(|P - V|, |P|) & \text{if } w \notin [0, 1] \end{cases}.
 \end{aligned} \tag{4.8}$$

Appendix B: Transformations

The transformation matrices²² for the affine transformation are defined as:

²² Farin *et al.*, 2013, p. 199–234.

$$\begin{aligned}
 T_{\text{translate}} &= \begin{bmatrix} 1 & 0 & 0 & \Delta x \\ 0 & 1 & 0 & \Delta y \\ 0 & 0 & 1 & \Delta z \\ 0 & 0 & 0 & 1 \end{bmatrix}, & T_{\text{rotx}} &= \begin{bmatrix} 1 & 0 & 0 & 0 \\ 0 & \cos \vartheta & -\sin \vartheta & 0 \\ 0 & \sin \vartheta & \cos \vartheta & 0 \\ 0 & 0 & 0 & 1 \end{bmatrix}, \\
 T_{\text{scale}} &= \begin{bmatrix} s_x & 0 & 0 & 0 \\ 0 & s_y & 0 & 0 \\ 0 & 0 & s_z & 0 \\ 0 & 0 & 0 & 1 \end{bmatrix}, & T_{\text{roty}} &= \begin{bmatrix} \cos \varphi & 0 & \sin \varphi & 0 \\ 0 & 1 & 0 & 0 \\ -\sin \varphi & 0 & \cos \varphi & 0 \\ 0 & 0 & 0 & 1 \end{bmatrix}, \\
 T_{\text{shear}} &= \begin{bmatrix} 1 & h_{xy} & h_{xz} & 0 \\ h_{yx} & 1 & h_{yz} & 0 \\ h_{zx} & h_{zy} & 1 & 0 \\ 0 & 0 & 0 & 1 \end{bmatrix}, & T_{\text{rotz}} &= \begin{bmatrix} \cos \psi & -\sin \psi & 0 & 0 \\ \sin \psi & \cos \psi & 0 & 0 \\ 0 & 0 & 1 & 0 \\ 0 & 0 & 0 & 1 \end{bmatrix}.
 \end{aligned} \tag{4.9}$$

The rotation matrices were multiplied in the following order:

$$T_{\text{rotate}} = T_{\text{rotz}} T_{\text{roty}} T_{\text{rotx}}. \tag{4.10}$$

Chapter 5

Edema and seed displacements affect intraoperative permanent prostate brachytherapy dosimetry

Adapted from: H Westendorp, TT Nuver, CJ Hoekstra, MA Moerland and AW Minken (2016). 'Edema and Seed Displacements Affect Intraoperative Permanent Prostate Brachytherapy Dosimetry'. *Int J Radiat Oncol Biol Phys*, 96(1):197–205

Abstract

Purpose: We sought to identify the intraoperative displacement patterns of seeds and to evaluate the correlation of intraoperative dosimetry with Day 30 for permanent prostate brachytherapy.

Materials and methods: We analyzed the data from 699 patients. Intraoperative dosimetry was acquired with transrectal ultrasonography (TRUS) and C-arm cone-beam computed tomography (CBCT). Intraoperative dosimetry ($D_{40} - D_{95}$) was compared with Day 30 for both modalities. An additional edema-compensating comparison was performed for D_{90} . Stranded seeds were linked between TRUS and CBCT using an automatic and fast linking procedure. Displacement patterns were analysed for each seed implantation location.

Results: On average an intraoperative (TRUS to CBCT) D_{90} decline of $10.6 \pm 7.4\%$ was observed. Intraoperative CBCT D_{90} showed a greater correlation ($R^2=0.33$) with respect to Day 30 than did TRUS ($R^2=0.17$). Compensating for edema the correlation increased to 0.41 for CBCT and 0.38 for TRUS. The mean absolute intraoperative seed displacement was 3.9 ± 2.0 mm. The largest seed displacements were observed near the rectal wall. The central and posterior seeds showed less caudal displacement than lateral and anterior seeds. Seeds that were implanted close to the base showed more divergence than seeds close to the apex.

Conclusion: Intraoperative CBCT D_{90} showed a greater correlation with Day 30 dosimetry than intraoperative TRUS. Edema seems to cause most of the systematic difference between intraoperative and Day 30 dosimetry. Seeds near the rectal wall showed most displacement, comparing TRUS and CBCT, probably because of TRUS probe-induced prostate deformation.

Introduction

International guidelines recommended dosimetry for permanent ^{125}I prostate implants a month after the implantation procedure, when prostate swelling from edema has resolved.¹ The dosimetry at Day 30 correlates with the clinical treatment outcome.² However, it is difficult to predict Day 30 dosimetry during the implantation procedure.³ Factors like contouring and registration inaccuracy,⁴ edema,⁵ transrectal ultrasound (TRUS) probe-induced deformation⁶ and difficult localization of implanted seeds on TRUS⁷ can lead to a hampered estimate of the delivered dose to the prostate and organs at risk (OAR).⁸ Edema affects dosimetry already during the implantation procedure.⁹

Furthermore, during implantation seeds can move, which cannot be accurately visualized using TRUS.¹⁰ Therefore TRUS-based live procedures have limited capability of capturing the final positions of the seeds. An accurate intraoperative identification of all final seed positions will potentially lead to a better prediction of the Day 30 dosimetry.

In the present study we analysed systematic patterns of edema and seed displacements. This is only feasible if the data processing is fully automated. Therefore, we developed an automated registration method that links stranded seeds between the different image sets of the permanent prostate implants.¹¹

The purpose of the present study was to assess intraoperative edema, quantify seed displacements, and evaluate corresponding effects on dosimetry. We compared intraoperative C-arm Cone Beam Computed Tomography (CBCT)-based seed localization and dosimetry with standard TRUS-based observations, using our automated procedure. We quantified the geometric and dosimetric consequences of intraoperative edema and differences in seed localization between TRUS and CBCT for 699 patients and related these findings to Day 30 dosimetry.

¹ Ash *et al.*, 2000; Davis *et al.*, 2012; Nath *et al.*, 2009; Salembier *et al.*, 2007.

² Davis *et al.*, 2012; Henry *et al.*, 2015; Potters *et al.*, 2001; Stock *et al.*, 1998.

³ Acher *et al.*, 2010; Han *et al.*, 2003b; Igidbashian *et al.*, 2008; Moerland *et al.*, 2009; Nag *et al.*, 2008; Nath *et al.*, 2009; Polo *et al.*, 2010.

⁴ Brabandere *et al.*, 2012.

⁵ Shaikh *et al.*, 2015.

⁶ D Liu *et al.*, 2015.

⁷ Polo *et al.*, 2010.

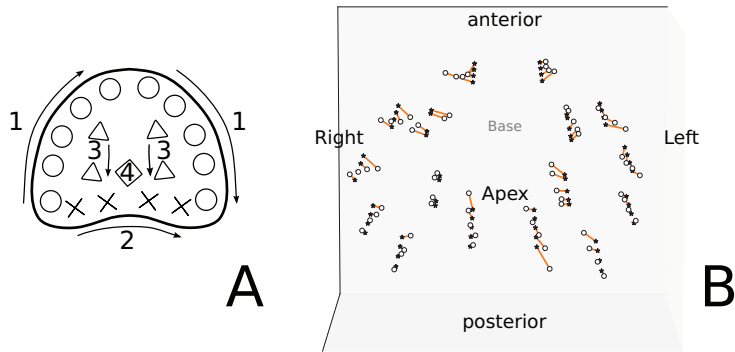
⁸ Kirisits *et al.*, 2014.

⁹ Yamada *et al.*, 2003.

¹⁰ Nag *et al.*, 2008; Polo *et al.*, 2010; Stone *et al.*, 2003.

¹¹ Westendorp *et al.*, 2015.

Figure 5.1: (A). Implantation order: 1. Periphery (○), 2. Posterior (×), 3. Central right and left (△), 4. Central posterior (◇). (B) Linking of seeds from cone-beam CT (○) to TRUS (★), viewed caudally. The corresponding seeds in both distributions are linked by orange lines.



Methods and Materials

Patients

From October 2007 to June 2012, 740 patients with prostate cancer who had undergone ¹²⁵I seed implantation, were eligible for the present study. The prescribed dose was 145 Gy for patients receiving monotherapy (81%). Patients receiving a boost after external beam radiotherapy (19%) were prescribed 110 Gy. Excluded were those patients who had not received a standard treatment or who had undergone trans urethral resection of the prostate before implantation. Of the 740 patients, 41 had an incomplete image data set, leaving 699 cases available for analysis.

Implantation procedure

A preplan was made using a treatment planning system (TPS)¹², approximately 2 weeks before the implantation procedure, to determine the appropriate source strength and number of seeds to be ordered.

In the operating theater, 4 fiducial gold markers, $\varnothing 1.0 \times 5.0$ mm¹³ were placed using 2 needles. Using the left needle, markers were placed near the base and apex, and using the right needle markers were placed near the midplane and base of the prostate. The fiducial markers show improved visibility compared with the seeds, facilitating (rigid) image registration.

¹² Variseed 7.1 – 8.0.2; Varian Medical Systems, Inc., Palo Alto, CA, USA

¹³ Heraeus GmbH, Hanau, Germany

Item	Input			Analyses
	Contours	Seed positions	Registration	
Intraoperative TRUS	TRUS pre implant ^a	TRUS intra operative	N/A	Edema, dosimetry and displacements
Intraoperative CBCT	TRUS post implant ^b	CBCT post implant ^c	Least squares minimization ^d	Edema, dosimetry and displacements
Day 30	TRUS pre implant	CT Day 30	Least squares minimization	Edema, dosimetry

Abbreviations: CBCT = cone-beam CT; CT = computed tomography; NA = not applicable; TRUS = transrectal ultrasonography.

^a Intraoperatively acquired before implantation.

^b Intraoperatively acquired immediately after implantation.

^c Intraoperatively acquired after post implant TRUS.

^d Rigid registration on fiducial gold markers.

Table 5.1: Overview of analyses and data sources.

Subsequently, the preplan was adjusted to the actual prostate size and shape at the moment of implantation using a TRUS scan¹⁴ with 5 mm spaced slices.

The periphery of the prostate was implanted with stranded seeds clockwise, viewed from the observer, as shown in [figure 5.1-A](#). After placing all peripheral needles, the seeds were deposited. The position of the deposited strands was manually determined using transversal and sagittal TRUS imaging, seeds were individually digitized. The dose distribution was updated and the number and location of seeds to be placed posteriorly was planned, placed and recorded. The planning was repeated for the central positions, and the implant was finished.

A final dose distribution was calculated using the preimplant TRUS contours ([table 5.1](#)). On average 72 ± 8 seeds were implanted. Stranded seeds with a strength of 0.419 to 0.876 U and dimensions of $\varnothing 0.8 \times 4.6$ mm were used¹⁵. Spacing between seeds was equidistant (10 mm center to center) in most strands. Strands with varying spacing were applied mainly for the central locations (3 and 4 in [figure 5.1-A](#)).

Next, a new TRUS scan was made with 2.5 mm spaced slices and minimal pressure to the rectal wall to limit deformation of the prostate. The prostate was contoured on this TRUS dataset anew. The TRUS probe was removed, the legs of the patient were lowered, and a CBCT with 2.5 mm spaced slices was acquired¹⁶. The CBCT was acquired approximately 5 minutes after the postimplant TRUS acquisition and <10 minutes after finishing the implant. The CBCT and TRUS datasets were registered using the fiducial gold markers and dosimetry was evaluated.

¹⁴ Falcon 2101 EX and Flex Focus 400, BK Medical; Herlev, Denmark

¹⁵ IBt 1251L; Seneffe, Belgium, IBt-Bebig I25.S06; Berlin, Germany, Bard STM1251; Murray Hill, NJ, USA

¹⁶ Siemens Arcadis Orbic 3D; Siemens Medical Systems, Erlangen, Germany

¹⁷ Westendorp *et al.*, 2007.¹⁸ Brilliance CT Big Bore;
Philips Healthcare, Best, The
Netherlands¹⁹ Westendorp *et al.*, 2007.

If deemed necessary the implant was adapted by placing remedial seeds.¹⁷

Postimplant dosimetry was performed at Day 30 using CT¹⁸ to obtain the seed positions. For cases in which an implant had been adapted in the operating room, an additional postplan was created. In this postplan, the source strength of the remedial seeds was set to 0, omitting the dose contribution of remedial seeds. The present study focused on intraoperative effects and how these translated to Day 30 dosimetry. Therefore, the contribution of remedial seeds was omitted in Day 30 dosimetry. Thus, the currently reported values of intraoperative CBCT-based dosimetry and dosimetry at Day 30 do not correspond to the actual values we achieved.

The dosimetry at Day 30 was based on the seed locations on the Day 30 CT and preimplant contours on the TRUS scan. Registration of both datasets was done by matching the fiducial gold markers using the least squares method of the TPS. If needed the registration was manually adjusted. This method closely resembles the method proposed by Bowes *et al.* (2013), with the major difference that we use fiducial gold markers for the registration instead of the urethra. A detailed description of our procedure has been previously published.¹⁹

Analysis

The intraoperative dosimetry was compared with the Day 30 dosimetry. In addition to a direct comparison, we determined the relationship between edema-compensated intraoperative and Day 30 dosimetry. The effect of edema on D₉₀ (Minimal dose to 90% of the volume) was compensated for the inverse square law $(r/r_{\text{ref}})^2$ and attenuation $(r/r_{\text{ref}})^{0.7}$ using an equation proposed by Moerland (1998).

$$D_{90 \text{ comp.}} = D_{90} \left(\frac{\bar{r}}{\bar{r}_{\text{ref}}} \right)^{(2.0+0.7)} \quad (5.1)$$

Where \bar{r} is the mean distance of all seeds to their center of mass (COM). The compensated D₉₀ (D_{90 comp.}) was plotted against the D₉₀ of Day 30 (reference, \bar{r}_{ref}). V_x (% of volume receiving minimal x% of the prescribed dose) does not scale with the radius. No compensation for V_x was determined.

The seed positions obtained by intraoperative TRUS were linked and registered to seed positions acquired by CBCT imaging using a strand-

based algorithm that has been described and evaluated in detail.²⁰ The registration of TRUS- and CBCT-based seeds allowed for translation and rotation. A typical result of the automated linking procedure is shown in [figure 5.1-B](#). All seeds in the CBCT distribution are linked to seeds in the TRUS distribution. The displacements are visualized.

²⁰ Westendorp *et al.*, 2015.

The differences in linked seed positions, (i.e. displacements) were analysed. The TRUS-based seed positions were taken as the reference to analyse seed displacements. In [figure 5.3](#), the reference seed positions of all implants, plotted together, cluster at specific locations. These locations resemble the coordinates of commonly used holes in the implantation template.

The *X* (left – right) and *Y* (anterior – posterior) coordinates of all seeds were plotted, and 19 clusters were identified. Seed positions were attributed to one of the clusters using K-Means clustering.²¹

²¹ Oliphant, 2007.

The prostate was subdivided in four transversal slices ([figure 5.3](#)). The slices coincided with the positions of seeds in strands containing 4 seeds, which were the most common. For each slice, the seeds were visualized by plotting all seed positions as dots, with colors showing displacements in craniocaudal direction. Per cluster, the mean resulting in-plane displacement, in that slice, was depicted as a vector.

Next, the individual clusters were displayed sagittally ([figure 5.4](#)). Each cluster was subdivided in the *Z* (cranial – caudal) direction in the number of seed positions in that cluster. The centers of the seed clusters were determined visually, and seeds were assigned to these seed clusters using K-means clustering. For each needle, all corresponding seed clusters were analysed. Each seed position was shown as a dot in the *Z*–*Y* plane with the color representing the length of the (3-dimensional) displacement. The mean *Z*–*Y* displacement of each seed cluster was visualized as a vector. The analyses and corresponding data sources are listed in [Table table 5.1](#).

Table 5.2: Dosimetry (mean ± SD) at Day 0 and Day 30.

	Intraoperative (Day 0)		Day 30
	TRUS	CBCT	CT
D ₄₀	154 ± 9	148 ± 10	164 ± 14
D ₆₀	139 ± 7	131 ± 9	144 ± 11
D ₈₀	125 ± 5	119 ± 8	127 ± 10
D ₉₀	118 ± 5	107 ± 8	116 ± 9
D _{90 comp.}	122 ± 13	119 ± 15	116 ± 9
D ₉₅	113 ± 5	101 ± 9	107 ± 9
V ₁₀₀	99.5 ± 1.1	94 ± 5	97 ± 3
V ₁₅₀	44 ± 10	37 ± 10	53 ± 12
UD ₃₀	119 ± 6	116 ± 10	137 ± 15
V _{Prostate} (cm ³)	39 ± 11	39 ± 11	38 ± 11

D_x: Minimal (% of prescribed) dose to x% of the prostate.

D_{90 comp.}: Minimal dose to 90% of the prostate, edema compensated by equation (5.1).

V_x: % of volume receiving minimal x% of prescribed dose.

UD₃₀: Minimal (% of prescribed) dose to 30% of the urethra.

Results

Dosimetry

Dosimetric data for 699 patients were obtained at Day 0 using TRUS and CBCT and at Day 30 using CT. The dosimetric results are summarized in table 5.2. On average a decline of 10.6 ± 7.4% (1 standard deviation, percentage of prescribed dose) for D₉₀ and 5.1 ± 5.2 % for V₁₀₀ was observed at the operating theatre comparing CBCT acquired dosimetry to that of TRUS. On Day 30 D₉₀ was 1.8 ± 8.5 % lower than intraoperatively based on TRUS and 8.7 ± 8.0% higher than using intraoperative CBCT. Day 30 dosimetry showed, on average, a 2.6 ± 3.1% lower V₁₀₀ compared to TRUS and a 2.4 ± 4.5% higher V₁₀₀ compared to CBCT.

Figure 5.2 shows the correlation of the intraoperative dosimetry with the Day 30 dosimetry. The intraoperative D₉₀ (based on TRUS and CBCT) was compared with Day 30 D₉₀. The correlation of D₉₀ TRUS dosimetry is represented by an R² of 0.17. The CBCT dosimetry correlation showed an R² of 0.33. In the lower row of subfigures, D₉₀ was compensated for edema and attenuation using equation (5.1). Compensating for edema by applying equation (5.1), the correlation (R²) increased to 0.38 and 0.41 for TRUS and CBCT based D₉₀ respectively. For all correlations

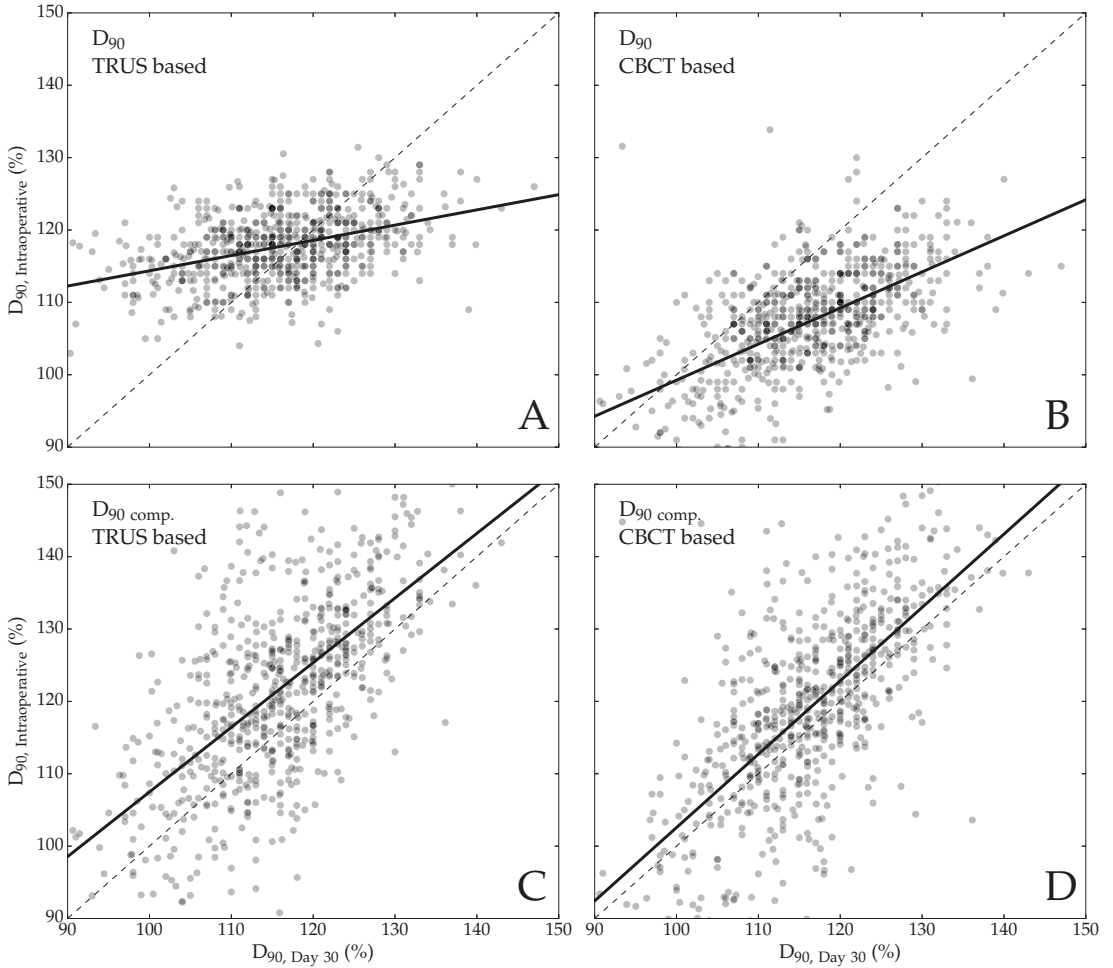


Figure 5.2: Correlation of intraoperative TRUS (A, C) and CBCT (B, D) D_{90} with Day 30 D_{90} . A ($R^2 = 0.17$) and B ($R^2 = 0.33$) represent raw data whereas C ($R^2 = 0.38$) and D ($R^2 = 0.41$) are compensated for edema effects by using equation (5.1). The linear regression for each situation is plotted as a solid black line. For comparison purposes a (dashed) unity line is shown.

a P -value $\ll 10^{-6}$ was found. For the compensated situation, the linear regression slope was 0.89 for TRUS-based and 1.01 for CBCT-based dosimetry compared with Day 30 values.

Displacement

In total 49 722 seeds were linked between TRUS (reference) and CBCT. An average displacement (vector length) of 3.9 ± 2.0 mm was observed. Relative to the COM, the standard deviation of the displacements was 1.8 mm in the left – right, 2.1 mm in the anteroposterior and 3.4 mm in the craniocaudal direction. The relative distance to the COM ($\bar{r}/\bar{r}_{\text{ref}}$) was 1.01 ± 0.04 for TRUS and 1.04 ± 0.04 for CBCT compared with Day 30. After scaling the distribution to account for edema, the mean displacement vector length reduced from 3.9 to 3.7 mm.

Figure 5.3 shows the displacements, between TRUS and CBCT, in 4 equidistant transverse slices. The seeds diverged more from the central axis when deposited more towards the base. Seeds in the base slice displaced caudally, on average 0.6 ± 3.2 mm. This was mainly caused by seeds in the anterior outer ring. Seeds in the apex showed a mean displacement of 0.8 ± 3.5 mm cranially, predominantly caused by the central and posterior seeds in the apex slice. The linking algorithm compensates for rotation²² resulting in a residual rotation of 0° .

²² Westendorp *et al.*, 2015.

The displacement is shown in figure 5.4 for each needle and corresponding seed cluster separately. The position of the left and right needles (symmetric) are depicted with the identification number of both needle positions in the central column. On the left and right side, the seeds assigned to the corresponding needles are displayed as dots. The color illustrates the total displacement of each seed. The vectors visualize the mean displacement of each cluster in the anteroposterior and craniocaudal directions. The corresponding length of each vector is presented as a number. Needles 1 to 11 and 14 were subdivided into 4 clusters; in needles 12 and 13, 5 clusters were identified; and in the central needles (15 – 19) 2 clusters were defined.

The least displacement was observed in the central seed clusters of needle 4 to 7, with a mean displacement of 3.1 ± 1.5 to 3.4 ± 2.0 mm. The most displacement was observed in needles 12, 13, and 19. The clusters in needle 19 presented with a mean displacement of 5.1 ± 3.0 mm, the basal cluster displacement equaled 4.5 mm. The outer clusters in needle 12 and 13 showed displacements of 4.6 ± 2.2 mm. Seeds displaced depending on their position. In the outer ring (needles 2 – 9) seeds displace predominantly caudally (figure 5.4).

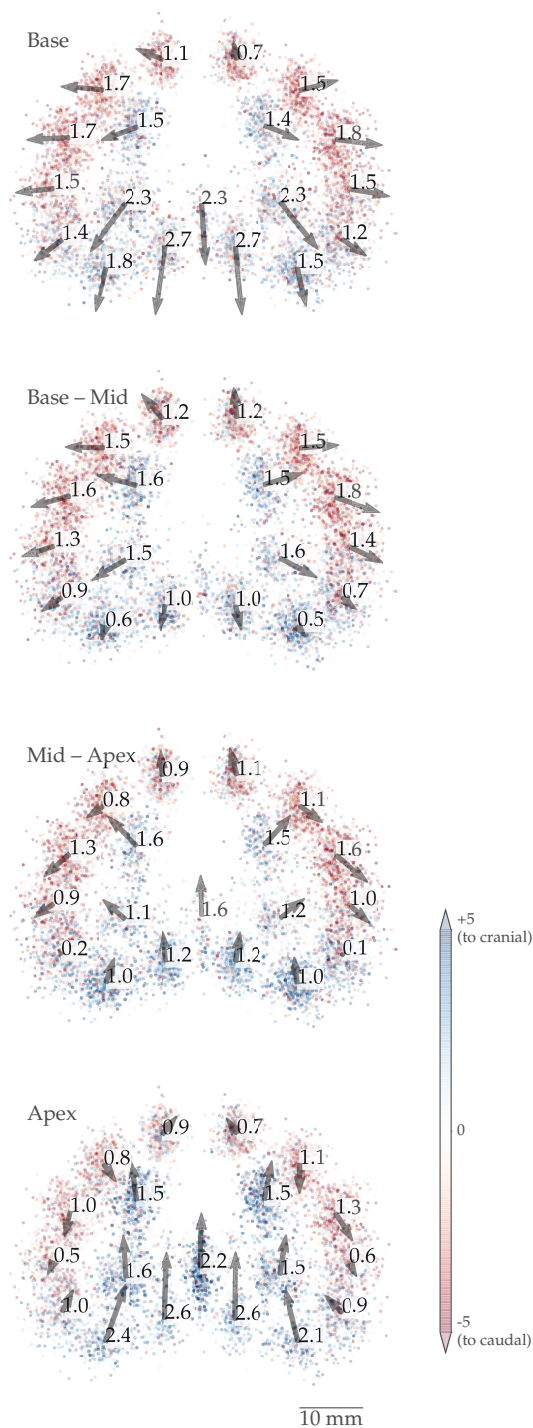


Figure 5.3: Displacement patterns differ considerably per slice and position. Reference positions of all 49722 seeds in transversal slices depicted as dots. The colors of the dots represent the displacement, from TRUS to CBCT, in cranio-caudal direction. For every needle in each slice the average inplane displacements are shown as vectors with the corresponding inplane length (mm) as a number.



Figure 5.4: Seed-(cluster) displacements of TRUS to CBCT. The location of the corresponding needles, as depicted in column A and C, is shown in column B. Each dot represents a seed, the color shows the corresponding (3D) length of the displacement. Vectors visualize the mean in plane movement of each cluster with the length in mm.

Discussion

The present study is the first to show the displacement of seeds and dosimetric consequences during the implantation procedure for a large group ($n=699$) of patients. The size of the group allowed the investigation of systematic displacement patterns of seeds.

Differences in dosimetry were observed for intraoperative acquisitions with TRUS and CBCT and the postoperative dosimetry at Day 30 (table 5.2). The systematic difference in D_{90} can be attributed to edema. A simple model compensating for the inverse square law and attenuation (equation (5.1)) seems to explain the systematic difference between Day 0 and Day 30 (5.2). Furthermore, after compensation for edema, CBCT based dosimetry shows a better correlation of D_{90} at Day 30 than did TRUS based dosimetry (figure 5.2). However, this improved correlation does not allow for individual, CBCT based dosimetry predictions for Day 30.

Random differences were not reduced after edema compensation. The simple spherical model cannot compensate for the nonuniform displacements present in figures 5.3 and 5.4 and decreased the mean displacement by only 0.2 mm. Also, stranded seeds might, because of strand rigidity, respond differently to prostatic edema in the craniocaudal than in lateral directions. We have previously shown that this effect is fairly limited.²³ However, loose seed implants could exhibit slightly different edema. Consequently, residual displacements would still affect dosimetry, just as would seed identification, contouring, registration uncertainties, and movement in the implantation channels.

Using the linking method,²⁴ we linked seed positions in the TRUS and CBCT datasets and quantified the corresponding displacements. A rigid registration between the TRUS and CBCT datasets minimized the distance between the seeds. The minimization of distance between seeds in both datasets could have resulted in an overcompensation of displacement patterns. For example, if all seeds would show a displacement in caudal direction, this would have been compensated by an equal translation. This was verified by comparing the seed positions with the prostate contours. The physician contoured the prostate before and after implantation. We evaluated whether the seeds were displaced between TRUS and CBCT by comparing the seed distribution and most basal contour. We did not find indications for systematic shifts.

²³ Westendorp *et al.*, 2012.

²⁴ Westendorp *et al.*, 2015.

Figures 5.3 and 5.4 show left – right symmetry of the displacement patterns. The pattern of displacements, as visualized by the vectors was continuous, with neighbouring clusters showing similar displacement.

Displacements originate from multiple underlying mechanisms. Among others, the following were found to play a role. The first factor was the pressure of the ultrasound probe to the prostate. This pressure was minimized, but does still deform the prostate, as shown previously by D Liu *et al.* (2015). Seeds near the rectum (probe) displace to posterior near prostate base and to anterior near the prostate apex. TRUS probe-induced prostate deformation affects the seeds' positions and the prostate shape. D Liu *et al.* (2015) reported that dosimetry changes due to TRUS probe removal mainly resulted in changes in seed positions and to a lesser extend to contour changes. The second factor was that the posterior needles, placed close to the rectum, were intentionally placed at an angle, using the beveled needle tip, to follow the prostate – rectum interface. The TPS did not allow angles for strands on the real-time TRUS images. For CT image data sets, angles were allowed. This amplifies the effect of the TRUS probe induced prostate deformation. Finally, the presence of edema will move seeds away from the COM.

Edema is difficult to predict but it results in considerable consequences on the dosimetry during the implantation procedure. This effect has also been observed by other groups that compare dosimetry shortly after implantation with Day 30 dosimetry.²⁵ The amount of edema observed in this study agrees well with results from an earlier study in which we reported a spherical volume change of 12%, corresponding to (\bar{r}/\bar{r}_{ref}) of 1.04.²⁶ The contoured prostate volumes (table 5.2) did not show this amount of edema. This could have been caused by the different slice spacing of the data sets and the tendency to contour an additional slice to ensure full target coverage. The wider slice spacing (5 vs. 2.5 mm) of the preimplant TRUS scan could have led to an overestimation of the volume increase due to the presence of edema.

The use of stranded seeds might lead to an underestimation of edema in craniocaudal direction. Loose seeds might show more edema but this would not challenge the qualitative observations.

The anterior–lateral outer ring of seeds displaced caudally. In contrast, the central and outer posterior seeds displaced cranially. This could be an indication that the implantation order affects the displacements (figure 5.1-A). However, comparing left and right needle positions (fig-

²⁵ Ishiyama *et al.*, 2010; Ohashi *et al.*, 2007.

²⁶ Westendorp *et al.*, 2012.

ure 5.4) we did not observe differences between earlier and later placed seeds. Therefore, we do not believe that the displacement of seeds is directly related to the order of implantation.

Published data have indicated that underdosage occurs predominantly at the base of the prostate.²⁷ Edema, needle divergence, and the caudal displacement of the (outer) seeds may could result in underdosage in that region. If seeds have been not accurately identified during the implantation procedure, the underdosage will remain unnoticed. This could result in underdosage at Day 30. An adaptive brachytherapy procedure that includes CBCT may thus help to improve dosimetry. Further investigation of the consequences of adaptive brachytherapy is needed for verification.

The implantation technique could be slightly modified to anticipate the intraoperative displacement patterns. The observed divergence of needles could possibly be lowered by implanting needles in a slightly convergent geometry. The displacements caused by TRUS probe removal could be anticipated by placing seeds near the prostate base slightly more anterior than planned. The seeds in the outer anterior ring could be implanted slightly deeper. However, these suggestions depend on the implantation technique, model of seeds and strands, and the use of loose or stranded seeds.

Currently interest in focal treatments is increasing. Particularly for small lesions, accurate seed placement is important;²⁸ thus, knowing the displacement properties could help in such procedures. In addition to implantation technique enhancements, the TPS should allow for the registration of nonparallel needles during the implantation procedure.

²⁷ Merrick *et al.*, 2014; Moerland *et al.*, 2009; Nasser *et al.*, 2014.

²⁸ Al-Qaisieh *et al.*, 2015.

Conclusion

We visualized the intraoperative systematic displacements for a large group of implants (n=699) based on automated analysis of 49 722 seeds on TRUS and CBCT. The magnitude and orientation of displacements of seeds differ considerably for various positions in the prostate. Seeds close to the rectal wall show most displacement, probably resulting from TRUS probe-induced prostate deformation. Seeds close to the base show more divergent displacements than seeds close to the apex. The corresponding dosimetry was assessed. The intraoperative systematic

difference in D_{90} seems predominantly caused by edema. Compared to TRUS, the intraoperative CBCT-based D_{90} shows a higher correlation with Day 30. Automated analysis is a prerequisite for the results we obtained for this large group.

Chapter 6

Conebeam CT-based adaptive planning improves permanent prostate brachytherapy dosimetry: An analysis of 1266 patients

Adapted from: H Westendorp, CJ Hoekstra, JJ Immerzeel, SM van de Pol, CG Niël, RA Kattenvilder, TT Nuver, MA Moerland and AW Minken (2017a). 'Conebeam CT-based dynamic planning improves permanent prostate brachytherapy dosimetry: An analysis of 1266 patients'. Med Phys

Abstract

Purpose To evaluate adaptive planning for permanent prostate brachytherapy and to identify the prostate regions that needed adaptation.

Methods and materials After the implantation of stranded seeds, using real-time intraoperative planning, a transrectal ultrasound (TRUS)-scan was obtained and contoured. The positions of seeds were determined on a C-arm conebeam computed tomography (CBCT)-scan. The CBCT-scan was registered to the TRUS-scan using fiducial gold markers. If dose coverage on the combined image-dataset was inadequate, an intraoperative adaptation was performed by placing remedial seeds. CBCT based intraoperative dosimetry was analyzed for the prostate (D_{90} , V_{100} and V_{150}) and the urethra (D_{30}). The effects of the adaptive dosimetry procedure for Day 30 were separately assessed.

Results We analyzed 1266 patients. In 17.4% of the procedures an adaptation was performed. Without the dose contribution of the adaptation Day 30 V_{100} would be <95% for half of this group. On Day 0 the increase because of the adaptation was $11.8 \pm 7.2\%$ (1SD) for D_{90} and $9.0 \pm 6.4\%$ for V_{100} . On Day 30 we observed an increase in D_{90} of $12.3 \pm 6.0\%$ and in V_{100} of $4.2 \pm 4.3\%$. For the total group, a D_{90} of $119.6 \pm 9.1\%$ and V_{100} of $97.7 \pm 2.5\%$ was achieved. Most remedial seeds were placed anteriorly near the base of the prostate.

Conclusion CBCT based adaptive planning enables identification of implants needing adaptation and improves prostate dose coverage. Adaptations were predominantly performed near the anterior base of the prostate.

Introduction

Postimplant dosimetry forms an essential feature of permanent prostate brachytherapy, as the results of postimplant dosimetry correlate with clinical outcome.¹ For ¹²⁵I-implants GEC/ESTRO, ABS and AAPM recommend to perform this postimplant dosimetry approximately 30 days after the implantation procedure.² However, at Day 30, dose coverage of the prostate may be lower than intended during the implantation procedure.

A lower D_{90} ^{3,4} and V_{100} ^{5,6} at Day 30 correlate with poorer treatment outcome. Insufficient target coverage cannot be overcome by increasing the overall dose; an excessive dose might harm the organs at risk. A high V_{150} is correlated with urethral,⁷ bowel⁸ and erectile⁹ toxicity. Therefore, during implantation a balance needs to be found between a high V_{100} and a low V_{150} . Dose to urethra, bladder and rectum should be kept below critical levels.

Intraoperative dosimetry procedures have been developed to generate high quality implants. Intraoperative planning takes the actual size and shape at the day of implantation into account. With interactive planning, the treatment is adapted according to the needle tracks, mostly determined using transrectal ultrasound (TRUS), resulting in improved dosimetry¹⁰ and clinical outcome.¹¹ Dynamic planning introduces an interactive procedure in which the actual shape of the prostate and positions of the deposited seeds are dynamically updated, allowing a higher overall accuracy.¹²

Since 2007 we routinely apply an intraoperative C-arm conebeam CT (CBCT) based adaptive dosimetry technique.¹³ With the patient still anesthetized, source positions identified with CBCT are registered to a TRUS scan, resulting in accurate dosimetry. This enables immediate, fast adaptation of the implant. We report the dosimetric results of this procedure for 1266 patients. We identified the regions of the prostate where remedial seeds were placed and show resulting effects on dosimetry. To our best knowledge, this is the first study to present large scale intraoperative dosimetry results for an adaptive planning procedure and the dosimetrical consequences at Day 30.

¹ Henry *et al.*, 2010; Stone *et al.*, 2007; Wallner *et al.*, 2003; Zelefsky *et al.*, 2007a.

² Ash *et al.*, 2000; Davis *et al.*, 2012; Nath *et al.*, 2009; Salembier *et al.*, 2007.

³ dose that covers 90% of the prostate

⁴ Davis *et al.*, 2012; Henry *et al.*, 2015; Potters *et al.*, 2010.

⁵ % of the prostate that receives at least 100% of the prescription dose

⁶ Davis *et al.*, 2012; Orio *et al.*, 2007.

⁷ Keyes *et al.*, 2009; Merrick *et al.*, 2003; Vordermark *et al.*, 2009.

⁸ Pinkawa *et al.*, 2006; Vordermark *et al.*, 2009.

⁹ Kollmeier *et al.*, 2012.

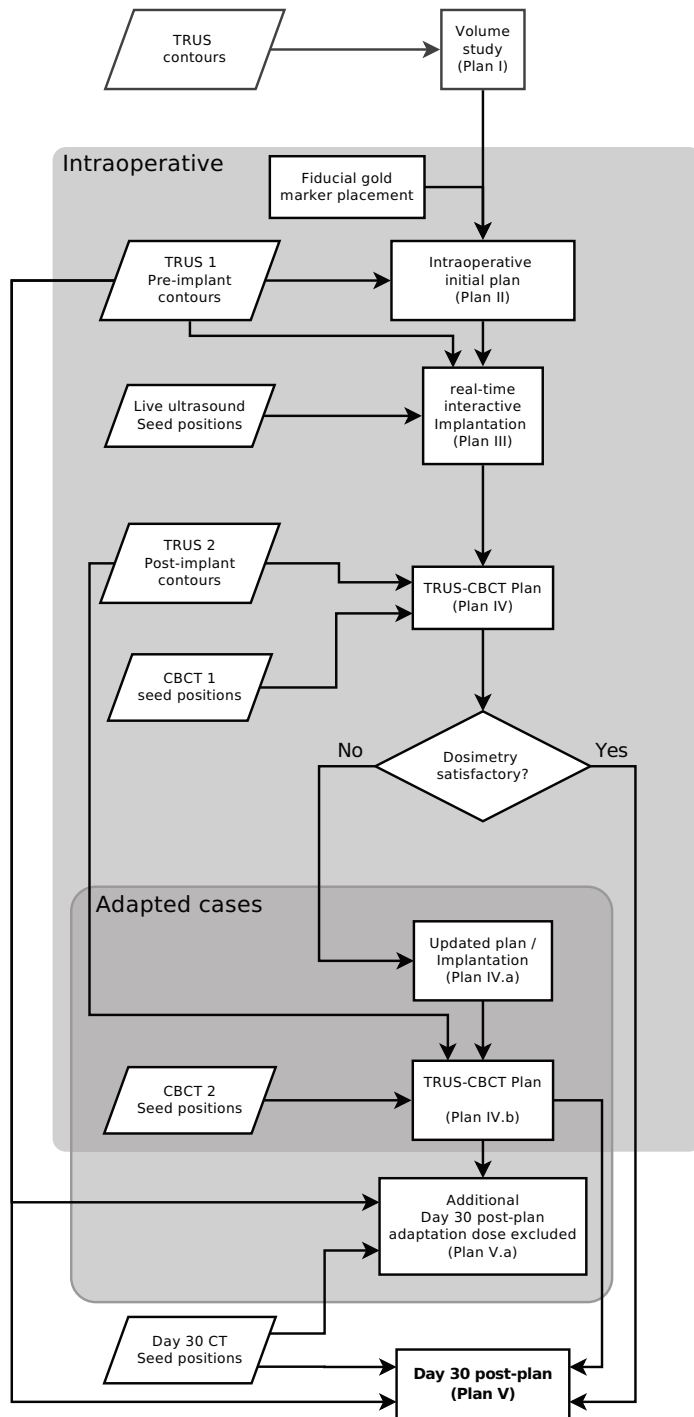
¹⁰ Polo *et al.*, 2010.

¹¹ Hinnen *et al.*, 2010b.

¹² Polo *et al.*, 2010.

¹³ Westendorp *et al.*, 2007.

Figure 6.1: Imaging and (adaptive) dosimetry. The trapezoidal boxes (left) show input of image data with corresponding contours and/or seed positions. The rectangles (right) show all plans. Plan IV, IV.a, IV.b, V and V.a include TRUS-(CB)CT registration.



Methods and materials

Patients

In the period of October 2007 to March 2016 we treated 1314 patients with localized prostate cancer (T1b – T2c) with ^{125}I brachytherapy. Patients were included in the analysis if they received the standard treatment and clinical follow-up. We excluded patients with incomplete datasets. Of the 1266 included cases 81% (1026 cases) received a monotherapy treatment of 145 Gy and 17% (211 cases) was treated with a boost of 110 Gy, 2% (29 cases) with a boost of 100 Gy. The boost treatment was given approximately 2 weeks after completion of external beam radiotherapy (EBRT).

Treatment technique

The implantation procedure, including all time points at which images were obtained or dosimetry was performed, is visualized in [figure 6.1](#). Implantations were performed with patients under spinal anaesthesia in dorsolithotomy position. Fluoroscopy¹⁴ and ultrasound¹⁵ were utilized to provide image feedback during implantation.

The implantation procedure started with the placement of four cylindrical fiducial gold markers¹⁶. The markers were used to register TRUS and CBCT at the end of the procedure and provided reference points in the prostate that facilitated navigation with fluoroscopy and TRUS. Patients receiving a boost had already four markers implanted prior to the preceding EBRT treatment for position verification.

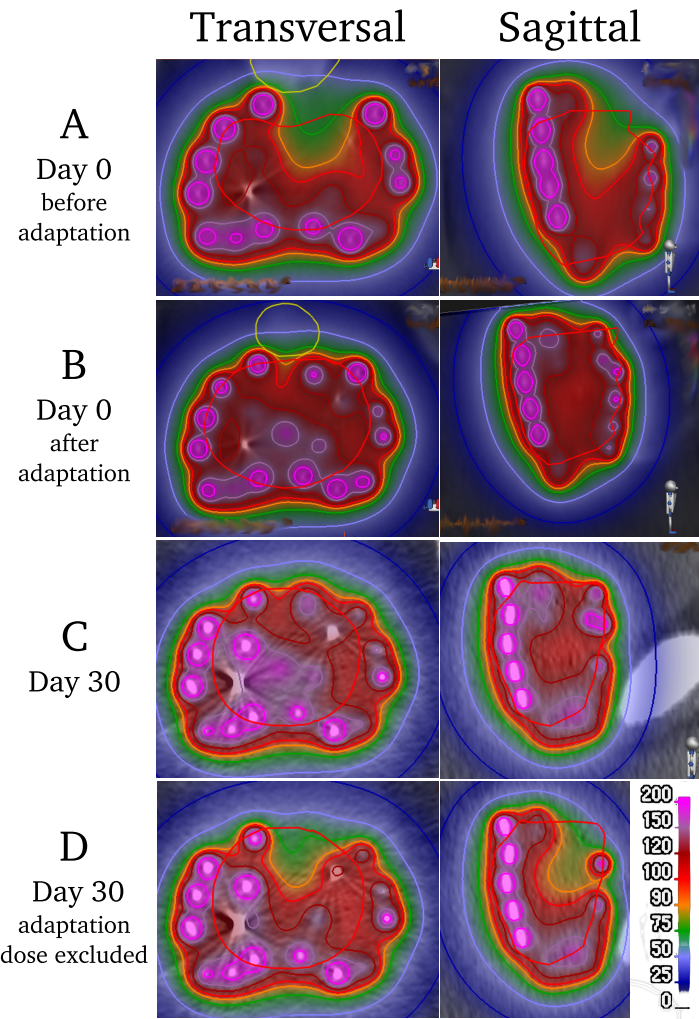
After marker placement, a TRUS-scan (TRUS 1) was obtained and the prostate (without margin), urethra and rectum were contoured. The urethra was contoured as a circle with fixed 5 mm diameter. On this dataset an intraoperative initial plan was made which served as a starting point for interactive, real-time implantation of seeds. The intraoperative starting point (Plan II) was based on a volume study (Plan I) that was made several weeks before implantation to exclude pubic arch interference and to determine the amount and strength of the ^{125}I seeds to be ordered. In our workflow, we improved intraoperative efficiency by editing Plan I instead of generating a plan anew. Plan II was modified according to the actual shape of the prostate and organs at risk contours on TRUS 1. Subsequently, the implantation was performed

¹⁴ Siemens Arcadis Orbic 3D; Siemens Medical Systems, Erlangen, Germany

¹⁵ Falcon 2101 EX and Flex Focus 400, BK Medical; Herlev, Denmark

¹⁶ $\varnothing 1 \times 5$ mm; Heraeus GmbH, Hanau, Germany

Figure 6.2: This example showed poor initial dose coverage (A, figure 6.1:Plan IV). The underdosages were adapted by placing remedial seeds (B, Plan IV.b). At Day 30 dose coverage was adequate (C, Plan V). However, excluding the adaptation of the remedial seeds, dose coverage would have been insufficient at Day 30 (D, Plan V.a). The colorbar represents the percentage of the prescribed dose (145 Gy). The prostate is contoured in red, the bladder in yellow.



¹⁷ Polo *et al.*, 2010.

¹⁸ 2007 – June 2008: IBt 1251L, Seneffe, Belgium; June 2008 – March 2010: IBt-Bebig I25.S06, Berlin, Germany; March 2008 – 2016: Bard STM1251, Murray Hill, NJ USA

(Plan III) using an interactive,¹⁷ real-time planning technique. Plan III is a key element of the adaptive planning procedure, in contrast to Plan I and Plan II that are specific for our implementation to improve the efficiency.

During the implantation, the position of stranded seeds¹⁸ was recorded on live TRUS images during release from the needles. First, seeds were implanted in the periphery of the prostate. Seed positions, visible on TRUS, were recorded in the TPS and the dose distribution was recalculated. The treatment plan was updated, the planned positions of the

remaining seeds were reoptimized. Next, seeds were implanted in the dorsal side of the prostate. Also these seed positions were recorded and, after calculating the actual dose distribution, the remaining, central seed positions were reoptimized. Finally the central seeds were placed and with their updated, optimized positions, final intraoperative TRUS-based dosimetry was obtained (Plan III).¹⁹

¹⁹ Westendorp *et al.*, 2016.

Following implantation the dosimetry of the implant was assessed. First, the legs of the patient were lowered as far as possible, with the feet of the patient remaining in the support. The pressure of the TRUS probe to the rectum was minimized to reduce possible deformation of the prostate. A TRUS-study (TRUS 2) was obtained with 2.5 mm spaced slices, on which the prostate and urethra were immediately contoured.

Directly after removal of the TRUS-probe and leg-support system a CBCT (CBCT 1) was acquired with the C-arm system that was also used for fluoroscopy. A transversal CT reconstruction with 2.5 mm thick slices was generated. Both the TRUS and the CBCT dataset were sent to the treatment planning system (TPS)²⁰. The seedfinder of the TPS identified the source-positions in the CBCT dataset. Resulting seed positions were visually inspected and, if necessary, corrected. In all cases the TPS identified the fiducial gold markers as seeds. Furthermore, occasionally, seeds close together were identified as one seed and seeds not displaying a bright spot on CBCT were not automatically found.

²⁰ Variseed 7.2 – 8.0.2; Varian Medical Systems, Inc., Palo Alto, CA USA

The TRUS study was registered to the CBCT dataset using the fiducial markers as reference points. The registration was visually checked by identifying the fiducial markers, seeds and urethral catheter in both datasets and manually adjusted if necessary.

A dose distribution (Plan IV) was calculated and inspected for underdosages. In case the radiation oncologist observed a critical underdosage, that was mostly also represented by a low V_{100} , the implant was adapted. In addition to the dosimetry, the decision to adapt was made by clinical considerations, such as the absolute value of the underdosage, and the location of the underdosage with respect to the index lesion. An updated plan (Plan IV.a) was made, using the CBCT-based postplan as starting point. Remedial seeds were implanted with the patient back in dorsolithotomy position and an additional CBCT-image (CBCT 2) dataset was acquired with the patient in imaging position. An extra postplan (Plan IV.b) based on CBCT 2 and the postimplant TRUS 2 (figure 6.1) was made after the implantation procedure had finished. Plans were made using

²¹ Rivard *et al.*, 2004.

the TG-43 line source approximation for seeds.²¹ Seeds had an average air kerma strength of 0.59 U (range 0.37–0.77 U) during placement. **Figure 6.2** gives an example of the consequences of the adaptation on dosimetry. More details of the clinical procedure, have been described before.²² In that study Day 0 dosimetry was assessed solely to show the feasibility of the procedure for a group of 20 patients.

²² Westendorp *et al.*, 2007, 2016.

Day 30 dosimetry

Day 30 dosimetry (Plan V) was performed. To locate the sources, a CT-dataset²³ was obtained with 2 mm thick slices. TRUS 1, that is not affected by edema,²⁴ was registered to the CT-dataset using the fiducial markers as reference points. If needed, the registration was manually adjusted. This method is similar to the methodology presented by Bowes *et al.* (2013); we use fiducial markers instead of the urethra for registration of the TRUS and CT data. Bowes *et al.* (2013) showed that this method results in similar values as MRI-CT dosimetry at Day 30.

²³ Brilliance Big Bore 16 Slice; Philips, Best, The Netherlands²⁴ Westendorp *et al.*, 2016.

The dosimetry for each patient was recorded. In case an implant had been adapted in the operating theatre, an additional postplan (Plan V.a) was made where we excluded the dose contribution of the remedial seeds, providing a situation as if no adaptation had been performed. An experienced technologist located remedial seeds visually, comparing intraoperative and postimplant seed distributions. This additional plan was used to quantify the dosimetric effects of the adaptation. **Figure 6.2** shows an example of the changes in isodoses as a consequence of the adaptation.

Analysis

The prostate D_{90} , V_{100} , V_{150} and the urethral D_{30} were determined for the adapted and the non adapted group, for Day 0 (intraoperative) as well as Day 30. Dosimetry of adapted and non adapted cases was visualized as density plots at various points in time (Plan III – V). The dose homogeneity index (HI) was calculated for Day 30 as $(V_{100} - V_{150})/V_{100}$.

Seed positions from 128 adapted implants were extracted from DICOM RT-Plan objects. Seeds present in Plan V but not in Plan V.a were identified as remedial seeds (**figure 6.1**). Projections of implants for the three main axes were displayed with the remedial seeds highlighted in a contrasting colour.

	Percent of implants with	$D_{90} > 100\%^a$ $V_{100} > 90\%^b$	$V_{100} > 95\%^b$
Day 0	non adapted	97	76
	adapted: before adaptation	35	4
	adapted: after adaptation	94	66
Day 30	non adapted	98.8	89
	adapted: adaptation dose excluded	85	51
	adapted: adaptation dose included	99.5	90

^a % of prescribed dose

^b % of prostate volume

Table 6.1: Percentage of implants with acceptable ($D_{90} > 100\%$ of prescribed dose, or equivalently, $V_{100} > 90\%$ of total volume) or preferable ($V_{100} > 95\%$ of total volume) dosimetry of the prostate.

Density distributions were constructed for the left–right (LR), anterior–posterior (AP) and craniocaudal (CC) axes to compare the positions of the remedial seeds with the positions of the initially implanted seeds.

Results

For the 1266 patients in our analysis adaptive CBCT based planning led to an adaptation in 218 (17.4%) cases. On average 71 seeds (range 36–94) were implanted. A median of 4 (range 1–10) remedial seeds were added during the implantation procedure.

The distributions of D_{90} , V_{100} and V_{150} at Day 0 are shown in figure 6.3 for several points in time at which dosimetry was obtained (see also figure 6.1). Figure 6.3 separately shows the distributions for adapted cases without the dose contribution of remedial seeds. The individual intraoperative dosimetry changes, resulting from adaptation, are displayed in figure 6.4.

CBCT acquisition, registration and dose review took approximately 10 min. The adaptation, including a second CBCT was performed in $\frac{1}{4}$ hour on average. This resulted in a mean procedure time (anaesthetized patient to finished implant) of $1\frac{1}{2}$ hour in case of an adaptation and $1\frac{1}{4}$ hour if no adaptation was performed.

In the adapted group, at Day 30, only 50% would have reached the

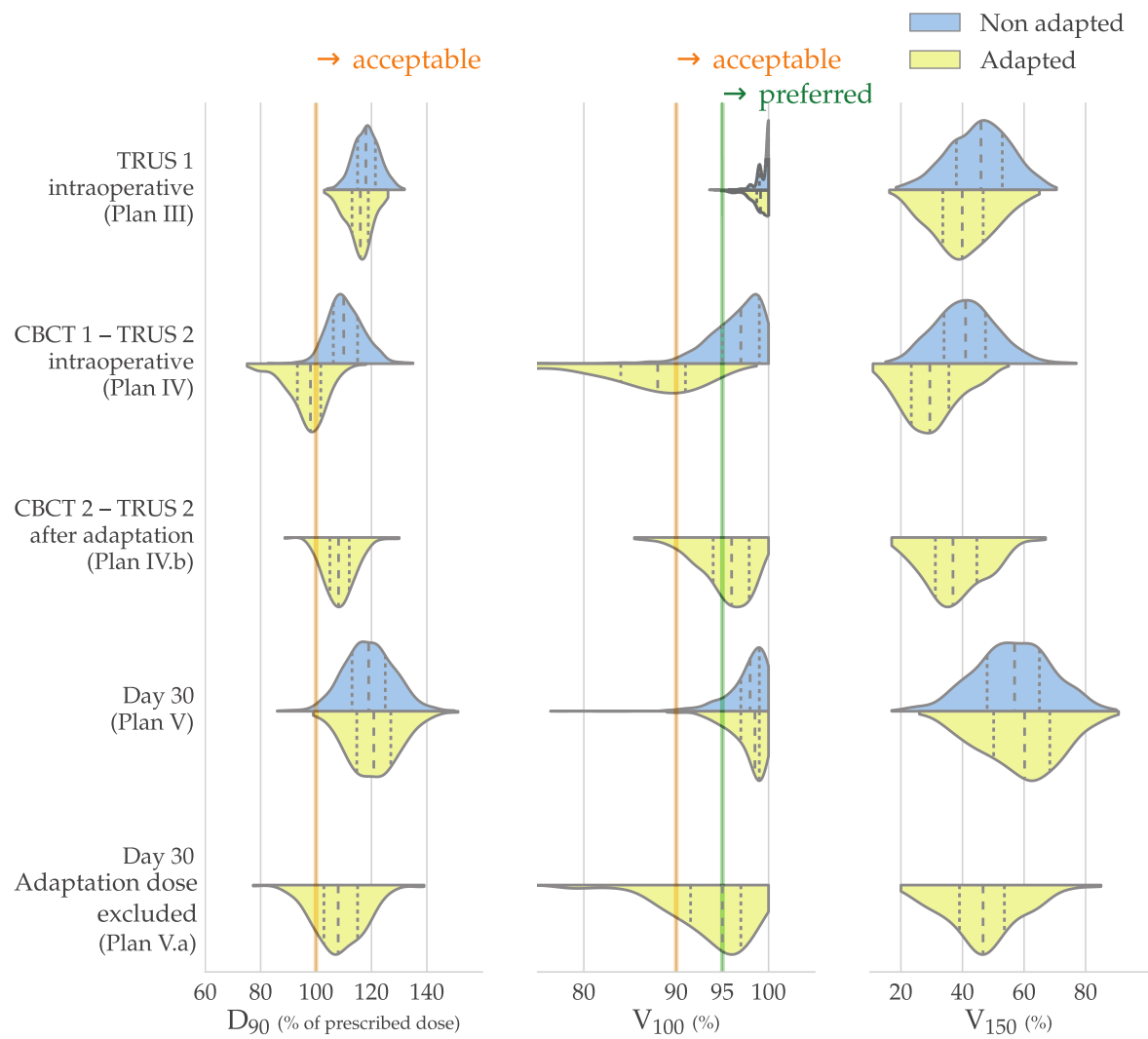


Figure 6.3: After adaptation (Plan IV.b, Plan V), dosimetry of the adapted cases is similar to the non adapted cases, before (Plan IV) and excluding the adaptation dose (Plan V.a) D_{90} and V_{100} are substantially poorer. The top half of each plot shows the non adapted cases and the bottom half the adapted cases. Dotted lines present the quartiles, dashed lines the median values. Timing of plans is clarified in figure 6.1. Areas under the curves are normalized.

preferred level of V_{100} if the adaptation would not have been performed. The adaptation increased this number to 90%. At Day 30, 89% of all cases had a $V_{100} > 95\%$, 99% showed a $V_{100} > 90\%$. The percentage of implants meeting the dosimetry criteria at Day 0 and Day 30 is displayed in [table 6.1](#).

In [table 6.2](#), the dosimetry at Day 0 and Day 30 is presented for both the adapted and the non adapted cases. For all adapted cases, two Day 30 plans were made: one with and one without the dose contribution of the remedial seeds. The adaptation led to an immediate (Day 0) average increase in D_{90} of $11.8 \pm 7.2\%$ (1 SD), V_{100} showed a mean increase of $9.0 \pm 6.4\%$. Comparing the corresponding Day 30 plans an increase in D_{90} of $12.3 \pm 6.0\%$ and an increase in V_{100} of $4.2 \pm 4.3\%$ was observed as a result of the dose contribution of the remedial seeds. The volume of adapted implants, contoured after implantation (Plan IV), was smaller ($35.1 \pm 9.8 \text{ cm}^3$) than that of non adapted implants ($39.3 \pm 10.9 \text{ cm}^3$).

Taking the average of dosimetry of all implants at Day 30, we observed a D_{90} of $119.6 \pm 9.1\%$, a V_{100} of $97.7 \pm 2.5\%$, a V_{150} of $57.0 \pm 12.6\%$ for the prostate and a D_{30} of $139.5 \pm 16.2\%$ for the urethra. The mean HI at Day 30 equaled 0.42 ± 0.12 . At Day 30, the mean HI for the adapted group was 0.40 ± 0.12 and for the non adapted group was 0.42 ± 0.12 .

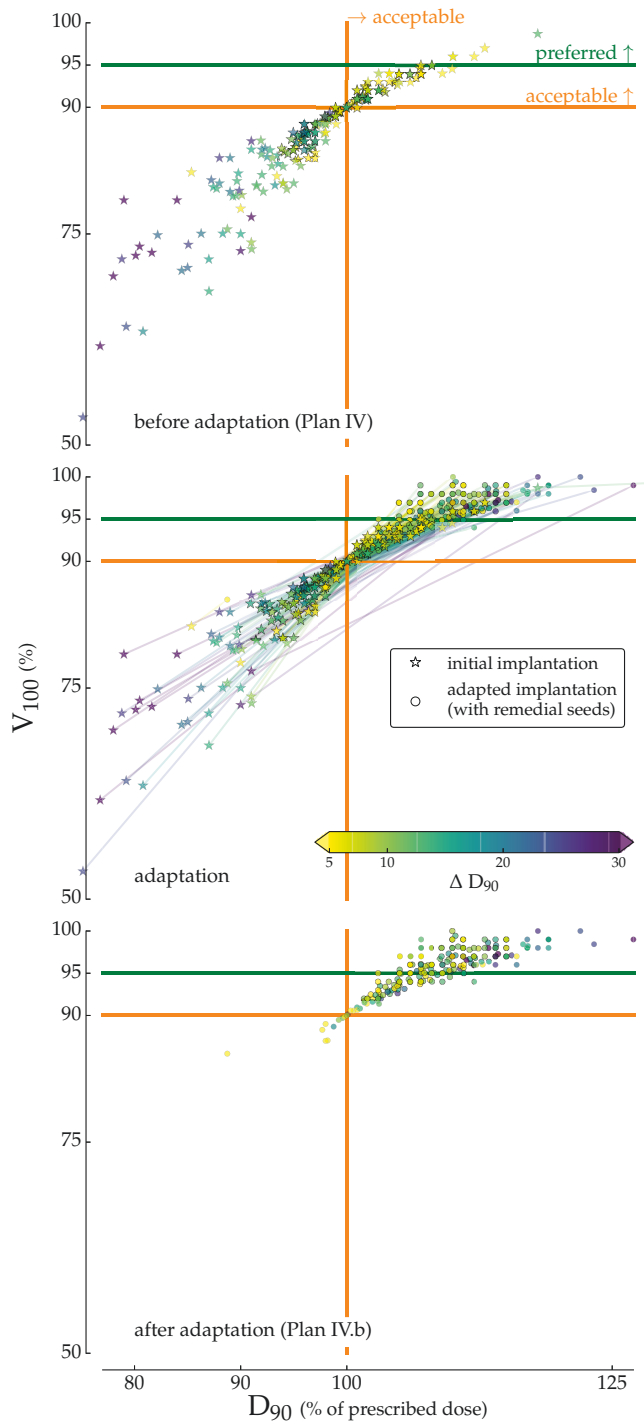
[Figure 6.5](#) shows the locations where the remedial seeds were placed. The orthogonal 2D projections and the 3D-view show that remedial seeds were predominantly placed at the base, anterior in the prostate.

Discussion

The dosimetric consequences of our adaptive planning technique are visualized in [figures 6.3](#) and [6.4](#). For the vast majority of cases, D_{90} and V_{100} move from unacceptable values (below 100% and 90% respectively) to acceptable values. Only 1% of the cases showed a $V_{100} < 90\%$ at Day 30. For most cases (89%) the preferred level of at least 95% for V_{100} was achieved. If no adaptations would have been performed, only 51% of the adapted group would have had a preferred V_{100} ($> 95\%$). The adaptation improved this number considerably to 90%. This shows that our procedure enabled identification of patients needing adaptation and that the selection at Day 0 correctly identified the group that otherwise would have shown coverage problems at Day 30.

[Table 6.2](#) shows that V_{150} for the adapted group is lower than for the

Figure 6.4: The adaptation of the adaptive planning procedure improves intraoperative dosimetry considerably for implants that initially show inadequate dose coverage of the prostate. Dosimetry is acceptable with a $V_{100} > 90\%$ and a $D_{90} > 100\%$, preferably V_{100} is above 95%.



		Prostate			Urethra
		D ₉₀ ^a	V ₁₀₀ ^b	V ₁₅₀ ^b	D ₃₀ ^a
Day 0	non adapted	mean ^c 110.7 ± 6.5 n ^d 1048	96.4 ± 3.0 1048	41.1 ± 10.1 1048	117.0 ± 10.6 1047
	adapted: before adaptation	mean 96.9 ± 7.1 n ^e 218	86.4 ± 7.0 218	29.9 ± 9.0 218	108.8 ± 11.9 216
	adapted: after adaptation	mean 108.6 ± 5.5 n ^e 214	95.4 ± 2.7 214	37.8 ± 9.7 214	115.5 ± 9.9 213
	non adapted	mean 119.3 ± 9.1 n ^d 1048	97.6 ± 2.5 1048	56.5 ± 12.5 1048	139.1 ± 16.3 1045
	adapted: adaptation dose excluded	mean 108.6 ± 8.9 n ^e 218	93.7 ± 5.1 218	46.9 ± 11.8 218	131.2 ± 15.7 218
	adapted: adaptation dose included	mean 120.9 ± 9.0 n ^e 218	97.8 ± 2.0 218	59.2 ± 12.6 218	141.1 ± 15.9 218

^a % of prescribed dose^b % of prostate volume^c Mean ± Standard Deviation^d Missing data if < 1048^e Missing data if < 218

Table 6.2: Dosimetric effects of adaptation.

non adapted group at Day 0 but higher at Day 30. In the adapted group dosimetry is based on CBCT 2 (Plan IV.b), which is acquired about 15 min later in the implant procedure compared to CBCT 1 (Plan IV), used for dosimetry in the non adapted group at Day 0.

Therefore, in the adapted group, dosimetry may be more affected by edema, resulting in increase of prostate volume and lower V₁₅₀. At Day 30 edema has resolved and V₁₅₀ is 2.7% higher for the adapted group.²⁵

²⁵ Westendorp *et al.*, 2016.

Considering the adapted group, table 6.2 and figures 6.3 and 6.4 show that, at Day 30, dosimetry would have been considerably poorer without adaptation. After the adaptation however, dosimetry almost equaled the non adapted group, both immediately after implantation and at Day 30. Not all patients showed Day 30 dosimetry above preferred levels, this is possibly caused by seed displacements.²⁶

²⁶ Westendorp *et al.*, 2016.

We compared Day 30 dosimetry after introduction of the CBCT technique to the dosimetry of 100 randomly selected patients (20 per year) from the period 2002–2006. Target coverage was improved from 110 ± 17 to 120 ± 9% for D₉₀ and 94 ± 5 to 98 ± 3% for V₁₀₀, at the same time

V_{150} decreased from 60 ± 11 to $57 \pm 13\%$ and the urethral D_{30} decreased from 145 ± 19 to $140 \pm 16\%$. This shows that the CBCT technique allowed more optimal implants, both for improving target coverage and for lowering dose to critical structures. Furthermore, the introduction of the CBCT technique significantly improved treatment outcome. For low risk prostate cancer 7 year biochemical disease free survival (BDFS) improved from 87.2% to 93.5% (log rank: $p=0.04$), for intermediate risk from 75.9% to 88.5 % ($p<0.001$) and for high risk from 57.1% to 85.0% ($p<0.001$) with the introduction of CBCT based adaptive planning.²⁷

²⁷ Peters *et al.*, 2017.

It is interesting that, using a state of the art, real-time intraoperative planning technique, implants may still show poor dosimetry. In previous work we compared the dosimetric results of our real-time intraoperative planning with that obtained with intraoperative CBCT. We found that edema and seed displacements were the major causes of underdosages needing adaptation.²⁸ In contrast to TRUS imaging, CBCT imaging allows for an accurate localisation of all final seed locations and is thus able to display dosimetry including intraoperative edema and seed displacements.

²⁸ Westendorp *et al.*, 2016.

We compared our results to other large scale studies (>150 patients), reporting postimplant dosimetry. Techniques that relied on (intraoperative) preplanning showed an average postoperative D_{90} of 100 – 111%, a V_{100} of 89 – 94% and a V_{150} of 56 – 61%.²⁹ Intraoperative real-time techniques showed a mean postoperative D_{90} of 105 – 126%, a V_{100} of 93 – 97% and a V_{150} of 32 – 70%.³⁰ In the present study Day 30 dosimetry shows an average D_{90} of 120%, a V_{100} of 98% and a V_{150} of 57%. Compared to values reported in literature the present study shows high values for V_{100} and D_{90} . This was realised by starting with a state of the art real-time interactive implantation procedure and adaptations of underdosages in 17% of the cases.

²⁹ Crook *et al.*, 2011; Nasser *et al.*, 2015; Al-Qaisieh *et al.*, 2009.

³⁰ Ishiyama *et al.*, 2010; Moerland *et al.*, 2009; Potters *et al.*, 2006; Shaikh *et al.*, 2015; Zelefsky *et al.*, 2007b.

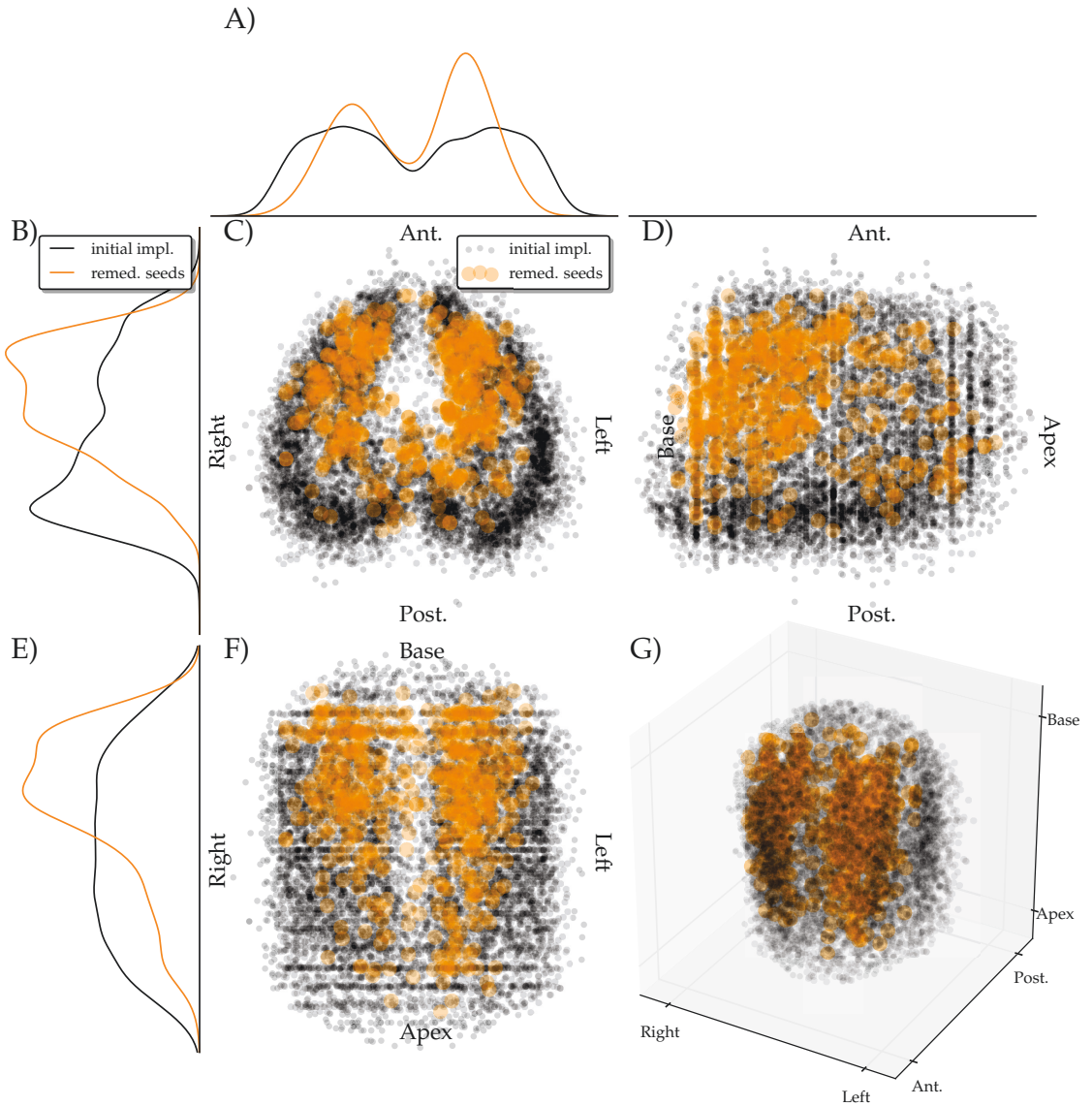


Figure 6.5: Remedial seeds were predominantly placed near the anterior base of the prostate. (A, B, E) Relative density of the distribution of positions of initially placed seeds compared with the positions of remedial seeds. (A) Right–Left. (B) Posterior–Anterior. (E) Apex–Base. (C, D, F) 2D views of the placement of initial and remedial seeds. (G) 3D view. Areas under the curves are normalized.

³¹ Crook *et al.*, 2011; Delouya *et al.*, 2015; Ishiyama *et al.*, 2010; Nasser *et al.*, 2015.

³² Keyes *et al.*, 2009; Merrick *et al.*, 2003; Vordermark *et al.*, 2009.

³³ Pinkawa *et al.*, 2006; Vordermark *et al.*, 2009.

³⁴ Kollmeier *et al.*, 2012.

We realized a HI of 0.42 on average, which is relatively high compared to values in recent literature, ranging from 0.29 to 0.41.³¹ This indicates that our adaptive technique allows for sparse implantation reducing V_{150} and associated risks of urethral,³² bowel³³ and erectile³⁴ toxicity as the technique provides the possibility to add remedial seeds if deemed necessary.

The final urethral D_{30} on Day 0 was comparable for the adapted (116%) and non adapted group (117%, table 6.2). The absolute urethral D_{30} values on Day 30 have limited value as the urethra contour originated from the intraoperative procedure (figure 6.1, TRUS 1) and, because of the absence of a urinary catheter, the urethra may not have the same shape at Day 30.

In the treated population an adaptation at Day 0 was deemed necessary in 17% of the cases. This seems a relatively large fraction. There are multiple reasons to adapt an implant. If the dosimetry is below the preferred level, and the dose at a clinically relevant volume is relatively low, the radiation oncologist usually decides for adaptation. The additional time to perform the adaptation is approximately $1/4$ hour, allowing remedial seeds to be placed with low effort. On average two needles were sufficient to place the four remedial seeds. To further improve efficiency of the procedure TRUS 2, CBCT 2, Plan I, Plan II, Plan IV.b and Plan V.a could be omitted, reducing overall workload at the expense of the loss of intermediate dosimetry data.

Immediately after introduction of the CBCT based technique in our clinic we performed adaptations more often than in recent years. Still, after almost 10 years of experience we perform an adaptation in more than one in ten implants. The relative ease to adapt an implant may have affected the initial implantation procedure. We can intentionally start with relatively sparse implants to reduce V_{150} and the OAR dose, knowing that the adaptive planning procedure allows eradication of cold spots by placing remedial seeds. However, we always ensure that dosimetry is adequate after finishing the real-time intraoperative planning (Plan III).

Figure 6.5 shows that remedial seeds were predominantly implanted in the anterior base of the prostate. Jastaniyah *et al.* (2013) and Moerland *et al.* (2009) also observed most coverage problems in this region. McParland *et al.* (2013) report the placement of extra seeds in this region. Some studies indicate that full coverage of this region might not be necessary,³⁵ while other studies show that cancerous tissues may also

³⁵ D'Amico *et al.*, 1999; Spadinger *et al.*, 2015.

be found in the anterior base.³⁶

In a separate analysis of the data we showed that, generally, seeds in the anterior base of the prostate have a tendency to displace caudally. Furthermore deeper implanted seeds tend to diverge from the central axis of the prostate.³⁷ Both mechanisms can cause the observed underdosages in the anterior base but the extent of the deviations cannot be predicted for an individual patient.

In a previous study³⁸ we showed that it is not possible to give an accurate individual prediction of Day 30 dosimetry during the implantation procedure. Using CBCT-based adaptive planning however, we were able to identify a subgroup of implants that needed adaptation, preventing insufficient target coverage at Day 30 for this subgroup (figures 6.3 and 6.4, table 6.2).

The use of intraoperative MRI is an attractive yet expensive and scarcely available alternative for performing dynamic dosimetry. It has potential to further increase the accuracy of the implantation procedure by providing visualization of lesions that may be boosted or focally treated.

Our adaptive planning technique would benefit from the inclusion of preoperative MRI. With MRI it is possible to define intraprostatic structures that cannot be visualized with TRUS. The addition of MRI may also improve the definition of the base and apex of the prostate.³⁹ However, the registered preoperative MRI may show a different prostate shape and size than the actual situation during implantation. Furthermore, the addition of preoperative MRI involves image registration, leading to registration uncertainties.

Registration and contouring uncertainties may have affected the results presented in the current study. In a separate study we found that the observed registration and contouring variability is smaller than underdosages that are adapted during the adaptive planning procedure.⁴⁰ Registration and contouring uncertainties result in uncertainties near the outer contour of the prostate, this region only partly overlaps with adapted underdosages. These adapted underdosages were located near the anterior base of the prostate but extended centrally. This is displayed in figure 6.5, which shows remedial seeds spread throughout the volume between the center and base of the (anterior) prostate.

The use of multiple modality imaging during the implantation procedure provides an opportunity to independently check the implant while

³⁶ Bittner *et al.*, 2013; Merrick *et al.*, 2007.

³⁷ Westendorp *et al.*, 2016, 2015.

³⁸ Westendorp *et al.*, 2016.

³⁹ Smith *et al.*, 2007.

⁴⁰ Westendorp *et al.*, 2017b.

the patient is still anaesthetized, thereby reducing the probability on errors.

In other studies an O-arm CBCT has been used to assess intraoperative dosimetry.⁴¹ These studies consider a limited amount of patients without applying the dosimetry feedback to improve the implant. Kuo *et al.* (2014) described a dynamic image guidance system using TRUS and fluoroscopy that was tested on 37 patients. To our best knowledge no large scale dosimetry study has been published about this interesting approach.

⁴¹ Ishiyama *et al.*, 2016; Zelefsky *et al.*, 2010.

Currently interest is growing in focal treatments⁴² and differential dose prescription strategies.⁴³ These techniques have the potential to reduce toxicity of the treatment without sacrificing outcome. Seed positioning becomes more critical when treating smaller targets.⁴⁴ A rapid adaptive planning feedback loop, as reported in the current study, may be beneficial to warrant high quality implants for smaller targets. The adaptive nature allows an immediate dose assessment of implants, possibly shortening the learning curve of new strategies.

⁴² Langley *et al.*, 2012.

⁴³ Rylander *et al.*, 2015.

⁴⁴ Al-Qaisieh *et al.*, 2015.

Conclusion

We present large scale (1266 patients) adaptive dosimetry results for permanent prostate brachytherapy. The addition of CBCT-imaging and intraoperative adaptation to the implantation procedure proves valuable, resulting in excellent Day 0 and Day 30 dosimetry. The presented technique is, quick, routinely feasible and allows a sparse implantation strategy, limiting V_{150} . Remedial seeds are predominantly placed near the anterior base of the prostate.

Chapter 7

Dosimetric impact of contouring and image registration variability on dynamic ^{125}I prostate brachytherapy

Adapted from: H Westendorp, K Surmann, CJ Hoekstra, SM van de Pol, RA Kattevilder, TT Nuver, MA Moerland and AW Minken (2017b). 'Dosimetric impact of inter- and intra-observer variability in contouring and image registration for intraoperative ^{125}I prostate brachytherapy dosimetry.' *Brachytherapy*

Abstract

Purpose: The quality of permanent prostate brachytherapy can be increased by addition of imaging modalities in the intraoperative procedure. This addition involves image registration, which inherently has inter- and intraobserver variability. We sought to quantify the inter- and intraobserver variability in geometry and dosimetry for contouring and image registration, and analyze the results for our dynamic ^{125}I brachytherapy procedure.

Methods and Materials: Five observers contoured 11 transrectal ultrasound (TRUS) datasets three times and 11 Computed Tomography (CT) datasets one time. The observers registered 11 TRUS and Magnetic Resonance Imaging (MRI) datasets to conebeam CT (CBCT) using fiducial gold markers. Geometrical as well as dosimetrical inter- and intraobserver variability were assessed. For the contouring study, structures were subdivided in 3 parts along the craniocaudal axis.

Results: We analyzed 165 observations. interobserver geometrical variability for prostate was 1.1 mm, resulting in a dosimetric variability of 1.6% for V_{100} and 9.3% for D_{90} . The geometric intraobserver variability was 0.6 mm with a V_{100} of 0.7% and D_{90} of 1.1%. TRUS–CBCT registration showed an interobserver variability in V_{100} of 2.0% and D_{90} of 3.1%. intraobserver variability was 0.9% and 1.6% respectively. For MRI–CBCT registration V_{100} and D_{90} was 1.3% and 2.1%. intraobserver variability was 0.7% and 1.1%, for the same.

Conclusion: Prostate dosimetry is affected by interobserver contouring and registration variability. The observed variability is smaller than underdosages that are adapted during our dynamic brachytherapy procedure.

Introduction

¹²⁵I prostate brachytherapy depends heavily on imaging. Intraoperative visual feedback for contouring and seed deposition is commonly provided by Transrectal Ultrasound (TRUS).¹ The quality of permanent prostate implants can be improved by using additional imaging modalities, like Magnetic Resonance Imaging (MRI) and conebeam CT (CBCT).²

With MRI, intraprostatic structures and lesions can be identified,³ allowing for boosting of subvolumes⁴ or focal treatments.⁵ Intraoperative CBCT enables more accurate localisation of the deposited seeds.⁶ When imaging modalities are added to the implantation procedure, a registration to the primary (TRUS) dataset needs to be performed. This registration requires manual interaction, resulting in additional inaccuracies due to inter- and intraobserver variability. This variability directly affects dosimetry.

In addition to registration, contouring is another major source of variability.⁷ interobserver variability depends on the imaging modality that is used for contouring.⁸ Contouring on CT results in more variability than contouring on TRUS and MRI.⁹ Prostate outer contours show similar variability on TRUS and MRI.¹⁰

De Brabandere *et al.* (2012) studied the dosimetric impact of interobserver variability in seed localisation, contouring and image registration in a multi-center setting. Eight observers contoured and registered post-implant CT and MRI for three patients. D_{90} showed a large dosimetric variability in contouring (17 – 23%) and image registration (6 – 16%). In this multi-center study, the authors suggested that personal or institutional habits could have played a major role in the large contouring variability. Training would probably help to lower contouring variability, whereas registration variability could possibly be reduced by using automated tools.

When adding imaging modalities to an implantation procedure, the benefit of improved accuracy of contouring should outweigh the additional uncertainties in dosimetry that are caused by the registration itself. Ideally, the registration variability should be small compared to other sources of uncertainty, like contouring and seed localization.

Since 2006 we routinely apply a dynamic dosimetry technique. After implantation, we acquire a C-arm CBCT scan and register it to a contoured TRUS image-dataset.¹¹ In a previous study we concluded that

¹ Nath *et al.*, 2009.

² Polo *et al.*, 2010.

³ Barentsz *et al.*, 2012; Puech *et al.*, 2014; Tanderup *et al.*, 2014.

⁴ Rylander *et al.*, 2015.

⁵ Langley *et al.*, 2012; Al-Qaisieh *et al.*, 2015; Tong *et al.*, 2013.

⁶ Ishiyama *et al.*, 2016; Westendorp *et al.*, 2007, 2016; Zelefsky *et al.*, 2010.

⁷ Brabandere *et al.*, 2012.

⁸ Smith *et al.*, 2007.

⁹ Smith *et al.*, 2007.

¹⁰ D Liu *et al.*, 2012; Smith *et al.*, 2007.

¹¹ Westendorp *et al.*, 2017a, 2007.

¹² Westendorp *et al.*, 2017a.

TRUS–CBCT based dosimetry enables identification of underdosed regions that need adaptation by placing remedial seeds.¹²

In the present study we assessed the inter- and intraobserver variability in contouring and registration for our dynamic implantation procedure. Anticipating the implementation of pretreatment MRI in our procedure, to enable focal treatments, we additionally incorporated the registration of MRI with CBCT. The purpose of this study was to quantify the dosimetric variability caused by contouring and registration and to compare this variability to the dosimetric improvements made by our dynamic dosimetry technique.

Materials and methods

Patients

Data from 11 prostate cancer patients, treated with a boost with stranded ¹²⁵I seeds after External Beam Radiation Therapy (EBRT), were used. Each patient had received 47 Gy (20 × 2.35 Gy) with EBRT and 110 Gy as a brachytherapy boost.

Treatment procedure

Prior to EBRT treatment, four gold fiducial markers¹³ were implanted for EBRT position verification and image registration. For EBRT, contouring of regions of interest (ROIs) was performed on a 2 mm thick sliced CT dataset¹⁴ registered with T1 and T2 weighted MRI datasets with a slice spacing of 2 mm¹⁵. The MRI dataset was acquired approximately 7 weeks before the implantation procedure.

Approximately two weeks after finishing EBRT, the brachytherapy procedure was performed. We used a dynamic dosimetry implantation procedure.¹⁶ The implantation procedure started with the acquisition of a TRUS scan¹⁷ with 5 mm spaced slices that were contoured. Immediately after finishing implantation, a second TRUS scan was acquired with 2.5 mm spaced slices on which the ROIs were contoured. This TRUS dataset was registered to a 2.5 mm thick sliced CBCT dataset¹⁸, on which implanted seeds were identified. The CBCT dataset was obtained directly after the TRUS scan. The registration was started using the least squares

¹³ Heraeus GmbH, Hanau, Germany

¹⁴ Brilliance Big Bore 16 Slice; Philips, Best, The Netherlands

¹⁵ Signa HDxt; GE Medical, Milwaukee, WI, USA

¹⁶ Westendorp *et al.*, 2017a, 2007, 2016.

¹⁷ FlexFocus 400; BK Medical, Herlev, Denmark

¹⁸ Siemens Arcadis Orbic 3D; Siemens Medical Systems, Erlangen, Germany

method in the treatment planning system (TPS)¹⁹ using the fiducial markers, and manually adjusted if deemed necessary. The hemispherical shape of the ends and the larger diameter (1.0 mm) improve visibility of fiducial markers considerably compared with ¹²⁵I seeds. A month after implantation, a CT dataset with 2 mm thick slices (CT 30) was acquired to assess the Day 30 dose distribution. More details of the procedure have been published previously.²⁰

¹⁹ Variseed 8.0.2; Varian Medical Systems Inc., Palo Alto, CA, USA

²⁰ Westendorp *et al.*, 2017a, 2007.

Multi-observer study

Five observers from our institute participated in the inter- and intraobserver variability study. The group of observers consisted of two experienced radiation oncologists that routinely perform the implantation procedure (CH, SP), a medical physicist with long term expertise (HW), a dedicated research brachytherapy technologist (RK) and the primary investigator (KS, trained by SP).

The observers contoured the prostate, urethra and rectum three times on the pre-implant TRUS. For comparison, the prostate and rectum were contoured once on CT 30. During the acquisition of CT 30, there was no catheter present to allow contouring of the urethra. To minimize bias, observers could not review their previous sessions. The sessions were at least one week apart.

Observers used the TPS to contour and register the datasets for all sessions. The data were exported in Dicom format and processed using MATLAB²¹.

TRUS–CBCT registrations were performed three times by each observer. To assess the impact of anticipated implementation of MRI we additionally performed three MRI–CBCT registrations. The observers were instructed to start the registration based on all fiducial markers. The least squares fit (points) registration algorithm of the TPS was used. After that, if needed, the registration was manually adjusted, guided by the visible seeds. After each registration, dosimetric parameters were recorded. For the prostate V_{100} and D_{90} were reported, for the urethra we recorded D_{30} and for the rectum V_{100} .

Fiducial markers were always implanted at four fixed locations: cranial left, cranial right, caudal left and caudal right, using two needles. If a fiducial marker could not be identified on the image dataset, the anatomical location (e.g. cranial left) of the missing fiducial marker was

²¹ Version 8.1.0.604; The MathWorks Inc., Natick, MA, USA

reported.

Two experienced radiation oncologists had reviewed the clinically used (TRUS) contours and both approved the result during the implantation procedure. These clinically used contours were regarded as the reference dataset for the interobserver variability studies. Clinical intraoperative (TRUS–CBCT) and day 30 (TRUS–CT) dosimetry were set as reference, both for the contouring and the registration study. CT contours were compared to the TRUS reference contours.

We contoured TRUS multiple times and assessed geometrical and dosimetrical variability. One session of CT contouring showed that interobserver variability in CT contouring was much higher than in TRUS. Therefore we decided to restrict the intraobserver variability study to TRUS contouring.

Contours were analyzed with a Matlab script. The prostate surface was sampled with 10° increments of the polar and azimuthal angles.²² The center of mass of the reference prostate was set to the origin (0, 0, 0) and all observations were relative to this center. For the urethra, the in-plane center was calculated for each slice. Urethra contours were analysed only on slices with prostate contours. The rectum was resampled around the center of the TRUS probe for each slice. Rectum contours were assessed over the length of the prostate under an angle of 25° left and right of the midline with an increment of 10°. A schematic drawing of the acquisition of the sample points is depicted in [figure 7.1](#). Each structure from the reference dataset was divided into three equal parts along the craniocaudal axis: superior, central and inferior.

The distance between the actual and the reference contour determined the geometrical interobserver variability. The distance between the actual contour and the mean of the three contouring sessions determined the intraobserver variability. The distance between the reference contours (inter) or mean of the three contouring sessions (intra) was calculated for each sample point. For each structure or part of a structure (superior, central, inferior) these sample points were averaged. Next, variabilities were calculated ([appendix A](#)).

The dosimetric contouring parameters were determined by the actual contours in the reference dose distribution. Dosimetric parameters were normalized to the reference (clinical situation for interobserver and average for intraobserver). The clinically obtained parameters served as references for the interobserver variability. For the intraobserver

²² Smith *et al.*, 2007.

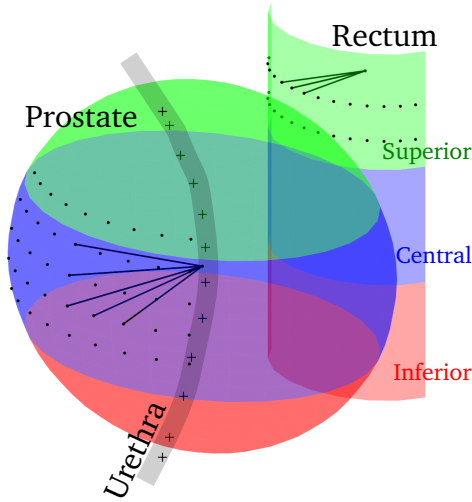


Figure 7.1: Sample points of the prostate (modelled as a sphere) were taken at each $10^\circ \times 10^\circ$ solid angle from the center of mass. The urethra was sampled at the center of each slice (+). Sample points of the rectum (modelled as a cylinder) were taken in each slice at each 10° between $-25^\circ - 25^\circ$. Each structure was divided into superior (green), central (blue) and inferior (red) parts based on the craniocaudal length of the prostate in the reference TRUS.

variability the mean of three sessions served as reference. The variability was reported as the standard deviations of the observations (SD_{inter} and SD_{intra} , [appendix A](#)).

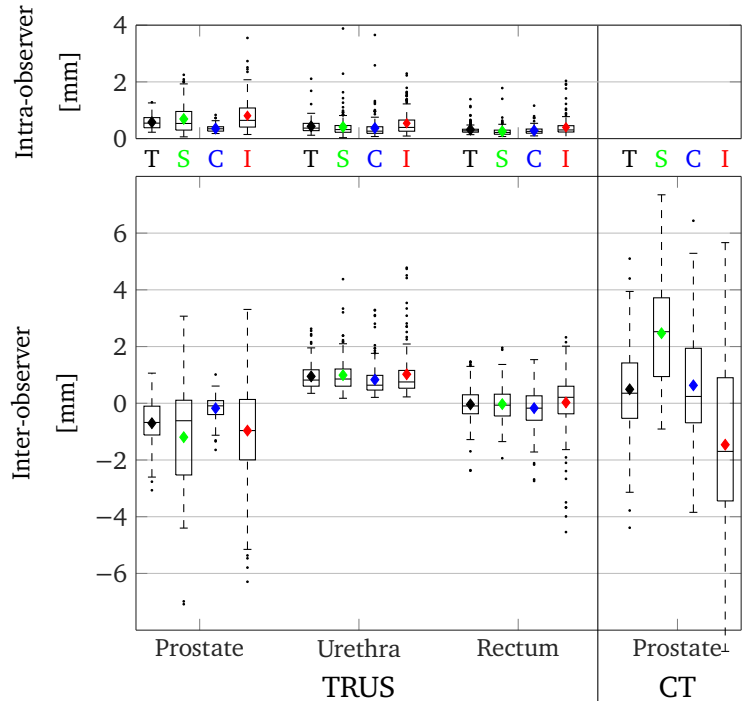
The registration study was conducted similarly as the contouring study. Reference contours and dose dose distributions were used, leaving the registration the only variable. The TPS did not report registration parameters (i.e. rotations and translations). We recorded dosimetric parameters only.

Results

Contouring variability

The interobserver variability in contouring (1 SD) for the whole prostate on TRUS was 1.1 mm and, splitting the prostate in three equal parts along the craniocaudal axis, 2.1 mm for the superior, 0.4 mm for the central and 2.0 mm for the inferior part. The intraobserver contouring variability (1 SD) was 0.6 mm for the whole structure and 0.9, 0.4 and 1.0 mm for superior, central and inferior parts, respectively. Regarding the urethra, an interobserver contouring variability of 1.1 mm and an intraobserver variability of 0.5 mm were observed. For the rectum, we found an interob-

Figure 7.2: intraobserver contouring variability (absolute values) and interobserver variability (signed values). interobserver contouring variability (compared to the reference: clinical TRUS contours) is smaller for TRUS than for CT. Variabilities are subdivided in total structure (T), superior (S), central (C) and inferior (I) parts of the prostate, urethra and rectum on TRUS (n=165) and the prostate on CT (n=55). A ♦ marks the average of each distribution.



server contouring variability of 0.6 mm and an intraobserver variability of 0.4 mm. All contouring variabilities are visualized as boxplots in figure 7.2. The observers contoured the prostate smaller than the reference, especially in the superior and inferior parts (figure 7.2). The superior and inferior parts had larger inter- and intraobserver variabilities than the central part.

The dosimetrical consequences of contouring variability are presented in figure 7.3 and table 7.1. Compared to the reference contours, the prostate was contoured smaller on TRUS, resulting in a higher D_{90} .

Contouring on CT resulted in an interobserver variability of 2.0 mm for the whole structure and 3.1, 2.4 and 3.8 mm for the superior, central and inferior parts, respectively. Large differences with the reference (TRUS) contours, of up to 5.1 mm, were observed. Prostate contouring on CT showed larger interobserver variabilities for V_{100} (5.9%) and for D_{90} (11.1%) than on TRUS: 1.6% for V_{100} and 9.3% for D_{90} (table 7.1).

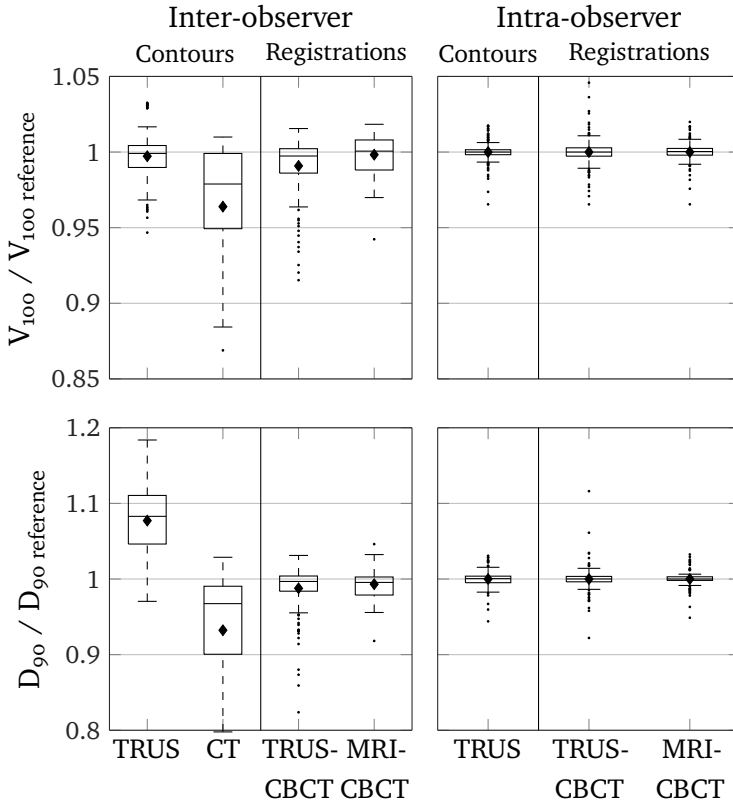


Figure 7.3: Contouring and registration variability affect dosimetry of the prostate. intraobserver variability is smaller than interobserver variability. Prostate V_{100} and D_{90} are normalized to the reference (clinical situation for interobserver and average for intraobserver). The \blacklozenge marks the mean of each distribution.

Registration variability

Observers localized 91.3% of the fiducial markers on TRUS, 100% on CBCT and 99.3% on MRI. After the automatic registration, the TRUS–CBCT registrations were manually adjusted in 78.2% of the observations. The observers reported that the seeds and urethra trajectory were used to manually improve the registration. For MRI–CBCT 17.6% of the registrations were manually adjusted.

Dosimetric results of the registrations are shown in figure 7.3. Table 7.1 lists the corresponding inter- and intraobserver variabilities, together with the corresponding dosimetric parameters. MRI–CBCT registrations had smaller interobserver variabilities than TRUS–CBCT registrations for the prostate V_{100} and D_{90} . The intraobserver TRUS– and MRI–CBCT registrations differed little in V_{100} and D_{90} .

Table 7.1: Inter- and intraobserver variability of the dosimetric parameters based on TRUS and CT contouring.

	Contours		Registrations	
	TRUS	CT	TRUS–CBCT	MRI–CBCT
Number	165	55	165	120
Prostate V ₁₀₀ [%]				
Average Reference	98.8	98.8	98.5	98.3
Average Observer	98.8	94.8	97.5	98.3
SD _{inter}	1.6	5.9	2.0	1.3
SD _{intra}	0.7	–	0.9	0.7
Prostate D ₉₀ [%]				
Average Reference	122.1	122.1	113.5	114.2
Average Observer	130.6	113.6	112.4	113.1
SD _{inter}	9.3	11.1	3.1	2.1
SD _{intra}	1.1	–	1.6	1.1
Urethra D ₃₀ [%]				
Average Reference	136.4	–	119.6	–
Average Observer	154.1	–	119.6	–
SD _{inter}	14.6	–	2.4	–
SD _{intra}	1.5	–	1.7	–
Rectum V ₁₀₀ [cm ³]				
Average Reference	0.83	0.83	–	–
Average Observer	2.33	1.00	–	1.21
SD _{inter}	0.43	0.51	–	0.57
SD _{intra}	0.23	–	–	0.49

Abbreviations SD_{inter} (1 SD with respect to the reference average) the interobserver variability; SD_{intra} (1 SD with respect to the observer average) the intraobserver variability.
– Not available.

Discussion

Contouring variability

We performed a multi-observer study, quantifying inter- and intraobserver contouring and registration variabilities for our dynamic planning technique.²³

The superior and inferior parts of the prostate showed the greatest contouring variabilities (figure 7.2). This is in agreement with other

²³ Westendorp *et al.*, 2017a, 2007.

studies.²⁴ The contouring variability of the whole prostate on CT is less than the contouring variability of its parts S, C and I (figure 7.2). This is a result of averaging of sample points (equations (7.3) and (7.4)). Larger contouring of the superior part and smaller contouring of the inferior part average out resulting in a smaller variability for the whole structure. Compared to CT, we found that TRUS contouring showed a smaller variation in geometrical differences (figure 7.2) as well as substantially smaller variations in dosimetric parameters (figure 7.3 and table 7.1). Observers mentioned that prostate contouring on CT scans was affected by the visible ¹²⁵I seeds, as the prostate boundary could not be identified accurately on CT. Poor prostate visualisation by CT results in large contouring variability compared to TRUS based prostate contouring variability. This observation agrees with previously published work.²⁵

Based on CT contouring alone, we found an interobserver V_{100} and D_{90} variability for the prostate of 5.9% and 11.1%. De Brabandere *et al.* (2012) found considerably larger interobserver variabilities (V_{100} : 11.7% and D_{90} : 23%) in a study that was performed by eight physicians from seven institutes. They suggested that training could help to improve the results. For this reason, we expected to find smaller variabilities as we conducted a single institution study.²⁶ Our results, with observers trained similarly, support the suggestion of De Brabandere *et al.* (2012).

In the present study we looked at the prostate as well as the rectum and urethra. To the best of our knowledge, this is the first contouring and registration variability study designed to incorporate these organs at risk. Urethra contouring on TRUS showed little variability (figure 7.2). The urethra visibility on TRUS is good because of the distinctive reflections of the urinary catheter. However, the dosimetric consequences are relatively large, with an SD_{inter} in D_{30} of 14.6% (table 7.1). This results from the small diameter of the urethra and its location in a region that is surrounded by steep dose gradients.

The variability of the rectum contours increased slightly from superior to inferior as the distance between the rectal wall and TRUS probe increased and the rectal wall contrasted less distinctly from the surrounding tissues (figure 7.2). The volume of the rectum that received the prescribed dose was small, the variability in V_{100} was within 0.5 cm³.

²⁴ D Liu *et al.*, 2012; Smith *et al.*, 2007.

²⁵ Khoo *et al.*, 2012; Smith *et al.*, 2007.

²⁶ Bowes *et al.*, 2013; Brabandere *et al.*, 2012; Kirisits *et al.*, 2014.

Registration variability

On TRUS, ¹²⁵I seeds cause bright reflections similar to those of fiducial markers, consequently seeds can be mistaken for fiducial markers. During registration however, the observer had an indication of the positions of the markers on the CBCT or MRI dataset, providing guidance to identify the fiducial markers on TRUS. With this guidance, observers were able to identify 91% of the fiducial markers on TRUS compared to 99.3% on MRI and 100% on CT.

The identification of gold markers on MRI (voids) and CBCT (bright spots) was straightforward and lead to an accurate automatic registration by the TPS. As no seeds were present in the MRI-dataset, observers had limited feedback to adjust the registration. The observers reported that they made less manual interactions during MRI–CBCT registrations (18%) than during TRUS–CBCT registrations (78%). The TPS did not allow for quantification of the translation and rotation resulting from the registration.

Registration of MRI with CBCT resulted in interobserver variabilities of 1.3% for the V_{100} and 2.1% for the D_{90} . De Brabandere *et al.* (2012) reported a V_{100} variability of 2.9% based on CT–T1–T2 registration together with a D_{90} variability of 7%. These variabilities based on multi-modality image registration are larger than the variabilities found in the present study. In line with the observations of the contouring study, the smaller variabilities of our study likely originate from the fact that the present study is performed with the assistance of well visible fiducial gold markers, in a single institute, with one set of instructions and training for all observers. Furthermore, the registration in our study started with an automated step, defining a good starting point for the registration and leaving the amount of manual interaction limited.

The mean difference between the normalized dosimetric parameters achieved with TRUS–CBCT and MRI–CBCT registration was <1% for V_{100} and D_{90} . We do not consider these differences to be clinically relevant.

MRI provides superior soft-tissue contrast compared to TRUS and CT.²⁷ It is possible to visualize suspect lesions in the prostate and define a volume for focal²⁸ or differential dose prescription brachytherapy.²⁹ The registration of TRUS and MRI datasets to CBCT introduces additional uncertainties. Table 7.1 shows that the intra- and interobserver variability is in the order of 1 to 3% for the prostate V_{100} and D_{90} and the urethral

²⁷ Brabandere *et al.*, 2012; Smith *et al.*, 2007.

²⁸ Tong *et al.*, 2013.

²⁹ Rylander *et al.*, 2015.

D_{30} . These values are expected to be higher for smaller volumes, e.g. focal or intraprostatic boost volumes.³⁰ Therefore, when incorporating a pretreatment MRI in the implantation procedure, treatment margins should be applied to correct for the registration uncertainties.³¹

³⁰ Polders *et al.*, 2015.

³¹ Rylander *et al.*, 2015.

General

Contouring and registration can be affected by the slice distance and slice thickness of the studied image data sets. Particularly, using TRUS, the variability in contouring of the base and the apex may be lower with closer spaced slices. Also the registration variability may reduce with closer spaced slices. Furthermore, the TPS affects the results. The automatic point based image registration, volume determination and dosimetric parameter calculation may depend on the software that is used.

The dosimetric inter- and intraobserver variability of TRUS contouring is higher than the variability in the registrations. The quality of the procedure can be improved most by reducing the greatest source of uncertainty: contouring variability.

Our study showed that within our institute, having the same training and protocols, the interobserver variability was considerably smaller than the values reported by De Brabandere *et al.* (2012). This demonstrates that training and guidelines can lead to better consensus in prostate contouring. This conclusion is in agreement with a study from Khoo *et al.* (2012), who reported reduced inter- and intraobserver variability after three training sessions, even for experienced radiation oncologists.

In our dynamic dosimetry procedure we strive to solve underdosages during the implantation procedure.³² Adaptations should not be made if the underdosage is an undesirable side effect of the registration of two datasets or a result of contouring variability. The present study points out that the variabilities in V_{100} , of 2.0% and 1.6% caused by registration and contouring, respectively (table 7.1), were smaller than the magnitude of underdosages we adapt ($9 \pm 6\%$).³³ The adaptation resulted in an increase of $15 \pm 9\%$ in D_{90} , whereas variabilities in D_{90} caused by registration and contouring were 3% and 9%, respectively (table 7.1). The underdosages that we observed in the implantation procedure are predominantly caused by other factors than registration or contouring variability. In our procedure, implant dynamics (e.g. edema

³² Westendorp *et al.*, 2007, 2016.

³³ Westendorp *et al.*, 2016.

³⁴ Westendorp *et al.*, 2017a, 2016.

³⁵ Khoo *et al.*, 2012.

³⁶ Westendorp *et al.*, 2015.

³⁷ Gellekom *et al.*, 2004.

and seed displacement) are therefore the main cause of underdosages that are adapted during implantation.³⁴

Both, contouring and registration, can be improved. Consistency of contouring can be increased by using guidelines and training.³⁵ Furthermore, accuracy can be gained in the registration procedure. For instance, the speed and accuracy of TRUS–CBCT registration could increase by applying a registration that uses all seeds that are localized on TRUS and CBCT.³⁶ Ideally the implantation is performed under live MRI-guidance,³⁷ obviating the registration step.

Conclusion

Prostate dosimetry is affected by interobserver contouring (2% for V_{100} , 9% for D_{90}) and registration variability (D_{90} , 3% for TRUS–CBCT and 2% for MRI–CBCT). The base and apex of the prostate show more geometric contouring variability than the central part. The observed dosimetrical variability is smaller than underdosages that are adapted during our dynamic brachytherapy procedure.

Appendix A: Calculation of the inter- and intraobserver variabilities

Each implant has its specific dosimetric parameters. We normalised these, for each implant, to the according reference dataset. All values were normalised to the values for the reference dataset in case of interobserver variability and to the mean of the observations in case of intraobserver variability.

The standard deviation was determined using [equation \(7.1\)](#) for interobserver variability and using [equation \(7.2\)](#) for intraobserver variability.

$$SD_{\text{inter}} = \sqrt{\frac{1}{P \ O \ S} \sum_{p=1}^P \sum_{o=1}^O \sum_{s=1}^S \left(\frac{X_{p,o,s}}{R_p} - \bar{R} \right)^2}, \quad (7.1)$$

with $\bar{R} = 1$ as a result of normalization,

$$SD_{\text{intra}} = \sqrt{\frac{1}{P \ O \ S} \sum_{p=1}^P \sum_{o=1}^O \sum_{s=1}^S \left(\frac{X_{p,o,s}}{\frac{1}{S} \sum_{s=1}^S X_{p,o,s}} - \bar{X} \right)^2},$$

$$\text{with } \bar{X} = \frac{1}{P \ O \ S} \sum_{p=1}^P \sum_{o=1}^O \sum_{s=1}^S \frac{X_{p,o,s}}{\frac{1}{S} \sum_{s=1}^S X_{p,o,s}}. \quad (7.2)$$

Where P represents the number of patients, O the number of observers and S the number of sessions. $X_{p,o,s}$ described the dosimetric parameter obtained for patient p by observer o during session s . R_p denotes the reference dosimetric parameter of patient p of the respective study, TRUS or CT.

To determine the geometrical variabilities, the distance between the patients reference contours (inter) or average of the three contouring sessions (intra) and the observer contours was calculated per sample point. This was averaged per structure or part before calculating SD_{geom} according to [equation \(7.3\)](#).

$$SD_{\text{geom}} = \sqrt{\frac{1}{P \ O \ S} \sum_{p=1}^P \sum_{o=1}^O \sum_{s=1}^S \left(D_{p,o,s} - \bar{D} \right)^2},$$

$$\text{with } \bar{D} = \frac{1}{P \ O \ S} \sum_{p=1}^P \sum_{o=1}^O \sum_{s=1}^S D_{p,o,s} \quad (7.3)$$

$D_{p,o,s}$ describes the average distance for patient p contoured by observer o during session s . For the interobserver variability, it was calculated as

$$D_{p,o,s} = \frac{1}{N} \sum_{n=1}^N \left(RO_{p,o,s,n} - RR_{p,n} \right), \quad (7.4)$$

with $RO_{p,o,s,n}$ as the observer absolute vector length for a point and $RR_{p,n}$ as the reference vector length for that point. N is the total number of sample points of the investigated structure.

For the intraobserver variability, it was calculated as

$$D_{p,o,s} = \frac{1}{N} \sum_{n=1}^N \left(RO_{p,o,s,n} - \frac{1}{S} \sum_{s=1}^S RO_{p,o,s,n} \right). \quad (7.5)$$

Chapter 8

Summary

THE AIM OF ^{125}I PROSTATE BRACHYTHERAPY is to cover the prostate with an adequate dose to control local disease and, at the same time, limit dose to healthy structures to minimize toxicity of the treatment.

The AAPM, ABS and GEC/ESTRO recommend to perform postimplant dosimetry approximately a month after implantation. Underdosages often are unnoticed until postimplant dosimetry takes place. However, in most cases, it is practically not feasible to correct underdosages at that time.

IN CHAPTER 2 WE INTRODUCE an efficient dynamic brachytherapy technique to correct underdosages already during the implantation procedure.

CHAPTER 2

After finishing the implant, a transrectal ultrasound (TRUS) scan was acquired on which the prostate was contoured by the physician. On TRUS images, implanted seeds cannot be visualized accurately. Therefore, cone-beam CT (CBCT) images were obtained using an isocentric C-arm. On these images ^{125}I seeds are clearly visible, however, anatomy is poorly visualized on this modality. Dose was calculated using the seed positions obtained with CBCT.

Three fiducial gold markers, being visible on both TRUS and CBCT, were used as reference points to register TRUS and CBCT imaging datasets. Following registration, the contours and the dose distribution were merged providing dosimetry during the implantation procedure. If the physician noticed underdosages at critical locations, an adaptive plan was made and remedial seeds were placed to resolve the underdosage.

In total, 20 patients were included in this pilot study. In 9 cases it was deemed necessary to add on average 4 remedial seeds, which resulted in a mean D_{90} of 108% and an improvement in D_{90} of 11% on average. During this first pilot study, an adaptation was performed within half an hour. This showed that the proposed method was feasible, effective and efficient.

CHAPTER 3

IMPLANTATION OF SEEDS CAUSES TRAUMA, which results in edema (swelling) of the prostate that affects dosimetry. Depending on the time trend and amount of edema this can result in an inadequate dose coverage of the target volume. In a study with 20 patients we quantified time trends in edema with 7 consecutive CT series. The change in seed positions was used as surrogate for edema

Two models to quantify prostate edema by scaling of seed distributions were compared, a cylindrical and a spherical model. In the cylindrical model seeds were linked across all 7 CT series. Distributions were aligned and scaled in cylindrical coordinates (radial and longitudinal) from which the volume changes were determined. This scaling reflected the implantation geometry more closely than the spherical model. In that model seeds were not linked, but the distance of the seeds to the center of gravity was used as a measure to determine the volume change.

The cylindrical model showed a prostate volume decrease of 18% in the first month after implantation, the spherical model demonstrated a decrease of 12%. One day after implantation both models showed a 9% larger volume than at one month. Apart from Day 0, both models provided similar estimated prostate volume changes. The amount of edema (during the first month after implantation) was relatively small in comparison with some values reported in literature (up to 100%), but showed good agreement with literature that reported results based on MRI imaging.

CHAPTER 4

THE METHOD TO QUANTIFY EDEMA was extended to track individual seeds between two imaging moments, taking into account *stranded* seed geometry. Whereas the cylindrical edema model from chapter 3 is capable of linking relatively similar seed distributions, the new method is more robust. It can link distributions in which seeds are displaced, missing or wrongly identified. The algorithm was applied to TRUS and CBCT data for 699 implants.

After an initial linking step, using the Hungarian Algorithm, strands were identified. In case curvature and distance constraints were violated, seeds were unlinked. If possible, these unlinked seeds were linked to other strands fulfilling the constraints. Finally, non-linked seeds were allowed to link, even when violating constraints to some extent. This process was repeated until a stable linking was reached or the 6th iteration ended.

All results were visually inspected, resulting in 12 uncertain matches and 11 mismatches, out of a total of 699 implants, 12 860 strands and 49 897 seeds. The algorithm was not only accurate, it was also fast: linking the distributions took 42 ms per case on average. With this new method we could analyse differences in seed positions between TRUS and C-arm CBCT based distributions in more detail.

CHAPTER 5

INTRAOPERATIVE EDEMA AND SEED DISPLACEMENT PATTERNS and their effects on dosimetry were identified using the seed tracking algorithm of chapter 4. Besides, we also studied the relation between TRUS and CBCT based intraoperative dosimetry and postoperative (Day 30) dosimetry. Using data from 699 patients we found a D_{90} decline of 11% between intraoperative TRUS based and CBCT based dosimetry. Intraoperative CBCT based dosimetry correlated better with Day 30 dosimetry than did TRUS based dosimetry. This correlation of D_{90} improved for both modalities when using a simple equation to compensate for the dosimetric effects of edema. Edema seemed to cause most of the systematic differences in D_{90} between implantation and postimplant dosimetry (Day 30).

Seed displacement patterns between intraoperative TRUS and CBCT were identified for various locations in the prostate. The largest displacements were observed near the rectal wall. This is probably caused by TRUS probe induced prostate deformation. The central and posterior

seeds showed less caudal displacements than did lateral and anterior seeds. Seeds that were implanted close to the base diverged more from the central prostate axis than did seeds close to the apex. The seed displacements, in the patterns we observed, are a plausible cause of underdosages occurring at the anterior base of the prostate.

Many groups reported a dose decline between TRUS based intraoperative and post implant dosimetry. In our study we observed a similar trend. Remarkably, CBCT based dosimetry showed an opposite effect, postimplant dose (D_{90}) is generally higher than intraoperatively CBCT acquired values.

We also showed that neither TRUS nor CBCT based intraoperative dosimetry accurately predict postimplant dosimetry at Day 30 for individual cases, probably because of seed displacements that occur after the patient leaves the operating theater.

CHAPTER 6

DOES CBCT BASED DYNAMIC BRACHYTHERAPY lead to improved postimplant dosimetry? In a study with data from 1266 patients, acquired over a period of 9 years, the dosimetrical effect of adaptations in the dynamic brachytherapy procedure was evaluated. Furthermore, regions that needed adaptation were identified. The CBCT based dynamic brachytherapy technique that was used resembled that of the pilot study (chapter 2) apart from efficiency improvements. In addition to the clinically achieved dosimetry, dosimetry was assessed excluding the dose contribution of the remedial seeds. This allowed us to quantify the dosimetric effect of adaptations also at Day 30.

We correctly selected candidate implants for adaptation by placement of remedial seeds. If these implants would not have been adapted, postimplant dosimetry would have been suboptimal, with half of the group showing an undesirable low V_{100} ($<95\%$).

In 17.4% of the patients an adaptation was performed. This resulted at Day 30 in a D_{90} of 121% and V_{100} of 98%. The group in which no adaptations were performed showed a mean D_{90} of 119% and V_{100} of 98%.

In contrast to a high V_{100} a relatively low V_{150} was obtained. This resulted in a favourable homogeneity index compared to values reported in literature. A low V_{150} correlates with low toxicity of the treatment, substantiating that CBCT based dynamic prostate brachytherapy allows

for high quality implants.

Most remedial seeds were placed near the anterior base of the prostate. The CBCT based implantation procedures were performed in $1\frac{1}{4}$ hour. An adaptation took $\frac{1}{4}$ hour of additional time. In conclusion, this study with a large number of patients showed that the CBCT method is effective and efficient for clinical routine.

THE VARIABILITY OF CONTOURING AND REGISTRATION in our procedure is discussed in chapter 7. The dosimetrical consequences of inter- and intra-observer contouring and registration variability were quantified and compared with the magnitude of the underdosages that were prevented during the adaptations made with the CBCT technique.

CHAPTER 7

Five observers participated in the study and performed 3 sessions on 11 patient datasets to quantify inter- and intra-observer variability. Variabilities were assessed geometrically (contours) and dosimetrically (contours and registrations). Contouring was performed on TRUS and CT image datasets and registrations were performed on TRUS-CBCT and MRI-CBCT. The prostate was subdivided in a superior, central and inferior part to identify the regions with most contouring variability.

Geometric inter-observer variability in contouring was 1.1 mm on average resulting in a dosimetric variability of 1.6% for V_{100} and 9% for D_{90} . TRUS-CBCT registration resulted in a V_{100} variability of 2% and a D_{90} variability of 3%. The superior and inferior part of the prostate showed more variability than the central part.

The study showed that contouring and registration variabilities affected dosimetry but were smaller than underdosages that were adapted in the implantation procedure. This underlines that the CBCT procedure increases dosimetric quality of ^{125}I prostate implants.

Chapter 9

Discussion & future outlook

PROSTATE CANCER PATIENTS treated with permanent ^{125}I brachytherapy have a good prognosis. The 7 – 15 year biochemical control rate is high with reported values of ~85–95% for low risk and ~80–90%¹ for intermediate risk prostate cancer. Adequate dose coverage of the prostate results in good biochemical control.² At the same time, dose should be limited to prevent damage to healthy tissues.³

A ^{125}I prostate brachytherapy procedure should result in good dose coverage for the prostate and limited dose to healthy tissues which should be validated by quality assurance. In case of permanent prostate brachytherapy quality assurance is recommended in the form of postimplant dosimetry.⁴ In techniques that only rely on Day 30 postimplant dosimetry, adaptation of underdosages requires scheduling of an additional procedure,⁵ which has a high threshold to act and is therefore seldom applied. Dynamic ^{125}I brachytherapy brings a great advantage in the potential to prevent underdosages by placing remedial seeds already during the initial implantation procedure.

WE DEVELOPED AND CLINICALLY INTRODUCED a dynamic implantation technique that is guided by TRUS and CBCT. Contouring of the prostate and organs at risk can accurately be performed on TRUS and ex-

¹ Cosset *et al.*, 2016; Crook *et al.*, 2011; Henry *et al.*, 2010; Peters *et al.*, 2017; Potters *et al.*, 2008; Stock *et al.*, 2006; Sylvester *et al.*, 2011; Zelefsky *et al.*, 2007b.

² Henry *et al.*, 2015; Henry *et al.*, 2010; Rasmusson *et al.*, 2016; Stock *et al.*, 2006; Zelefsky *et al.*, 2007b.

³ Keyes *et al.*, 2009; Kollmeier *et al.*, 2012; Merrick *et al.*, 2003; Pinkawa *et al.*, 2006.

⁴ Ash *et al.*, 2000; Davis *et al.*, 2012; Nath *et al.*, 2009; Salembier *et al.*, 2007.

⁵ Doyle *et al.*, 2012; Hughes *et al.*, 2005; Keyes *et al.*, 2004; Kumar *et al.*, 2015; Putora *et al.*, 2013.

act seed localisation is enabled by CBCT. Both modalities were registered using fiducial gold markers, visible on both datasets.

⁶ Nag *et al.*, 2001; Polo *et al.*, 2010.

The goal of a dynamic dose calculation procedure⁶ is to ensure adequate dose coverage while limiting dose to organs at risk for each patient. By identifying the positions of all seeds in the operating theater and determining the corresponding dose, dynamic brachytherapy improves the chance that dose coverage is adequate when the patient leaves the operating room. In our procedure, an adaptation that resolves underdosages can be performed immediately after the initial implantation procedure. In a study with 1266 patients we showed that adequate dose coverage was achieved, intraoperatively and after one month. We showed that we correctly selected implants that needed an adaptation. Without the adaptation approximately half of these implants would have shown a $V_{100} < 95\%$ at Day 30. However, an accurate, individual, prediction of Day 30 dosimetry was not possible. Edema and seeds displacement continue to affect dosimetry, also after the implantation procedure. Therefore postimplant dosimetry remains necessary, even after a dynamic brachytherapy.

⁷ Peters *et al.*, 2017.

In a recent study⁷ we compared treatment outcome in the period without use of the dynamic CBCT method to the period with CBCT use. This study showed that the biochemical relapse free survival significantly improved after introduction of the CBCT method.

DIRECT FEEDBACK ON THE DOSIMETRY of an implant helps radiation oncologists with improving the implantation skills. When we started with the CBCT method, one in four implants needed an adaptation, over the years this fraction decreased gradually to one in ten. For permanent prostate brachytherapy implants, experienced physicians show superior dosimetry compared to inexperienced physicians.⁸ However, even experienced physicians still have cases with poor quality,⁹ possibly because of seed displacements (just) after implantation. The CBCT technique allows for a final dosimetric check in the operating theater and thus enabled adequate dose coverage on Day 30 for almost all patients. This final check provides direct feedback on the implantation, allowing starting physicians to shorten the learning curve and giving both inexperienced and experienced physicians a possibility to compensate for displacements that cannot be predicted.

⁸ Merrick *et al.*, 2011.

⁹ Zelefsky *et al.*, 2013.

TO IMPROVE UNDERSTANDING OF IMPLANT DYNAMICS, we developed a new seed tracking algorithm. This algorithm enables linking of seeds in prostate implants acquired at different times with multiple imaging modalities, such as TRUS and CBCT.

Several applications may benefit from this algorithm. An accurate registration of image datasets is a prerequisite for many dynamic dosimetry techniques such as TRUS-fluoroscopy dynamic dosimetry.¹⁰ Our algorithm, being fast and accurate can be of benefit compared to slower, more complex, approaches such as those proposed by Chng *et al.* (2011) and Lobo *et al.* (2012). Furthermore, it can be used to identify displacements that take place between the implantation procedure and postimplant dosimetry. Probably, its parameters can be set to enable tracking of loose seeds distributions. The strand concept then needs to be replaced by a needle channel concept, with other curvature and distance properties. Another possible application is the comparison of displacements of different seed or strand designs. A better understanding of seed displacements could help to design seeds and strands that anchor in the tissue and limit displacements after implantation.

¹⁰ Kuo *et al.*, 2014.

The algorithm may also be used for automatic registration of datasets with seeds. With a certain number of seeds (automatically) identified, the algorithm can link both distributions and perform a registration. With minor adaptations of the algorithm this registration could also be deformable. Such an automatic registration can be of value to further improve efficiency of the intraoperative procedure and may also be used to register postimplant MRI and CT.

DOSIMETRY OF ¹²⁵I PROSTATE BRACHYTHERAPY is complicated by dynamic processes such as prostate edema and seed displacements. The seed tracking algorithm revealed prostate edema and seed displacements between intraoperative TRUS and CBCT for 699 implants. Edema mainly results from trauma that is caused by needle insertion. In our study we did not observe edema to the extent (50%) that is reported in literature.¹¹ We found volume changes up to 20% which is in agreement with recent studies that are based on MRI.¹² When intraoperative edema is quantified, a simple model¹³ can provide an improved estimate of postimplant dosimetry.

¹¹ Waterman *et al.*, 1998.

¹² Sloboda *et al.*, 2010.

¹³ Moerland, 1998.

Seed displacements are another cause of changes in dosimetry after implantation. The displacements that occur immediately after placement

have been studied and resulting underdosed subvolumes identified. The underdosages could adequately be compensated by placing remedial seeds.

MOST COVERAGE DEFICIENCIES were observed near the anterior base of the prostate. This is in agreement with the observations of other groups.¹⁴ It is disputed if tumor foci occur less often in the anterior base of the prostate¹⁵ and if this region should be covered by the prescribed dose.¹⁶ If coverage in (parts of) the prostate could be lower, toxicity of the treatment might decrease. It would be interesting to look more in detail which dose should be prescribed to which prostate region.¹⁷ Probably an index lesion should receive the highest dose, while other parts of the prostate can be treated with a lower dose than currently prescribed.¹⁸

A dynamic implantation technique exhibits considerable advantages over other techniques if the dose prescription becomes more complex. For example, the prostate can be implanted at the 'low' dose level, after which dosimetry is obtained. In a second step, the 'high' dose to the index lesion can be added, together with adaptation of underdosages in the low dose region. It has been suggested to use multiple source strengths in such an approach.¹⁹ The seed tracking algorithm could assist in identifying the sources and their respective strengths.

In selected cases the prostate could be treated partially or *focally*. In these treatments dose is prescribed to half of the prostate (hemi gland) or even smaller volumes, like the index lesion.²⁰ Laing *et al.* (2016) report a significant dose reduction to organs at risk in hemi gland treatments. Also for focal treatments the CBCT technique may help to accurately treat the region. Al-Qaisieh *et al.* (2015) showed that in focal treatments seed positioning is more critical than in whole prostate treatments, particularly if small lesions are treated. Our CBCT based dynamic technique allows for more accurate seed reconstruction than TRUS based approaches. This higher accuracy could be of benefit in focal prostate brachytherapy.

Starting with a new treatment approach, physicians need to be trained to adopt the new technique. We have shown that immediate dosimetric feedback helps to improve the treatment practice. For example, the use of the CBCT technique in a focal setting could accelerate the learning process.²¹

¹⁴ Merrick *et al.*, 2014; Moerland *et al.*, 2009; Nasser *et al.*, 2014; Spadinger *et al.*, 2015.

¹⁵ Bittner *et al.*, 2013; D'Amico *et al.*, 1999; Merrick *et al.*, 2007.

¹⁶ Spadinger *et al.*, 2015, 2011.

¹⁷ Haworth *et al.*, 2016.

¹⁸ Rylander *et al.*, 2015.

¹⁹ Mahdavi *et al.*, 2016; Todor *et al.*, 2011.

²⁰ Butler *et al.*, 2016.

²¹ Acher *et al.*, 2006; HW Liu *et al.*, 2010; Thaker *et al.*, 2014.

Focal prostate brachytherapy develops also into the direction of high dose rate (HDR) treatments, in which the C-arm CBCT technique can increase accuracy.

HIGH DOSE RATE (HDR) PROSTATE BRACHYTHERAPY treatments in our department are conducted with the C-arm CBCT as an addition to TRUS. Even *et al.* (2014) showed that needles were reconstructed more accurately on CBCT images than on TRUS images, improving the accuracy of the procedure. Using the C-arm CBCT unit, the patient can be imaged in treatment position. This could also be of benefit for other (fractionated) brachytherapy treatments, in which the position of the applicator with respect to the geometry need to be checked before treatment can commence. Most MRI and CT rooms are not adequately shielded to allow HDR brachytherapy and furthermore these imaging systems usually have a too tight schedule for HDR treatments. With the mobile C-arm CBCT an accurate 3D reconstruction can be made in a brachytherapy suite. Fiducial gold markers or surgical clips can provide references for the anatomy.

THERE ARE SEVERAL ALTERNATIVE METHODS to perform dynamic dosimetry. Since a TRUS only approach does not provide an accurate overview of the final seed positions, other imaging modalities need to be combined for accurate dosimetry.²²

Another approach is the combined use of TRUS and fluoroscopy. In addition to TRUS equipment, in many operating theaters the brachytherapy team has C-arm fluoroscopy available. Generally, a C-arm is used to make (2D) fluoroscopy images of the implant to obtain a qualitative measure of the implant geometry. However, by combining multiple 2D fluoroscopy images under different angles, a 3D reconstruction of the implant can be made. This is an attractive option because no additional investments in hardware need to be made. Several groups have developed algorithms to perform this type of reconstructions.²³ However, the clinical experience with TRUS-fluoroscopy dynamic planning is scarce. Today it is only applied in experimental settings. To let this approach break through it needs to become generally available in treatment planning software.

A more advanced technique with additional potential is MRI based implantation.²⁴ MRI allows for visualization of lesions within the prostate, enabling higher precision techniques, like focal therapy. There are

²² Chauveinc *et al.*, 2004; Han *et al.*, 2003b; Polo *et al.*, 2010; Xue *et al.*, 2005.

²³ Fallavollita *et al.*, 2010; French *et al.*, 2005; Gong *et al.*, 2002; Kuo *et al.*, 2014; Su *et al.*, 2004; Todor *et al.*, 2003.

²⁴ Gellekom *et al.*, 2004; Patriciu *et al.*, 2007.

²⁵ Leeuw *et al.*, 2013.

developments to perform seed localisation with MRI as well.²⁵ Downsides of this technique are the low availability of MRI systems equipped for brachytherapy, the cost and the limited space inside the bore to implant the prostate. The limited space requires the use of robotic systems to place ¹²⁵I seeds in the prostate.²⁶

²⁶ Bosch *et al.*, 2010; Song *et al.*, 2010.

IN CONCLUSION, WE INTRODUCED A NEW, cost-effective, efficient, accurate C-arm CBCT based dynamic prostate brachytherapy technique in clinical practice. Adaptations to prevent underdosages proved to be effective, intraoperatively as well as at postimplant dosimetry. Biochemical disease free survival of our ¹²⁵I prostate brachytherapy treatment increased significantly after introduction of the technique. Understanding of implant dynamics, resulting from edema and seed displacements, was gained by application of an automatic and fast linking method. The method provides immediate feedback in the operating theater and therefore shortens the learning curve for starting professionals and promotes continuous quality improvement for experienced professionals. It furthermore enables a safe introduction of new prostate brachytherapy treatments quickly leading to a high quality routine.

Bibliography

- Acher P, Popert R, Nichol J, Potters L, Morris S and Beaney R (2006). 'Permanent prostate brachytherapy: Dosimetric results and analysis of a learning curve with a dynamic dose-feedback technique.' *Int J Radiat Oncol Biol Phys*, 65 (3):694–8.
- Acher P, Puttagunta S, Rhode K *et al.* (2010). 'An analysis of intraoperative versus post-operative dosimetry with CT, CT-MRI fusion and XMR for the evaluation of permanent prostate brachytherapy implants.' *Radiother Oncol*, 96(2):166–71.
- Althof V, Haaren P van, Westendorp H *et al.* (2012). 'A quality assurance tool for helical tomotherapy using a step-wedge phantom and the on-board MVCT detector.' *J Appl Clin Med Phys*, 13 (1):3585.
- Ash D, Flynn A, Battermann J *et al.* (2000). 'ESTRO/EAU/EORTC recommendations on permanent seed implantation for localized prostate cancer.' *Radiother Oncol*, 57(3):315–21.
- Ash D, Al-Qaisieh B, Bottomley D, Carey B and Joseph J (2006). 'The correlation between D90 and outcome for I-125 seed implant monotherapy for localised prostate cancer.' *Radiother Oncol*, 79(2):185–9.
- Barentsz JO, Richenberg J, Clements R *et al.* (2012). 'ESUR prostate MR guidelines 2012.' *Eur Radiol*, 22(4):746–57.
- Beaulieu L, Evans DAR, Aubin S *et al.* (2007). 'Bypassing the learning curve in permanent seed implants using state-of-the-art technology.' *Int J Radiat Oncol Biol Phys*, 67(1):71–77.
- Bittner N, Merrick GS, Butler WM, Bennett A and Galbreath RW (2013). 'Incidence and pathological features of prostate cancer detected on transperineal template guided mapping biopsy after negative transrectal ultrasound guided biopsy.' *The Journal of urology*, 190 (2):509–14.
- Bosch MR van den, Moman MR, Vulpen M van *et al.* (2010). 'MRI-guided robotic system for transperineal prostate interventions: proof of principle.' *Phys Med Biol*, 55(5):N133–N140.
- Bowes D, Crook JM, Araujo C and Batchelar D (2013). 'Ultrasound-CT fusion compared with MR-CT fusion for postimplant dosimetry in permanent prostate brachytherapy.' *Brachytherapy*, 12(1):38–43.

- Brabandere M de, Hoskin P, Haustermans K, Heuvel F van den and Siebert FA (2012). 'Prostate post-implant dosimetry: interobserver variability in seed localisation, contouring and fusion.' *Radiother Oncol*, 104(2):192–8.
- Butler WM and Merrick GS (2016). 'Focal prostate brachytherapy with ^{103}Pd seeds'. *Physica Med*, 32(3):459–64.
- Chauveinc L, Flam T, Solignac S *et al.* (2004). 'Prostate cancer brachytherapy: is real-time ultrasound-based dosimetry predictive of subsequent CT-based dose distribution calculation? A study of 450 patients by the Institut Curie/Hospital Cochin (Paris) Group.' *Int J Radiat Oncol Biol Phys*, 59(3):691–5.
- Chng N, Spadinger I, Morris WJ, Usmani N and Salcudean S (2011). 'Prostate brachytherapy postimplant dosimetry: automatic plan reconstruction of stranded implants.' *Med Phys*, 38(1):327–42.
- Cosset JM, Flam T, Belin L *et al.* (2016). 'Long-term results of permanent implant prostate cancer brachytherapy: A single-institution study of 675 patients treated between 1999 and 2003'. *Cancer/Radiothérapie*, 20(4):261–7.
- Crezee J, Haaren P van, Westendorp H *et al.* (2009). 'Improving locoregional hyperthermia delivery using the 3-D controlled AMC-8 phased array hyperthermia system: a preclinical study.' *Int J Hyperthermia*, 25(7):581–92.
- Crook J, Borg J, Evans A *et al.* (2011). '10-year experience with I-125 prostate brachytherapy at the Princess Margaret Hospital: results for 1,100 patients'. *Int J Radiat Oncol Biol Phys*, 80(5):1323–9.
- D'Amico AV, Davis A, Vargas SO, Renshaw AA, Jiroutek M and Richie JP (1999). 'Defining the implant treatment volume for patients with low risk prostate cancer: does the anterior base need to be treated?' *Int J Radiat Oncol Biol Phys*, 43(3):587–90.
- Davis BJ, Horwitz EM, Lee WR *et al.* (2012). 'American Brachytherapy Society consensus guidelines for transrectal ultrasound-guided permanent prostate brachytherapy.' *Brachytherapy*, 11(1):6–19.
- Delouya G, Bahary P, Carrier JF *et al.* (2015). 'Refining prostate seed brachytherapy: Comparing high-, intermediate-, and low-activity seeds for I-125 permanent seed prostate brachytherapy.' *Brachytherapy*, 14(3):329–33.
- Dogan N, Mohideen N, Glasgow GP, Keys K and Flanigan RC (2002). 'Effect of prostatic edema on CT-based postimplant dosimetry.' *Int J Radiat Oncol Biol Phys*, 53(2):483–9.
- Doyle L, Hesney AJ, Chapman KL *et al.* (2012). 'Re-implantation of suboptimal prostate seed implantation: technique with intraoperative treatment planning.' *J Contemp Brachytherapy*, 4 (3):176–81.
- Even AJG, Nuver TT, Westendorp H, Hoekstra CJ, Slump CH and Minken AW (2014). 'High-dose-rate prostate brachytherapy based on registered transrectal ultrasound and in-room cone-beam CT images.' *Brachytherapy*, 13 (2):128–36.
- Fallavollita P, Aghaloo ZK, Burdette EC, Song DY, Abolmaesumi P and Fichtinger G (2010). 'Registration between ultrasound and fluoroscopy or CT in prostate brachytherapy.' *Med Phys*, 37(6):2749–60.

- Farin G and Hansford D (2013). *Practical Linear Algebra: A Geometry Toolbox, Third Edition*. Taylor & Francis, 199–234.
- French D, Morris J, Keyes M, Goksel O and Salcudean S (2005). 'Computing intra-operative dosimetry for prostate brachytherapy using TRUS and fluoroscopy.' *Acad Radiol*, 12(10):1262–72.
- Fuller DB, Jin H, Koziol JA and Feng AC (2005). 'CT-ultrasound fusion prostate brachytherapy: a dynamic dosimetry feedback and improvement method. A report of 54 consecutive cases.' *Brachytherapy*, 4(3):207–16.
- Fuller DB, Koziol JA and Feng AC (2004). 'Prostate brachytherapy seed migration and dosimetry: analysis of stranded sources and other potential predictive factors.' *Brachytherapy*, 3(1):10–19.
- Gellekom MPRV, Moerland MA, Battermann JJ and Lagendijk JJW (2004). 'MRI-guided prostate brachytherapy with single needle method – a planning study'. *Radiother Oncol*, 71(3):327–32.
- Gewanter RM, Wu C, Laguna JL, Katz AE and Ennis RD (2000). 'Intraoperative preplanning for transperineal ultrasound-guided permanent prostate brachytherapy.' *Int J Radiat Oncol Biol Phys*, 48(2):377–80.
- Gong L, Cho PS, Han BH *et al.* (2002). 'Ultrasonography and fluoroscopic fusion for prostate brachytherapy dosimetry.' *Int J Radiat Oncol Biol Phys*, 54(5):1322–30.
- Grimm P, Billiet I, Bostwick D *et al.* (2012). 'Comparative analysis of prostate-specific antigen free survival outcomes for patients with low, intermediate and high risk prostate cancer treatment by radical therapy. Results from the Prostate Cancer Results Study Group.' *BJU Int*, 109 Suppl 1:22–29.
- Haaren PMA van, Riet A van't, Moerland MA, Koedooder C and Westendorp H (2011). 'Dose to fingertips of staff preparing stranded iodine-125 seeds for permanent prostate implants.' *Radiat Prot Dosimetry*, 145(1):61–65.
- Han BH, Wallner K, Merrick G, Badiozamani K and Butler W (2003a). 'The effect of interobserver differences in post-implant prostate CT image interpretation on dosimetric parameters.' *Med Phys*, 30(6):1096–102.
- Han BH, Wallner K, Merrick G, Butler W, Sutlief S and Sylvester J (2003b). 'Prostate brachytherapy seed identification on post-implant TRUS images.' *Med Phys*, 30(5):898–900.
- Haworth A, Mears C, Betts JM *et al.* (2016). 'A radiobiology-based inverse treatment planning method for optimisation of permanent I-125 prostate implants in focal brachytherapy.' *Physics in medicine and biology*, 61 (1):430–44.
- Henry AM, Rodda SL, Mason M *et al.* (2015). 'The effect of dose and quality assurance in early prostate cancer treated with low dose rate brachytherapy as monotherapy.' *Clin Oncol*, 27(7):382–6.
- Henry AM, Al-Qaisieh B, Gould K *et al.* (2010). 'Outcomes following iodine-125 monotherapy for localized prostate cancer: the results of Leeds 10-year single-center brachytherapy experience.' *Int J Radiat Oncol Biol Phys*, 76(1):50–56.

- Hinnen KA, Battermann JJ, Roermund JGH van *et al.* (2010a). 'Long-term biochemical and survival outcome of 921 patients treated with I-125 permanent prostate brachytherapy.' *Int J Radiat Oncol Biol Phys*, 76(5):1433–8.
- Hinnen KA, Moerland MA, Battermann JJ *et al.* (2010b). 'Loose seeds versus stranded seeds in I-125 prostate brachytherapy: differences in clinical outcome.' *Radiother Oncol*, 96(1):30–33.
- Holm HH, Juul N, Pedersen JF, Hansen H and Strøyer I (1983). 'Transperineal ^{125}I Iodine seed implantation in prostatic cancer guided by transrectal ultrasonography.' *J Urol*, 130(2):283–6.
- Hughes L, Waterman FM and Dicker AP (2005). 'Salvage of suboptimal prostate seed implantation: Reimplantation of underdosed region of prostate base.' *Brachytherapy*, 4(2):163–70.
- Hunter J (2007). 'Matplotlib: A 2D Graphics Environment'. *Comput Sci Eng*, 9(3):90–95.
- Igdbashian L, Donath D, Carrier JF *et al.* (2008). 'Poor predictive value of intraoperative real-time dosimetry for prostate seed brachytherapy.' *Int J Radiat Oncol Biol Phys*, 72(2):605–9.
- IKNL (2016a). *Cijfers over kanker*. Ed. by Integraal Kankercentrum Nederland. URL: <http://www.cijfersoverkanker.nl/> (visited on 19/10/2016).
- IKNL (2016b). *Oncoline*. Ed. by Integraal Kankercentrum Nederland. URL: <http://oncoline.nl/> (visited on 31/10/2016).
- Ishiyama H, Nakamura R, Satoh T *et al.* (2010). 'Differences between intraoperative ultrasound-based dosimetry and postoperative computed tomography-based dosimetry for permanent interstitial prostate brachytherapy.' *Brachytherapy*, 9(3):219–23.
- Ishiyama H, Sekiguchi A, Satoh T *et al.* (2016). 'Dosimetry of permanent interstitial prostate brachytherapy for an interoperative procedure, using O-arm based CT and TRUS.' *J Contemp Brachytherapy*, 8(1):7–16.
- Jain AK, Zhou Y, Mustufa T, Burdette EC, Chirikjian GS and Fichtinger G (2005). 'Matching and reconstruction of brachytherapy seeds using the Hungarian algorithm (MARSHAL).' *Med Phys*, 32(11):3475–92.
- Jastaniyah N, Sloboda R, Kamal W *et al.* (2013). 'Regional treatment margins for prostate brachytherapy.' *Brachytherapy*, 12(6):596–602.
- Kaplan ID, Meskell P, Oldenburg NE, Saltzman B, Kearney GP and Holupka EJ (2006). 'Real-time computed tomography dosimetry during ultrasound-guided brachytherapy for prostate cancer.' *Brachytherapy*, 5(3):147–51.
- Keyes M, Miller S, Moravan V *et al.* (2009). 'Predictive factors for acute and late urinary toxicity after permanent prostate brachytherapy: long-term outcome in 712 consecutive patients.' *Int J Radiat Oncol Biol Phys*, 73(4):1023–32.
- Keyes M, Pickles T, Agranovich A, Kwan W and Morris WJ (2004). ' ^{125}I reimplantation in patients with poor initial dosimetry after prostate brachytherapy.' *Int J Radiat Oncol Biol Phys*, 60(1):40–50.
- Kho0 ELH, Schick K, Plank AW *et al.* (2012). 'Prostate contouring variation: can it be fixed?' *Int J Radiat Oncol Biol Phys*, 82(5):1923–9.

- Kirisits C, Rivard MJ, Baltas D *et al.* (2014). 'Review of clinical brachytherapy uncertainties: analysis guidelines of GEC-ESTRO and the AAPM.' *Radiother Oncol*, 110 (1):199–212.
- Kollmeier M, Scala L, Kunaprayoon D *et al.* (2012). 'V150 predicts erectile outcome in patients undergoing low-dose-rate (LDR) brachytherapy alone for prostate cancer'. *Radiother Oncol*, 103(103):S81–.
- Kuhn HW (1955). 'The Hungarian method for the assignment problem'. *Nav Res Logist Q*, 2(1-2):83–97.
- Kumar R, Le Y, Deweese T and Song DY (2015). 'Re-implantation following suboptimal dosimetry in low-dose-rate prostate brachytherapy: technique for outpatient source insertion using local anesthesia'. *J Radiat Oncol*, 5(1):103–8.
- Kuo N, Dehghan E, Deguet A *et al.* (2014). 'An image-guidance system for dynamic dose calculation in prostate brachytherapy using ultrasound and fluoroscopy.' *Med Phys*, 41(9):091712.
- Laing R, Franklin A, Uribe J, Horton A, Uribe-Lewis S and Langley S (2016). 'Hemi-gland focal low dose rate prostate brachytherapy: An analysis of dosimetric outcomes'. *Radiother Oncol*, 121(2):310–5.
- Langley S, Ahmed HU, Al-Qaisieh B *et al.* (2012). 'Report of a consensus meeting on focal low dose rate brachytherapy for prostate cancer.' *BJU Int*, 109 Suppl 1:7–16.
- Leclerc G, Lavallée MC, Roy R, Vigneault E and Beaulieu L (2006). 'Prostatic edema in ^{125}I permanent prostate implants: dynamical dosimetry taking volume changes into account.' *Med Phys*, 33(3):574–83.
- Leeuw H de, Seevinck P and Bakker C (2013). 'Center-out radial sampling with off-resonant reconstruction for efficient and accurate localization of punctate and elongated paramagnetic structures'. *Magn Reson Med*, 69(6):1611–22.
- Liu D, Meyer T, Usmani N *et al.* (2015). 'Implanted brachytherapy seed movement reflecting transrectal ultrasound probe-induced prostate deformation.' *Brachytherapy*, 14(6):809–17.
- Liu D, Usmani N, Ghosh S *et al.* (2012). 'Comparison of prostate volume, shape, and contouring variability determined from preimplant magnetic resonance and transrectal ultrasound images.' *Brachytherapy*, 11(4):284–91.
- Liu HW, Malkoske K, Sasaki D *et al.* (2010). 'The dosimetric quality of brachytherapy implants in patients with small prostate volume depends on the experience of the brachytherapy team.' *Brachytherapy*, 9 (3):202–7.
- Lobo JR, Moradi M, Chng N *et al.* (2012). 'Use of needle track detection to quantify the displacement of stranded seeds following prostate brachytherapy.' *IEEE Trans Med Imaging*, 31(3):738–48.
- Mahdavi SS, Spadinger IT, Chng NT and Morris WJ (2016). 'Robustness to source displacement in dual air kerma strength planning for focal low-dose-rate brachytherapy of prostate cancer.' *Brachytherapy*, 15 (5):642–9.
- Matzkin H, Chen J, German L and Mabweesh NJ (2013). 'Comparison between pre-operative and real-time intraoperative planning ^{125}I permanent prostate brachytherapy: long-term clinical biochemical outcome'. *Radiat Oncol*, 8(1):288.

- McKinney W (2010). 'Data structures for statistical computing in Python'. *Proceedings of the 9th Python in Science Conference*, 51–56.
- McLaughlin P, Narayana V, Pan C *et al.* (2006). 'Comparison of day 0 and day 14 dosimetry for permanent prostate implants using stranded seeds.' *Int J Radiat Oncol Biol Phys*, 64(1):144–50.
- McParland N, Chng N and Keyes M (2013). 'The dosimetric impact of supplementing pre-planned prostate implants with discretionary ¹²⁵I seeds'. *J Radiother Pract*, 12(03):226–36.
- Merrick GS, Butler WM, Dorsey AT and Walbert HL (1998). 'Influence of timing on the dosimetric analysis of transperineal ultrasound-guided, prostatic conformal brachytherapy.' *Radiat Oncol Investig*, 6(4):182–90.
- Merrick GS, Butler WM, Grimm P *et al.* (2014). 'Multisector prostate dosimetric quality: Analysis of a large community database.' *Brachytherapy*, 13(2):146–51.
- Merrick GS, Butler WM, Wallner KE *et al.* (2003). 'Dysuria after permanent prostate brachytherapy.' *Int J Radiat Oncol Biol Phys*, 55(4):979–85.
- Merrick GS, Gutman S, Andreini H *et al.* (2007). 'Prostate cancer distribution in patients diagnosed by transperineal template-guided saturation biopsy.' *Eur Urol*, 52 (3):715–23.
- Merrick GS, Lief JH, Grimm P, Sylvester J, Butler WM and Allen ZA (2011). 'The effect of Pro-Qura case volume on post-implant prostate dosimetry.' *Int J Radiat Oncol Biol Phys*.
- Moerland MA, Wijrdeman HK, Beersma R, Bakker CJ and Battermann JJ (1997). 'Evaluation of permanent I-125 prostate implants using radiography and magnetic resonance imaging.' *Int J Radiat Oncol Biol Phys*, 37(4):927–33.
- Moerland MA (1998). 'The effect of edema on postimplant dosimetry of permanent iodine-125 prostate implants: a simulation study'. *J Brachyther Int*, 14:225–32.
- Moerland MA, Deursen MJ van, Elias SG, Vulpen M van, Jürgenliemk-Schulz IM and Battermann JJ (2009). 'Decline of dose coverage between intraoperative planning and post implant dosimetry for I-125 permanent prostate brachytherapy: comparison between loose and stranded seed implants.' *Radiother Oncol*, 91(2):202–6.
- Mueller A, Wallner K, Merrick G *et al.* (2002). 'Modification of prostate implants based on postimplant treatment margin assessment.' *Med Phys*, 29(12):2782–7.
- Nag S, Beyer D, Friedland J, Grimm P and Nath R (1999). 'American Brachytherapy Society (ABS) recommendations for transperineal permanent brachytherapy of prostate cancer.' *Int J Radiat Oncol Biol Phys*, 44(4):789–99.
- Nag S, Bice W, DeWyngaert K, Prestidge B, Stock R and Yu Y (2000). 'The American Brachytherapy Society recommendations for permanent prostate brachytherapy postimplant dosimetric analysis.' *Int J Radiat Oncol Biol Phys*, 46(1):221–30.

- Nag S, Ciezki JP, Cormack R *et al.* (2001). 'Intraoperative planning and evaluation of permanent prostate brachytherapy: report of the American Brachytherapy Society.' *Int J Radiat Oncol Biol Phys*, 51(5):1422–30.
- Nag S, Shi P, Liu B, Gupta N, Bahnson RR and Wang JZ (2008). 'Comparison of real-time intraoperative ultrasound-based dosimetry with postoperative computed tomography-based dosimetry for prostate brachytherapy.' *Int J Radiat Oncol Biol Phys*, 70(1):311–7.
- Narayana V, Roberson PL, Pu AT, Sandler H, Winfield RH and McLaughlin PW (1997). 'Impact of differences in ultrasound and computed tomography volumes on treatment planning of permanent prostate implants.' *Int J Radiat Oncol Biol Phys*, 37(5):1181–5.
- Nasser NJ, Sappiatzer J, Wang Y, Borg J and Saibishkumar EP (2015). 'Dosimetric evaluation of clinical target volume in the postimplant analysis of low-dose-rate brachytherapy for prostate cancer.' *Brachytherapy*, 14(2):189–96.
- Nasser NJ, Wang Y, Borg J and Saibishkumar EP (2014). 'Sector analysis of dosimetry of prostate cancer patients treated with low-dose-rate brachytherapy.' *Brachytherapy*, 13(4):369–74.
- Nath R, Bice WS, Butler WM *et al.* (2009). 'AAPM recommendations on dose prescription and reporting methods for permanent interstitial brachytherapy for prostate cancer: report of Task Group 137.' *Med Phys*, 36(11):5310–22.
- Ohashi T, Yorozu A, Toya K *et al.* (2007). 'Comparison of intraoperative ultrasound with postimplant computed tomography–dosimetric values at Day 1 and Day 30 after prostate brachytherapy.' *Brachytherapy*, 6(4):246–53.
- Oliphant TE (2007). 'Python for Scientific Computing'. *Comput Sci Eng*, 9(3):10–20.
- Orio P, Wallner K, Merrick G *et al.* (2007). 'Dosimetric parameters as predictive factors for biochemical control in patients with higher risk prostate cancer treated with Pd-103 and supplemental beam radiation.' *Int J Radiat Oncol Biol Phys*, 67(2):342–6.
- Pasteau O and Degrais P (1914). 'The radium treatment of cancer of the prostate.' *Arch Roentg Ray*, (28):396–410.
- Patriciu A, Petrisor D, Muntener M, Mazilu D, Schar M and Stoianovici D (2007). 'Automatic brachytherapy seed placement under MRI guidance'. *IEEE T Bio-Med Eng*, 54(8):1499–506.
- Perez F and Granger BE (2007). 'IPython: a system for interactive scientific computing'. *Comput Sci Eng*, 9(3):21–29.
- Peters M, Voort van Zyp JRN van der, Moerland MA *et al.* (2016a). 'Development and internal validation of a multivariable prediction model for biochemical failure after whole-gland salvage iodine-125 prostate brachytherapy for recurrent prostate cancer.' *Brachytherapy*, 15 (3):296–305.
- Peters M, Hoekstra CJ, Voort van Zyp JRN van der *et al.* (2016b). 'Rectal dose constraints for salvage iodine-125 prostate brachytherapy.' *Brachytherapy*, 15 (1):85–93.

- Peters M, Smit Duijzentkunst DA, Westendorp H *et al.* (2017). 'Adaptive cone-beam CT planning improves long-term biochemical disease-free survival for ^{125}I prostate brachytherapy'. *Brachytherapy*.
- Peters M, Voort van Zyp JRN van der, Moerland MA *et al.* (2016c). 'Multivariable model development and internal validation for prostate cancer specific survival and overall survival after whole-gland salvage Iodine-125 prostate brachytherapy.' *Radiother Oncol*, 119 (1):104–10.
- Peters M, Voort van Zyp J van der, Hoekstra C *et al.* (2015). 'Urethral and bladder dosimetry of total and focal salvage Iodine-125 prostate brachytherapy: Late toxicity and dose constraints.' *Radiother Oncol*, 117 (2):262–9.
- Pinkawa M, Fishedick K, Piroth MD *et al.* (2006). 'Health-related quality of life after permanent interstitial brachytherapy for prostate cancer: correlation with postimplant CT scan parameters.' *Strahlenther Onkol*, 182(11):660–5.
- Polders DL, Steggerda MJ, van Herk M *et al.* (2015). 'Establishing implantation uncertainties for focal brachytherapy with I-125 seeds for the treatment of localized prostate cancer.' *Acta Oncol*, 54(6):839–46.
- Polo A, Salembier C, Venselaar J and Hoskin P (2010). 'Review of intraoperative imaging and planning techniques in permanent seed prostate brachytherapy.' *Radiother Oncol*, 94(1):12–23.
- Potters L, Cao Y, Calugaru E, Torre T, Fearn P and Wang XH (2001). 'A comprehensive review of CT-based dosimetry parameters and biochemical control in patients treated with permanent prostate brachytherapy.' *Int J Radiat Oncol Biol Phys*, 50(3):605–14.
- Potters L, Calugaru E, Jassal A and Presser J (2006). 'Is there a role for postimplant dosimetry after real-time dynamic permanent prostate brachytherapy?' *Int J Radiat Oncol Biol Phys*, 65 (4):1014–9.
- Potters L, Morgenstern C, Calugaru E *et al.* (2008). '12-year outcomes following permanent prostate brachytherapy in patients with clinically localized prostate cancer.' *J Urol*, 179 (5 Suppl):S20–S24.
- Potters L, Roach M, Davis BJ *et al.* (2010). 'Postoperative nomogram predicting the 9-year probability of prostate cancer recurrence after permanent prostate brachytherapy using radiation dose as a prognostic variable.' *Int J Radiat Oncol Biol Phys*, 76(4):1061–5.
- Prestidge BR, Bice WS, Kiefer EJ and Prete JJ (1998). 'Timing of computed tomography-based postimplant assessment following permanent transperineal prostate brachytherapy.' *Int J Radiat Oncol Biol Phys*, 40(5):1111–5.
- Puech P, Villers A, Ouzzane A and Lemaitre L (2014). 'Prostate cancer: diagnosis, parametric imaging and standardized report.' *Diagn Interv Imaging*, 95(7–8):743–52.
- Putora PM, Plasswilm L, Seelentag W *et al.* (2013). 'Re-implantation after insufficient primary ^{125}I permanent prostate brachytherapy.' *Radiat Oncol*, 8(1):194.

- Al-Qaisieh B, Ash D, Bottomley DM and Carey BM (2002). 'Impact of prostate volume evaluation by different observers on CT-based post-implant dosimetry.' *Radiother Oncol*, 62(3):267–73.
- Al-Qaisieh B, Mason J, Bownes P *et al.* (2015). 'Dosimetry modeling for focal low-dose-rate prostate brachytherapy.' *Int J Radiat Oncol Biol Phys*, 92(4):787–93.
- Al-Qaisieh B, Witteveen T, Carey B *et al.* (2009). 'Correlation between pre- and postimplant dosimetry for iodine-125 seed implants for localized prostate cancer.' *Int J Radiat Oncol Biol Phys*, 75(2):626–30.
- Raben A, Chen H, Grebler A *et al.* (2004). 'Prostate seed implantation using 3D-computer assisted intraoperative planning vs. a standard look-up nomogram: Improved target conformality with reduction in urethral and rectal wall dose.' *Int J Radiat Oncol Biol Phys*, 60(5):1631–8.
- Rasmusson E, Gunnlaugsson A, Kjellén E *et al.* (2016). 'Low-dose rate brachytherapy with I-125 seeds has an excellent 5-year outcome with few side effects in patients with low-risk prostate cancer.' *Acta Oncol*, 55 (8):1016–21.
- Reed DR, Wallner KE, Narayanan S, Sutlief SG, Ford EC and Cho PS (2005). 'Intraoperative fluoroscopic dose assessment in prostate brachytherapy patients.' *Int J Radiat Oncol Biol Phys*, 63(1):301–7.
- Rivard MJ, Coursey BM, DeWerd LA *et al.* (2004). 'Update of AAPM Task Group No. 43 Report: A revised AAPM protocol for brachytherapy dose calculations.' *Med Phys*, 31(3):633–74.
- Rossum G van *et al.* (1989). 'Python programming language'.
- Rylander S, Polders D, Steggerda MJ, Moonen LM, Tanderup K and Van der Heide UA (2015). 'Re-distribution of brachytherapy dose using a differential dose prescription adapted to risk of local failure in low-risk prostate cancer patients.' *Radiother Oncol*, 115(3):308–13.
- Salembier C, Lavagnini P, Nickers P *et al.* (2007). 'Tumour and target volumes in permanent prostate brachytherapy: A supplement to the ESTRO/EAU/EORTC recommendations on prostate brachytherapy.' *Radiother Oncol*, 83(1):3–10.
- Shah JN, Wu CS, Katz AE, Laguna JL, Benson MC and Ennis RD (2006). 'Improved biochemical control and clinical disease-free survival with intraoperative versus preoperative preplanning for transperineal interstitial permanent prostate brachytherapy.' *Cancer J*, 12 (4):289–97.
- Shaikh T, Zaorsky NG, Ruth K *et al.* (2015). 'Is it necessary to perform week three dosimetric analysis in low-dose-rate brachytherapy for prostate cancer when day o dosimetry is done? A quality assurance assessment.' *Brachytherapy*, 14(3):316–21.
- Shanahan TG, Nanavati PJ, Mueller PW and Maxey RB (2002). 'A comparison of permanent prostate brachytherapy techniques: preplan vs. hybrid interactive planning with postimplant analysis.' *Int J Radiat Oncol Biol Phys*, 53(2):490–6.
- Siebert FA, Brabandere MD, Kirisits C, Kovács G and Venselaar J (2007). 'Phantom investigations on CT seed imaging for interstitial brachytherapy.' *Radiother Oncol*, 85(2):316–23.

- Sloboda R, Usmani N, Pedersen J, Murtha A, Pervez N and Yee D (2010). 'Time course of prostatic edema post permanent seed implant determined by magnetic resonance imaging.' *Brachytherapy*, 9(4):354–61.
- Smith WL, Lewis C, Bauman G *et al.* (2007). 'Prostate volume contouring: A 3D analysis of segmentation using 3DTRUS, CT, and MR.' *Int J Radiat Oncol Biol Phys*, 67(4):1238–47.
- Solhjem MC, Davis BJ, Pisansky TM *et al.* (2004). 'Prostate volume measurement by transrectal ultrasound and computed tomography before and after permanent prostate brachytherapy.' *Int J Radiat Oncol Biol Phys*, 60(3):767–76.
- Song SE, Cho NB, Fischer G *et al.* (2010). 'Development of a pneumatic robot for MRI-guided transperineal prostate biopsy and brachytherapy: New approaches'. *2010 IEEE International Conference on Robotics and Automation*. IEEE, 2580–5.
- Spadinger I, Chu J, Afsari Golshan M *et al.* (2015). 'Regional dose metrics as predictors of biochemical failure and local recurrence after low-dose-rate prostate brachytherapy.' *Brachytherapy*, 14(3):350–8.
- Spadinger I, Morris WJ, Keyes M *et al.* (2011). 'Quadrant dosimetry as a predictor of biochemical relapse in ¹²⁵I prostate brachytherapy.' *Brachytherapy*, 10(2):87–97.
- Steggerda MJ, Boom F van den, Witteveen T and Moonen LMF (2015). 'How well can we predict the dose distribution from TRUS images made at the OR after I-125 brachytherapy of the prostate?' *Radiother Oncol*, 115(S1):S62–S63.
- Steggerda MJ, Moonen LMF, Poel HG van der and Schneider CJ (2007). 'The influence of geometrical changes on the dose distribution after I-125 seed implantation of the prostate.' *Radiother Oncol*, 83(1):11–17.
- Steggerda MJ, Schneider C, Herk M van, Zijp L, Moonen L and Poel H van der (2005). 'The applicability of simultaneous TRUS-CT imaging for the evaluation of prostate seed implants.' *Med Phys*, 32(7):2262–70.
- Stewart J (2015). *Multivariable Calculus*. Cengage Learning, 877–82.
- Stock RG, Stone NN, Tabert A, Iannuzzi C and DeWyngaert JK (1998). 'A dose-response study for I-125 prostate implants.' *Int J Radiat Oncol Biol Phys*, 41(1):101–8.
- Stock RG, Stone NN, Cesaretti JA and Rosenstein BS (2006). 'Biologically effective dose values for prostate brachytherapy: effects on PSA failure and posttreatment biopsy results.' *Int J Radiat Oncol Biol Phys*, 64(2):527–33.
- Stone NN, Hong S, Lo YC, Howard V and Stock RG (2003). 'Comparison of intraoperative dosimetric implant representation with postimplant dosimetry in patients receiving prostate brachytherapy.' *Brachytherapy*, 2(1):17–25.
- Stone NN, Potters L, Davis BJ *et al.* (2007). 'Customized dose prescription for permanent prostate brachytherapy: insights from a multicenter analysis of dosimetry outcomes.' *Int J Radiat Oncol Biol Phys*, 69(5):1472–7.
- Stone NN, Stock RG, Cesaretti JA and Unger P (2010). 'Local Control Following Permanent Prostate Brachytherapy: Effect of High Biologically Effective Dose

- on Biopsy Results and Oncologic Outcomes'. *Int. J. Radiat. Oncol. Biol. Phys.* 76(2):355–60.
- Su Y, Davis BJ, Herman MG and Robb RA (2004). 'Prostate brachytherapy seed localization by analysis of multiple projections: identifying and addressing the seed overlap problem.' *Med Phys*, 31(5):1277–87.
- Sylvester JE, Grimm PD, Wong J, Galbreath RW, Merrick G and Blasko JC (2011). 'Fifteen-year biochemical relapse-free survival, cause-specific survival, and overall survival following ^{125}I prostate brachytherapy in clinically localized prostate cancer: Seattle experience.' *Int J Radiat Oncol Biol Phys*, 81 (2):376–81.
- Tanaka O, Hayashi S, Matsuo M *et al.* (2007). 'Effect of edema on postimplant dosimetry in prostate brachytherapy using CT/MRI fusion.' *Int J Radiat Oncol Biol Phys*, 69(2):614–8.
- Tanderup K, Viswanathan AN, Kirisits C and Frank SJ (2014). 'Magnetic resonance image guided brachytherapy.' *Semin Radiat Oncol*, 24(3):181–91.
- Taussky D, Austen L, Toi A *et al.* (2005). 'Sequential evaluation of prostate edema after permanent seed prostate brachytherapy using CT-MRI fusion.' *Int J Radiat Oncol Biol Phys*, 62(4):974–80.
- Thaker NG, Kudchadker RJ, Swanson DA *et al.* (2014). 'Establishing high-quality prostate brachytherapy using a phantom simulator training program.' *Int J Radiat Oncol Biol Phys*, 90 (3):579–86.
- Todor DA, Zaider M, Cohen GN, Worman MF and Zelefsky MJ (2003). 'Intraoperative dynamic dosimetry for prostate implants.' *Phys Med Biol*, 48(9):1153–71.
- Todor DA, Barani LJ, Lin PS and Anscher MS (2011). 'Moving Toward Focal Therapy in Prostate Cancer: Dual-Isotope Permanent Seed Implants as a Possible Solution'. *Int J Radiat Oncol Biol Phys*, 81(1):297–304.
- Tong WY, Cohen G and Yamada Y (2013). 'Focal low-dose rate brachytherapy for the treatment of prostate cancer.' *Cancer Manag Res*, 5:315–25.
- UpToDate® (2016). *uptodate.com*. URL: <https://www.uptodate.com/contents/active-surveillance-for-men-with-low-risk-clinically-localized-prostate-cancer> (visited on 31/10/2016).
- Vordermark D, Noe M, Markert K *et al.* (2009). 'Prospective evaluation of quality of life after permanent prostate brachytherapy with I-125: importance of baseline symptoms and of prostate-V150.' *Radiother Oncol*, 91(2):217–24.
- Wallner K, Merrick G, True L, Sutlief S, Cavanagh W and Butler W (2003). ' ^{125}I versus ^{103}Pd for low-risk prostate cancer: preliminary PSA outcomes from a prospective randomized multicenter trial.' *Int J Radiat Oncol Biol Phys*, 57(5):1297–303.
- Waterman FM, Yue N, Corn BW and Dicker AP (1998). 'Edema associated with I-125 or Pd-103 prostate brachytherapy and its impact on post-implant dosimetry: an analysis based on serial CT acquisition.' *Int J Radiat Oncol Biol Phys*, 41(5):1069–77.

- Waterman FM, Yue N, Reisinger S, Dicker A and Corn BW (1997). 'Effect of edema on the post-implant dosimetry of an I-125 prostate implant: a case study.' *Int J Radiat Oncol Biol Phys*, 38(2):335–9.
- Westendorp H, Hoekstra CJ, Immerzeel JJ *et al.* (2017a). 'Cone-beam CT-based dynamic planning improves permanent prostate brachytherapy dosimetry: An analysis of 1266 patients'. *Med Phys*.
- Westendorp H, Hoekstra CJ, Riet A van 't, Minken AW and Immerzeel JJ (2007). 'Intraoperative adaptive brachytherapy of iodine-125 prostate implants guided by C-arm cone-beam computed tomography-based dosimetry.' *Brachytherapy*, 6(4):231–7.
- Westendorp H, Kattevilder R, 't Riet A van *et al.* (2012). 'Objective automated assessment of time trends in prostate edema after ^{125}I implantation'. *Brachytherapy*, 11(5) (5):327–33.
- Westendorp H, Nuver TT, Hoekstra CJ, Moerland MA and Minken AW (2016). 'Edema and Seed Displacements Affect Intraoperative Permanent Prostate Brachytherapy Dosimetry'. *Int J Radiat Oncol Biol Phys*, 96(1):197–205.
- Westendorp H, Nuver TT, Moerland MA and Minken AW (2015). 'An automated, fast and accurate registration method to link stranded seeds in permanent prostate implants'. *Phys Med Biol*, 60(20):N391–N403.
- Westendorp H, Riet A van 't, Bouwman R *et al.* (2004). 'Assessment of prostate volume determining parameters in I-125 therapy.' *Radiother Oncol*, 71(S2):S4.
- Westendorp H, Surmann K, Hoekstra CJ *et al.* (2017b). 'Dosimetric impact of inter- and intra-observer variability in contouring and image registration for intraoperative ^{125}I prostate brachytherapy dosimetry.' *Brachytherapy*.
- Wilkinson DA, Lee EJ, Ciezki JP *et al.* (2000). 'Dosimetric comparison of pre-planned and or-planned prostate seed brachytherapy.' *Int J Radiat Oncol Biol Phys*, 48(4):1241–4.
- Xue J, Waterman F, Handler J and Gressen E (2005). 'Localization of linked ^{125}I seeds in postimplant TRUS images for prostate brachytherapy dosimetry.' *Int J Radiat Oncol Biol Phys*, 62(3):912–9.
- Yamada Y, Potters L, Zaider M, Cohen G, Venkatraman E and Zelefsky MJ (2003). 'Impact of intraoperative edema during transperineal permanent prostate brachytherapy on computer-optimized and preimplant planning techniques.' *Am J Clin Oncol*, 26(5):e130–e135.
- Yue N, Chen Z, Peschel R, Dicker AP, Waterman FM and Nath R (1999). 'Optimum timing for image-based dose evaluation of ^{125}I and ^{103}Pd prostate seed implants.' *Int J Radiat Oncol Biol Phys*, 45(4):1063–72.
- Zelefsky MJ, Cohen GN, Bosch WR *et al.* (2013). 'Results from the Quality Research in Radiation Oncology (QRRO) survey: Evaluation of dosimetric outcomes for low-dose-rate prostate brachytherapy.' *Brachytherapy*, 12 (1):19–24.
- Zelefsky MJ, Kuban DA, Levy LB *et al.* (2007a). 'Multi-institutional analysis of long-term outcome for stages T1-T2 prostate cancer treated with permanent seed implantation.' *Int J Radiat Oncol Biol Phys*, 67(2):327–33.

- Zelevsky MJ, Worman M, Cohen GN *et al.* (2010). 'Real-time intraoperative computed tomography assessment of quality of permanent interstitial seed implantation for prostate cancer.' *Urology*, 76(5):1138–42.
- Zelevsky MJ, Yamada Y, Cohen GN *et al.* (2007b). 'Intraoperative real-time planned conformal prostate brachytherapy: post-implantation dosimetric outcome and clinical implications.' *Radiother Oncol*, 84(2):185–9.
- Zelevsky MJ and Zaider M (2006). 'Low-dose-rate brachytherapy for prostate cancer: preplanning vs. intraoperative planning-intraoperative planning is best.' *Brachytherapy*, 5(3):143–4, discussion 146.

Samenvatting

HET DOEL VAN ^{125}I PROSTAAT BRACHYTHERAPIE is een goede dosisbedekking van de prostaat om lokale ziekte onder controle te krijgen en, tegelijkertijd, een dosisbeperking in gezonde weefsels, met als doel bijwerkingen van de behandeling te beperken.

De AAPM, ABS en GEC/ESTRO adviseren om ongeveer één maand na implantatie postimplant-dosimetrie uit te voeren. Onderdoseringen blijven vaak onopgemerkt tot dat moment van dosimetrie. Het is dan vaak in praktijk niet meer haalbaar om onderdoseringen te corrigeren.

IN HOOFDSTUK 2 INTRODUCEREN WE een efficiënte dynamische brachytherapie-techniek waarmee we onderdoseringen al tijdens de implantatieprocedure corrigeren.

HOOFDSTUK 2

Na het voltooiën van het implantaat, werd een transrectale ultrasound (TRUS)-opname verkregen waarop de prostaat door de arts werd ingetekend. Op deze TRUS-beelden kunnen geïmplanteerde zaadjes niet nauwkeurig zichtbaar gemaakt worden. Daarom werden met een isocentrische C-boog cone-beam CT (CBCT)-beelden gemaakt. Op deze beelden zijn de ^{125}I zaadjes duidelijk te onderscheiden; de anatomie is met deze modaliteit echter slecht zichtbaar. Uitgaande van de met CBCT verkregen zaadjes posities werd de dosisverdeling berekend.

Met behulp van drie goudstaafjes als referentiepunten, zichtbaar op zowel TRUS als CBCT, werden de TRUS- en CBCT-beelden geregistreerd (op dezelfde manier gepositioneerd). Daarna werden de intekening en dosisverdeling gecombineerd waarmee, nog tijdens de implantatieprocedure, dosimetrie werd verkregen. Als de arts op kritische plaatsen

onderdoseringen waarnam, werd een adaptief plan gemaakt waarna zaadjes werden bijgeplaatst om de onderdosering op te heffen.

In totaal werden 20 patiënten in deze pilot studie geïncludeerd. In negen gevallen werd het noodzakelijk geacht om gemiddeld vier zaadjes bij te plaatsen. Dat resulteerde in een gemiddelde D_{90} van 108% en een verbetering in D_{90} van 11%. In deze eerste pilot studie kostte het uitvoeren van een adaptatie minder dan een half uur. Daarmee bleek de voorgestelde methode haalbaar, effectief en efficiënt.

HOOFDSTUK 3

HET IMPLANTEREN VAN ZAADJES VEROOORZAAKT LETSEL met zwelling (oedeem) van de prostaat tot gevolg. Deze zwelling beïnvloedt vervolgens de dosimetrie. Afhankelijk van de omvang en het tijdsverloop van het oedeem kan dit tot een ontoereikende dosisbedekking van het doelgebied leiden. In een studie met 20 patiënten kwantificeerden we het tijdsverloop van oedeem met zeven opeenvolgende CT-scans. De verandering van de zaadjesposities werd gebruikt als parameter voor oedeem.

Het prostaatoedeem werd gekwantificeerd door het schalen van de zaadjesverdelingen. Twee modellen werden vergeleken, een cilindrisch en een sferisch model. In het cilindrische model werden zaadjes tussen alle zeven CT-scans gekoppeld. De verdelingen werden uitgelijnd en geschaald in cilindrische coördinaten (radiaal en longitudinaal) waaruit volumeveranderingen bepaald werden. Deze schaling vertoonde meer gelijkenis met de geometrie van het implantaat dan de schaling met het sferische model. In dat model werden zaadjes niet gekoppeld maar werd de afstand van zaadjes tot het zwaartepunt gebruikt als een maat om volumeveranderingen te bepalen.

Het cilindrische model toonde een volumeafname van de prostaat van 18% in de eerste maand na implantatie; het sferische model liet een afname van 12% zien. Eén dag na implantatie demonstreerden beide modellen een 9% groter volume dan na één maand. Afgezien van Dag 0 lieten beide modellen een vergelijkbaar verloop van geschatte prostaat-volumeveranderingen zien. De hoeveelheid oedeem was (gedurende de eerste maand na implantatie) relatief gering in vergelijking met enkele in de literatuur gerapporteerde waarden (tot aan 100%), maar toonde een goede overeenkomst met studies gebaseerd op MRI-beeldvorming.

DE METHODE OM OEDEEM TE KWANTIFICEREN is verder uitgebreid. Hierbij is rekening gehouden met de geometrie van zaadjes in een *strand* (strip). Individuele zaadjes konden zo tussen twee afbeeldingsmomenten worden gevolgd. Waar het cilindrische model van hoofdstuk 3 uitsluitend in staat is om zaadjes in elkaar gelijkende distributies te koppelen, is de nieuwe methode robuuster. De nieuwe methode kan ook distributies koppelen waarbij zaadjes zijn verplaatst, ontbreken of onjuist zijn geïdentificeerd. Het algoritme werd toegepast op TRUS- en CBCT-data van 699 implantaten.

Na een initiële koppeling werden, gebruikmakend van het 'Hongaarse Algoritme', de strands geïdentificeerd. Bij schending van krommings- en afstandsrandvoorwaarden werden de zaadjes ontkoppeld. Zo mogelijk werden deze ontkoppelde zaadjes gekoppeld aan andere strands waarbij de randvoorwaarden wel werden vervuld. Uiteindelijk werden de zaadjes gekoppeld ook als de randvoorwaarden enigszins geschonden werden. Dit proces werd herhaald totdat een stabiele situatie werd bereikt, of na de zesde iteratie.

Alle resultaten werden visueel geïnspecteerd, wat resulteerde in 12 onzekere en 11 incorrecte situaties op een totaal van 699 implantaten, 12 860 strands en 49 897 zaadjes. Het algoritme was niet alleen accuraat, het was ook snel: het koppelen van distributies duurde gemiddeld 42 ms per geval. Met deze nieuwe methode konden we verschillen in zaadjesposities tussen TRUS- en C-boog-CBCT-gebaseerde distributies in meer detail analyseren.

HOOFDSTUK 4

INTRAOPERATIEVE OEDEEM EN ZAADJES-VERPLAATSINGSPATRONEN en de gevolgen op dosimetrie werden bepaald met de methode van hoofdstuk 4. Daarnaast keken we ook naar de relatie tussen TRUS- en CBCT-gebaseerde dosimetrie en postoperatieve (Dag 30) dosimetrie. Met de data van 699 patiënten vonden we een afname in D_{90} van 11% tussen intraoperatieve TRUS- en CBCT-gebaseerde dosimetrie. Intraoperatieve CBCT-gebaseerde dosimetrie correleerde beter met Dag 30 dosimetrie dan TRUS-gebaseerde dosimetrie. Een eenvoudige vergelijking verbeterde deze correlatie van D_{90} voor beide modaliteiten. Oedeem leek het grootste deel van de systematische veranderingen in D_{90} tussen implantatie en postimplant (Dag 30) dosimetrie te veroorzaken.

HOOFDSTUK 5

Voor diverse locaties in de prostaat werden de patronen van zaadjesverplaatsingen tussen intraoperatieve TRUS en CBCT bepaald. In de buurt van de rectumwand werden de grootste verplaatsingen gevonden. Dit werd waarschijnlijk veroorzaakt door TRUS-sonde-geïnduceerde prostaatvervorming. Centrale en posterior gelegen zaadjes toonden minder caudale verplaatsingen dan laterale en anterior gelegen zaadjes. Zaadjes die nabij de prostaatbasis geplaatst werden, divergeerden meer van de centrale as dan zaadjes in de buurt van de apex. De verplaatsingen van zaadjes, in de door ons waargenomen patronen, zijn een aannemelijke oorzaak van onderdoseringen die bij de anterior-basis van de prostaat ontstaan.

Er zijn veel groepen die rapporteerden over een afname van dosis tussen TRUS-gebaseerde intraoperatieve en postimplant-dosimetrie. In onze studie zagen we een vergelijkbare trend. Opmerkelijk is dat CBCT-gebaseerde dosimetrie een tegenovergesteld effect laat zien; de postimplant dosis (D_{90}) is over het algemeen hoger dan intraoperatieve CBCT-gebaseerde waarden.

We lieten ook zien dat voor individuele gevallen TRUS- noch CBCT-gebaseerde intraoperatieve dosimetrie een nauwkeurige voorspelling kan geven voor postimplant-dosimetrie op Dag 30. Dit komt waarschijnlijk door zaadjesverplaatsingen die optreden nadat de patiënt de operatiekamer verlaten heeft.

HOOFDSTUK 6

LEIDT DYNAMISCHE CBCT-GEBASEERDE BRACHYTHERAPIE tot betere postimplant-dosimetrie? In een studie met data van 1266 patiënten, verkregen in een periode van negen jaar, werd het effect van de adaptaties in de dynamische brachytherapieprocedure geëvalueerd. Daarnaast werden regio's geïdentificeerd waar een adaptatie nodig was. Afgezien van enkele efficiëntieverbeteringen leek de CBCT-gebaseerde dynamische dosimetrietechniek op de techniek die werd gebruikt voor de pilotstudie (hoofdstuk 2). In aanvulling op de klinisch bereikte dosimetrie werd dosimetrie bepaald zonder de dosisbijdrage van bijgeplaatste zaadjes. Dit maakte het mogelijk het dosimetrisch effect van adaptaties ook op Dag 30 te bepalen.

We waren in staat om de juiste implantaten voor bijplaatsing van zaadjes te selecteren. Als we in deze implantaten geen zaadjes bijge-

plaatst zouden hebben, zou de dosimetrie niet optimaal zijn. Hierbij zou de helft van de groep een onwenselijk lage V_{100} ($<95\%$) hebben gekregen.

Bij 17,4% van de patiënten werd een adaptatie uitgevoerd. Dit resulteerde op Dag 30 in een D_{90} van 121% en een V_{100} van 98%.

In tegenstelling tot de hoge V_{100} werd juist een lage V_{150} verkregen. Dit leidde tot een gunstige homogeniteitsindex vergeleken met in de literatuur beschreven waarden. Een lage V_{150} correleert met een lagere toxiciteit van de behandeling. Dit geeft aan dat een CBCT-gebaseerde dynamische prostaatbrachytherapie implantaten van hoge kwaliteit mogelijk maakt.

De meeste bijgeplaatste zaadjes werden in de buurt van de anterior-basis van de prostaat geplaatst. De CBCT-gebaseerde implantatieprocedures werden uitgevoerd in $1\frac{1}{4}$ uur. Een adaptatie kostte een kwartier extra tijd. Concluderend toont deze studie met een groot aantal patiënten aan dat de CBCT-methode effectief en efficiënt is en geschikt voor de klinisch routine.

DE VARIABILITEIT IN HET INTEKENEN EN DE REGISTRATIE van onze procedure wordt besproken in hoofdstuk 7. De dosimetrische gevolgen van inter- en intra-observatorvariabiliteit in de intekening en registratie werden gekwantificeerd. Vervolgens werden deze vergeleken met de omvang van de onderdoseringen die werden voorkomen gedurende de adaptaties met de CBCT-techniek.

Vijf observatoren namen deel aan de studie en voerden drie sessies uit voor datasets van elf patiënten om de inter- en intra-observatorvariabiliteit te kwantificeren. De variabiliteiten werden geometrisch (intekeningen) en dosimetrisch (intekeningen en registraties) bepaald. TRUS- en CT-beelden werden gebruikt om op in te tekenen en registraties vonden plaats op TRUS-CBCT en MRI-CBCT. De prostaat werd onderverdeeld in een superior, centraal en inferior deel om de regio's met de meeste intekenvariabiliteit te identificeren.

De geometrische inter-observatorvariabiliteit was gemiddeld 1,1 mm voor het intekenen, wat resulteerde in een dosimetrische variabiliteit van 1,6% voor V_{100} en 9% voor D_{90} . TRUS-CBCT-registratie leidde tot een V_{100} variabiliteit van 2% en een D_{90} variabiliteit van 3%. Het superior en

HOOFDSTUK 7

inferior deel van de prostaat toonden meer variabiliteit dan het centrale deel.

Deze studie laat zien dat inteken- en registratie-variabiliteiten de dosimetrie beïnvloedden. Toch was deze invloed kleiner dan de onderdoseringen waarvoor adaptatie plaatsvond in de implantatieprocedure. Dit onderstreept dat de CBCT-procedure de dosimetrische kwaliteit van ¹²⁵I implantaten verhoogt.

Dankwoord

De omgeving geeft een rit zijn schoonheid, de omgeving draagt bij aan het succes. Het onderzoek waarmee ik mij de afgelopen jaren bezig heb gehouden voelt als een lange rittenkoers. Vele etappes moesten worden afgelegd, sommige waren goed te doen, andere kostten me veel inspanning. Wat dat betreft was het een interessant mengsel van genieten en afzien. Nu, met de meet in zicht, overheerst de vreugde dat ik kan terugkijken op een periode waarin ik veel mooie dingen heb gedaan. Dit alles is alleen mogelijk geweest door de bijdrage van velen. Mensen die ik erg dankbaar ben.

Allereerst denk ik daarbij aan André. Je motiveerde me als een ploegleider om aan deze rit te starten en bood mij alle gelegenheid hem tot een goed einde te brengen.

Ook ben ik heel blij met de hulp uit Utrecht. Rien, je kent de kneepjes van de discipline prostaat brachytherapy heel goed. Onderweg gaf je me aanwijzingen die het resultaat naar een substantieel hoger plan brachten. Jan, heel erg bedankt voor de kans die ik kreeg om deze rit in Utrecht te finishen.

Mijn teammaten, Vincent en Tonnis. Dank voor al die tijd dat ik uit de wind kon rijden. Tonnis, jouw kritische aanwijzingen hebben tot grote verbeteringen geleid; bij het schrijven kon ik me geen betere ploeggenoot wensen.

Een rittenkoers kan alleen plaatsvinden als daarvoor de ruimte is; ruimte die niet voor andere zaken ingezet kan worden. Karin, ik ben heel blij dat je mij die ruimte in Deventer hebt geboden.

Een goede start is het halve werk. Dat goede begin vond zijn oorsprong in werk dat Arie, Carel en Jos al ruim voor mijn aanstelling in Deventer waren begonnen. Geweldig bedankt voor de vliegende start. Arie, mooi dat jouw kunst, met lage-energie- γ -straling, de

blikvanger mag zijn van dit boekje dat gaat over een laagenergetische bestralingsbehandeling.

Dan de brachyclub, ons multidisciplinaire team herbergt talenten op verschillende terreinen. Juist dat maakt ons team sterk en dat leidt weer tot mooie resultaten. Rob, Ada en collega's, als mechaniekers stonden jullie mij terzijde door enorme hoeveelheden data te registreren en mijn vele vragen te beantwoorden. Jos, Carel, Sandrine en Charles, enorm bedankt voor jullie deskundige werk, het was een basis en voorwaarde voor ons onderzoek. Het materiaal (lees: de data) moet goed zijn om iets te kunnen presteren. En Max natuurlijk, ik ben je heel dankbaar dat jij met Daan het voor mij te steile stuk van de klinische outcome opgegaan bent; we zijn zeer content met jouw analyse.

Artsen, jullie métier ziet er anders uit dan het mijne, laboranten zonder jullie hands-on bijdrage zou het niets worden. Dank jullie allemaal voor het interessant houden van de rit en de andere strategieën die het juist bij elkaar een waardevol geheel maken. Het peloton bestaat uit een grote groep mensen, met velen had ik geregeld contact. Dit geldt in het bijzonder voor de groep Klinische Fysica in Deventer. Heel erg bedankt voor de gesprekken over ons vak en ver daarbuiten over algoritmes, hardware, open source, fietsen, kinderen, het instituut, geloof, techniek, drijfveren. . .

En natuurlijk ook de fietsmaten van YKC/TWTC en BZZ, wat heeft onze gemeenschappelijke hobby de zaak opgevrolijkt. De koers, de klim, de TTT, de baan, het kraken, Maratona, Hermann, Paris – Roubaix (de *volledige* terugkeer), genuil, gefilosofeer en wat dies meer zij, super.

Menno, Pieter, Sandar, al 20 jaar verheugen we ons elk jaar opnieuw op een weekend met MTB, dominicanen, RiSK en vele andere tradities, voor mij elke keer opnieuw een zeer welkome ravitaillering. Dank voor de vriendschap die spiegelt en adviseert.

Papa en mama, dank jullie wel voor de kans om mogelijkheden te benutten, het vertrouwen dat de rit ergens toe leiden zou. Hans en Harriët, jullie bedankt voor de vele aanmoedigingen onderweg. Zussen, zwagers, schoonzus de '*allez*'-tjes die ik van jullie kreeg, hebben me enorm geholpen.

Fietsen kost veel tijd, onderzoek ook. Tijd die alleen komt met enthousiasme van thuis.

Lieve Andrea, jou aan mijn zij te hebben is onmisbaar gebleken in voorspoed maar ook juist in de donkere periodes. De rust(dagen) die

jij me helpt te nemen, maken alles mooier. Simone, Eline en Matthijs, hoe fijn is het om met jullie samen te zijn en met elkaar iets leuks te doen. Gelukkig hebben we daar, ondanks de tijd die naar andere dingen uitging, al heel veel van kunnen genieten. Dank dat jullie me, als geen ander helpen om werk, onderzoek en sport in een weidser perspectief te zien. Een perspectief dat ons weten ver overtreft.

List of publications

- H Westendorp, CJ Hoekstra, A van 't Riet, AW Minken and JJ Immerzeel (2007). 'Intraoperative adaptive brachytherapy of iodine-125 prostate implants guided by C-arm cone-beam computed tomography-based dosimetry.' *Brachytherapy*, 6(4):231–7
- J Crezee, P van Haaren, H Westendorp, M de Greef, H Kok, J Wiersma, G van Stam, J Sijbrands, P Zum Vörde Sive Vörding, J van Dijk, M Hulshof and A Bel (2009). 'Improving locoregional hyperthermia delivery using the 3-D controlled AMC-8 phased array hyperthermia system: a preclinical study.' *Int J Hyperthermia*, 25(7):581–92
- PMA van Haaren, A van't Riet, MA Moerland, C Koedooder and H Westendorp (2011). 'Dose to fingertips of staff preparing stranded iodine-125 seeds for permanent prostate implants.' *Radiat Prot Dosimetry*, 145(1):61–65
- H Westendorp, R Kattenvilder, A van 't Riet, AW Minken, TT Nuver, JJ Immerzeel and CJ Hoekstra (2012). 'Objective automated assessment of time trends in prostate edema after ^{125}I implantation'. *Brachytherapy*, 11(5) (5):327–33
- V Althof, P van Haaren, H Westendorp, T Nuver, D Kramer, M Ikink, A Bel and A Minken (2012). 'A quality assurance tool for helical tomotherapy using a step-wedge phantom and the on-board MVCT detector.' *J Appl Clin Med Phys*, 13 (1):3585
- AJG Even, TT Nuver, H Westendorp, CJ Hoekstra, CH Slump and AW Minken (2014). 'High-dose-rate prostate brachytherapy based on registered trans-rectal ultrasound and in-room cone-beam CT images.' *Brachytherapy*, 13 (2):128–36
- M Peters, J van der Voort van Zyp, C Hoekstra, H Westendorp, S van de Pol, M Moerland, M Maenhout, R Kattenvilder and M van Vulpen (2015). 'Urethral and bladder dosimetry of total and focal salvage Iodine-125 prostate brachytherapy: Late toxicity and dose constraints.' *Radiother Oncol*, 117 (2):262–9

- H Westendorp, TT Nuver, MA Moerland and AW Minken (2015). 'An automated, fast and accurate registration method to link stranded seeds in permanent prostate implants'. *Phys Med Biol*, 60(20):N391–N403
- M Peters, JRN van der Voort van Zyp, MA Moerland, CJ Hoekstra, S van de Pol, H Westendorp, M Maenhout, R Kattevilder, HM Verkooijen, PSN van Rossum, HU Ahmed, TT Shah, M Emberton and M van Vulpen (2016a). 'Development and internal validation of a multivariable prediction model for biochemical failure after whole-gland salvage iodine-125 prostate brachytherapy for recurrent prostate cancer.' *Brachytherapy*, 15 (3):296–305
- H Westendorp, TT Nuver, CJ Hoekstra, MA Moerland and AW Minken (2016). 'Edema and Seed Displacements Affect Intraoperative Permanent Prostate Brachytherapy Dosimetry'. *Int J Radiat Oncol Biol Phys*, 96(1):197–205
- M Peters, JRN van der Voort van Zyp, MA Moerland, CJ Hoekstra, S van de Pol, H Westendorp, M Maenhout, R Kattevilder, HM Verkooijen, PSN van Rossum, HU Ahmed, TT Shah, M Emberton and M van Vulpen (2016c). 'Multivariable model development and internal validation for prostate cancer specific survival and overall survival after whole-gland salvage Iodine-125 prostate brachytherapy.' *Radiother Oncol*, 119 (1):104–10
- M Peters, CJ Hoekstra, JRN van der Voort van Zyp, H Westendorp, SMG van de Pol, MA Moerland, M Maenhout, R Kattevilder and M van Vulpen (2016b). 'Rectal dose constraints for salvage iodine-125 prostate brachytherapy.' *Brachytherapy*, 15 (1):85–93
- M Peters, DA Smit Duijzentkunst, H Westendorp, SMG van de Pol, RAJ Kattevilder, A Schellekens, JRN van der Voort van Zyp, MA Moerland, M van Vulpen and CJ Hoekstra (2017). 'Adaptive cone-beam CT planning improves long-term biochemical disease-free survival for ¹²⁵I prostate brachytherapy'. *Brachytherapy*
- H Westendorp, CJ Hoekstra, JJ Immerzeel, SM van de Pol, CG Niël, RA Kattevilder, TT Nuver, MA Moerland and AW Minken (2017a). 'Cone-beam CT-based dynamic planning improves permanent prostate brachytherapy dosimetry: An analysis of 1266 patients'. *Med Phys*
- H Westendorp, K Surmann, CJ Hoekstra, SM van de Pol, RA Kattevilder, TT Nuver, MA Moerland and AW Minken (2017b). 'Dosimetric impact of inter- and intra-observer variability in contouring and image registration for intraoperative ¹²⁵I prostate brachytherapy dosimetry.' *Brachytherapy*

Curriculum Vitae

Rik Westendorp werd op 13 oktober 1977 in Woerden geboren. In 1996 behaalde hij aan het Ichthus College te Kampen het VWO diploma, waarna hij begon aan een studie Technische Natuurkunde te Twente. Daar studeerde hij in 2002 af bij de vakgroep Biofysische Technieken. In mei 2002 startte hij met de opleiding tot klinisch fysicus radiotherapie in het Catharina Ziekenhuis te Eindhoven. Deze opleiding zette hij in 2003 voort in het RISO te Deventer, waarna in 2006 registratie als klinisch fysicus plaatsvond.

Sindsdien vervult hij een betrekking als klinisch fysicus radiotherapie in het RISO, later Radiotherapiegroep, te Deventer met als belangrijkste aandachtspunten treatment planning en ^{125}I prostaat brachytherapie. Rik is getrouwd met Andrea. Zij zijn de dankbare ouders van Simone, Eline en Matthijs.



List of Abbreviations

^{125}I	Iodine 125 (radioactive isotope of Iodine)
2D	Two Dimensional
3D	Three Dimensional
AAPM	American Association of Physicists in Medicine
ABS	American Brachytherapy Society
AP	Anterior Posterior
BDFS	Biochemical Disease Free Survival
C	Central
CBCT	ConeBeam Computed Tomography
CC	CranioCaudal
COM	Center Of Mass
CT	Computed Tomography
dlf	distance to linefit
D_x	Minimal Dose (% of prescribed) to x% of volume
EBRT	External Beam Radiation Therapy
ESTRO	European SocieTy for Radiotherapy & Oncology
GEC	Groupe Européen de Curiethérapie
HDR	High Dose Rate
HI	Homogeneity index
I	Inferior
LDR	Low Dose Rate
lf	linefit
ll	link length
LR	Left Right
MRI	Magnetic Resonance Imaging
OAR	Organ At Risk
PDR	Pulsed Dose Rate
PSA	Prostate Specific Antigen
RMS	Root Mean Square
ROI	Region Of Interest
S	Superior
SD	Standard Deviation
T	Total volume
TPS	Treatment Planning System
TRUS	Trans Rectal UltraSound
V	Volume
V_y	% of Volume receiving minimal y% of prescribed dose

